AD-A178 223 A UNIFIED DIRECT-INVERSE PROCEDURE FOR TWO-DIMENSIONAL BOUNDARY LAYERS US. (U) PENNSYLVANIA STATE UNIV STATE COLLEGE APPLIED RESEARCH LAB K C KAUFMAN ET AL. FEB 87 1/2

UNCLASSIFIED TR-87-001 F/G 12/1 NL

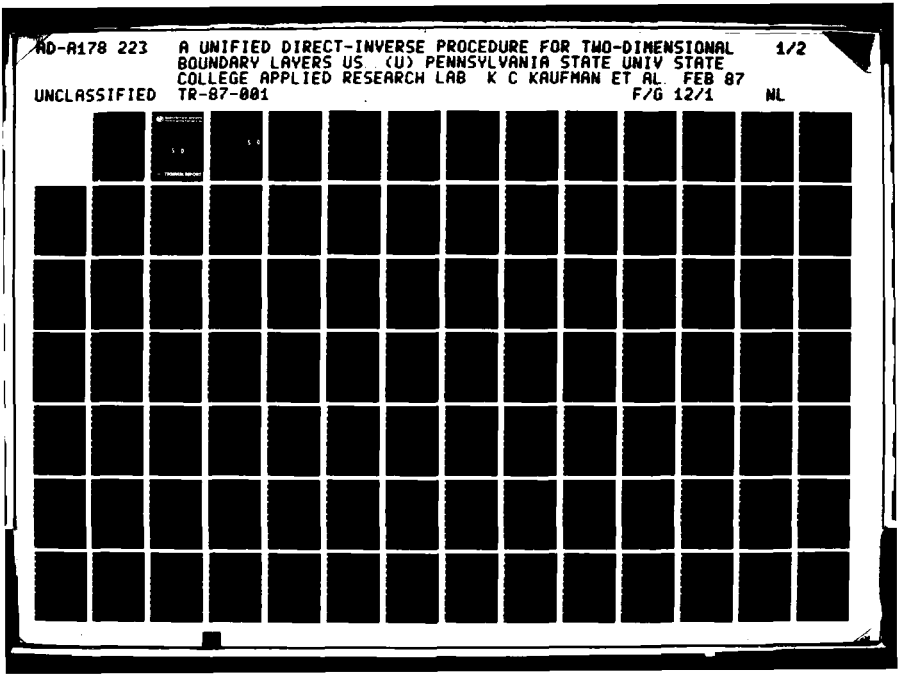

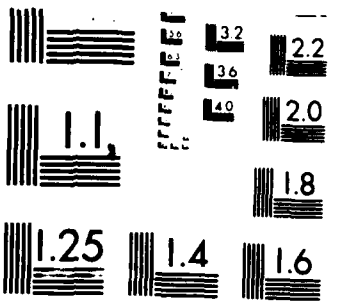

MICROCOPY RESOLUTION TEST CHART
NATIONAL BUREAU OF STANDARDS 1963 A

AD-A178 223

Applied Research Laboratory
The Pennsylvania State University

A UNIFIED DIRECT-INVERSE PROCEDURE FOR TWO-DIMENSIONAL BOUNDARY LAYERS USING SPLINE/FINITE DIFFERENCE DISCRETIZATION

by

K. C. Kaufman and G. H. Hoffman

DTIC
ELECTE
MAR 2 3 1987
S D
D

DTIC FILE COPY

DISTRIBUTION STATEMENT A
Approved for public release
Distribution Unlimited

ARL-PSU

TECHNICAL REPORT

873 20 006

(12)

The Pennsylvania State University
APPLIED RESEARCH LABORATORY
P. O. Box 30
State College, PA 16804

A UNIFIED DIRECT-INVERSE PROCEDURE FOR TWO-DIMENSIONAL BOUNDARY LAYERS USING SPLINE/FINITE DIFFERENCE DISCRETIZATION

by

K. C. Kaufman and G. H. Hoffman

DTIC
ELECTE
MAR 2 3 1987
S D
D

Technical Report No. TR-87-001
February 1987

Supported by:
Naval Sea Systems Command

L. R. Hettche, Director
Applied Research Laboratory

Approved for public release; distribution unlimited

Unclassified
SECURITY CLASSIFICATION OF THIS PAGE

ADA178223

REPORT DOCUMENTATION PAGE

1a. REPORT SECURITY CLASSIFICATION Unclassified	1b. RESTRICTIVE MARKINGS
2a. SECURITY CLASSIFICATION AUTHORITY	3. DISTRIBUTION / AVAILABILITY OF REPORT
2b. DECLASSIFICATION / DOWNGRADING SCHEDULE	
4 PERFORMING ORGANIZATION REPORT NUMBER(S)	5. MONITORING ORGANIZATION REPORT NUMBER(S)
6a. NAME OF PERFORMING ORGANIZATION Applied Research Laboratory The Pennsylvnaia State University 6b. OFFICE SYMBOL (If applicable) ARL	7a. NAME OF MONITORING ORGANIZATION Naval Sea Systems Command Department of the Navy
6c. ADDRESS (City, State, and ZIP Code) P. O. Box 30 State College, PA 1680r	7b. ADDRESS (City, State, and ZIP Code) Washington, DC 20362
8a. NAME OF FUNDING / SPONSORING ORGANIZATION Naval Sea Systems Command 8b. OFFICE SYMBOL (If applicable) NAVSEA	9. PROCUREMENT INSTRUMENT IDENTIFICATION NUMBER
8c. ADDRESS (City, State, and ZIP Code) Department of the Navy Washington, DC 20362	10 SOURCE OF FUNDING NUMBERS PROGRAM ELEMENT NO. / PROJECT NO. / TASK NO. / WORK UNIT ACCESSION NO.

11 TITLE (Include Security Classification)
A Unified Direct-Inverse Procedure for Two-Dimensional Boundary Layers Using Spline/Finite Difference Discretization (Unclassified)

12 PERSONAL AUTHOR(S)
K. C. Kaufman and G. H. Hoffman

13a TYPE OF REPORT	13b TIME COVERED	14. DATE OF REPORT (Year, Month, Day)	15. PAGE COUNT
M.S. Thesis	FROM _____ TO _____	February 1987	167

16 SUPPLEMENTARY NOTATION

17 COSATI CODES			18. SUBJECT TERMS (Continue on reverse if necessary and identify by block number)
FIELD	GROUP	SUB-GROUP	incompressible, boundary layer, spline, finite difference Mechul, wall shear, skin friction, turbulent flow, Levy-Lees Newton-Raphson

19 ABSTRACT (Continue on reverse if necessary and identify by block number)

A unified approach is presented for solving the two-dimensional incompressible boundary layer equations. Solutions are obtained for direct and inverse options using the same equation formulation by a simple interchange of boundary conditions. A modified form of the mechul function scheme obtains inverse solutions with specification of transformed wall shear, skin friction coefficient, or displacement thickness distributions. Turbulent flow is treated using a two-piece algebraic eddy viscosity model, with the modified Levy-Lees transformation applied to capture the growth of laminar and turbulent layers. Fourth-order spline discretization approximates normal derivatives with three- and two-point backward differences approximating streamwise derivatives, yielding a fully implicit

20 DISTRIBUTION / AVAILABILITY OF ABSTRACT ☒ UNCLASSIFIED/UNLIMITED ☐ SAME AS RPT. ☐ DTIC USERS	21. ABSTRACT SECURITY CLASSIFICATION Unclassified
22a NAME OF RESPONSIBLE INDIVIDUAL	22b TELEPHONE (Include Area Code) 814/865-6344 / 22c. OFFICE SYMBOL

DD FORM 1473, 84 MAR 83 APR edition may be used until exhausted. All other editions are obsolete.

SECURITY CLASSIFICATION OF THIS PAGE
Unclassified

19. Abstract (continued)

solution method. The resulting spline/finite difference equations are solved by Newton-Raphson iteration together with partial pivoting. Numerical solutions are presented for several nonsimilar flows and compared with published results.

ABSTRACT

A unified approach is presented for solving the two-dimensional incompressible boundary-layer equations. Solutions are obtained for direct and inverse options using the same equation formulation by a simple interchange of boundary conditions. A modified form of the mechul function scheme obtains inverse solutions with specification of transformed wall shear, skin friction coefficient, or displacement thickness distributions. Turbulent flow is treated using a two-piece algebraic eddy viscosity model, with the modified Levy-Lees transformation applied to capture the growth of laminar and turbulent layers. Fourth-order spline discretization approximates normal derivatives with three- and two-point backward differences approximating streamwise derivatives, yielding a fully implicit solution method. The resulting spline/finite difference equations are solved by Newton-Raphson iteration together with partial pivoting. Numerical solutions are presented for several nonsimilar flows and compared with published results.

DTIC
COPY
INSPECTED
6

Accesion For
NTIS CRA&I ☒
DTIC TAB ☐
Unannounced ☐
Justification .....
By .....
Distribution /
Availability Codes
Dist | Avail and / or Special
A-1

LIST OF TABLES

LIST OF FIGURES

LIST OF FIGURES (Continued)

LIST OF FIGURES (Continued)

NOMENCLATURE

English Letters:

A,B,C	4 X 4 block tridiagonal matrix coefficients
$\hat{A},\hat{B},\hat{C},\hat{D},\hat{E},\hat{F},\hat{G}$	linearized momentum equation coefficients
C_f	skin friction coefficient = $\dfrac{\tau_w}{1/2\ \rho_\infty u_{ref}^2}$
H	boundary-layer shape factor
K	number of steps in normal direction
L	boundary-layer reference length
L^g	spline derivative approximation for $\dfrac{\partial^2 g}{\partial N^2}$
L,P,Q,T	known right-hand sides of linearized spline equations
M	number of steps in streamwise direction
N	adaptive normal coordinate
R	column vector of known quantities
Re	reference Reynolds number = $\rho_\infty\ u_\infty\ L/\mu_\infty$
V	Reynolds scaled normal velocity component, $v\sqrt{Re}$
Y	Reynolds scaled normal coordinate, $y\sqrt{Re}$
Z	column vector of solution variable corrections
b	eddy viscosity coefficient, μ_t/μ_{t_e}
b^*	reciprocal of eddy viscosity coefficient
f	pseudo-self-similar streamfunction
h	normal stepsize
ℓ^g	spline derivative approximation for $\dfrac{\partial g}{\partial N}$
u,v	untransformed streamwise and normal velocity components
x,y	untransformed streamwise and normal coordinates

Greek Letters:

δ	boundary-layer thickness
δ^*	boundary-layer displacement thickness
τ_w	wall shear
$\hat{\tau}$	Klineberg and Steger transformed wall shear
ρ	fluid density
μ	fluid viscosity
ψ	two-dimensional streamfunction
η	modified Levy-Lees normal coordinate
ξ	modified Levy-Lees streamwise coordinate
ε	eddy viscosity
β	streamwise pressure gradient parameter
σ	normal stepsize ratio
Θ	FLARE coefficient

Subscripts:

e	denotes edge value
i,j	denotes spline/finite difference grid nodal points
t	denotes turbulent value
w	denotes wall value
∞	denotes reference/freestream value
η	denotes normal partial derivative
ξ	denotes streamwise partial derivative

Superscripts:

n	denotes iteration level
*	denotes dimensional quantities
$\hat{}$	denotes transformed quantities

ACKNOWLEDGEMENT

The author has the deepest gratitude for the support, both technical and moral, of Dr. Gilbert H. Hoffman. This work, and the experience gained from it, would not have been possible without his aid. The author wishes to thank Dr. Shaaban Abdallah for countless hours of enjoyable discussion concerning this thesis. The author also appreciates the time and effort of Mrs. Lynne Stewart for typing the manuscript.

This research was supported by E/F funding at the Applied Research Laboratory/The Pennsylvania State University.

Chapter 1

INTRODUCTION

1.1 Problem Background

The two standard computational techniques for treating boundary-layer flows are the direct and inverse methods. The direct method, which involves specifying a pressure or inviscid edge velocity distribution, has been widely used for many years. The pioneering work of Smith and Clutter [1] is an excellent example of a direct boundary-layer solution method. This approach performs well for attached shear layers but cannot treat separating boundary layers, due to the singularity that exists at the separation point when the edge velocity is specified [2,3]. This singularity prevents the use of the direct method for regions of backflow, including separation bubbles and trailing edge separation.

These regions of backflow are usually of great interest to the fluid dynamicist, since they can have a significant effect on the overall flow. To obtain solutions for separated boundary layers, several types of inverse methods have been developed. By specifying distributions of displacement thickness, wall shear, or similar quantities, and obtaining the streamwise pressure distribution, these methods eliminate the singularity in the boundary-layer equations at separation. The equations of motion may then be integrated through the region of separation under the condition that the extent of separation is small (backflow velocities less than ten percent of the edge velocity). The boundary-layer equations remain valid under the assumption that the shear layer is thin ($d\delta/dx \ll 1$). For shear layers which violate this condition, upstream influences become significant and

the boundary-layer equations alone can no longer accurately describe the flow.

Catherall and Mangler [4] originated the inverse procedure, specifying a displacement thickness distribution near the separation point to obtain regular solutions into a region of backflow. Once inside the separated zone, however, the procedure developed instabilities which required a progressive increase in convergence limits as the solution continued downstream. Since the boundary-layer equations are parabolic, these instabilities arise from marching in a direction opposite to the streamwise velocity.

Reyhner and Flugge-Lotz [5] originated the FLARE approximation which eliminates the instabilities by setting all streamwise convection terms to zero inside the region of backflow. Since the x-convective terms are small in this region, for thin separated zones, this introduces only minor errors while allowing a forward-marching procedure to continue through the separated region. Since it was presented, the FLARE approximation has been a standard part of the majority of inverse methods which seek to resolve regions of separated flow.

An iterative procedure developed by Williams [6] improved on the FLARE approach by making repeated downstream and upstream passes through the separated zone. On the first downstream pass, FLARE is used to define the extent of the separation zone. An upstream pass, using a direct solution, is then made inside the region of backflow to determine the convective terms. The downstream pass is then repeated without FLARE, using the results obtained from the upstream solution. This process is repeated for several cycles until convergence is reached. The DUIT (Downstream-Upstream Iteration) procedure produces more accurate velocity profiles for the separated region, and has been used

successfully by Cebeci, Keller, and Williams [7]. A drawback inherent in the iterative process, however, is that only closed separation bubbles or separated regions which reach an asymptotic state can be treated. The DUIT procedure has presently been tested only on laminar flows.

The majority of inverse studies have only considered laminar boundary layers. These studies include the work of Keller and Cebeci [8], Klineberg and Steger [9], Horton [10,11], and Carter, [12,13]. Recently, several studies of turbulent separating boundary layers have been presented, including Carter and Wornom [14], Cebeci [15], Carter [16], and Whitfield, Swafford, and Jacocks [17]. These are difference methods, with the exception of the integral method in Reference 17.

The quantities specified by these inverse methods vary, with most specifying the Reynolds stretched displacement thickness [4] or a wall shear. A method presented by Carter [16] is unique in specifying the mass flow, $\bar{m}$. Carter [12,13] has considered the specification of both displacement thickness and wall shear, but reformulated the equations for each case. Cebeci [15], however, considers the specification of skin friction coefficient C_{f_e} and displacement thickness with a minimum of reformulation. Cebeci also presents both direct and inverse methods in this work, although the equations must be put in variational form to obtain an inverse solution.

Table 1 presents a sample of the inverse methods referenced in this study, with a brief summary of their important features.

Table 1

Sampling of Inverse Method Investigations

Authors	Specify	Flow Type	Method/Discretization
1. Catherall and Mangler (1966)	δ^*	Lam	Crank-Nicolson
2. Reyhner and Flugge-Lotz (1968)	δ^*	Com/Lam	Implicit F.D./Integral
3. Keller and Cebeci (1972)	f_w''	Lam	Eigenvalue/Keller Box
4. Cebeci and Keller (1973)	f_w''	Lam	Mechul Fun./Keller Box
5. Klineberg and Steger (1974)	$\hat{\tau}$	Lam	Modified Box
6. Horton (1974)	f_w''	Lam	Shooting
7. Carter (1974)	τ_w/δ^*	Lam	Modified Box
8. Carter (1975)	τ_w/δ^*	Lam	Global It./Modified Box
9. Carter and Wornum (1975)	δ^*	Lam/Tur	Modified Box
10. Cebeci (1976)	C_f/δ^*	Com/Lam/Tur	Variational Eq. Keller Box
11. Carter (1978)	$\delta^*/\bar{m}$	Com/Lam/Tur	Crank-Nicolson
12. Cebeci, Keller, and Williams (1979)	δ^*	Lam	DUIT/Keller Box
13. Horton (1981)	δ^*	Lam	Implicit F.D./Imbedding
14. Whitfield, Swafford, and Jacocks (1981)	δ^*	Lam/Tur	Integral

1.2 Applications

Before discussing the present approach to solving the boundary-layer equations, a brief consideration of the applications of direct and inverse boundary-layer methods is appropriate. If the solution method cannot be applied to important, existing problems, any innovations in the solution approach are worthless.

As is stated in the previous section, the direct method is applicable only to attached flows. It is typically used to obtain skin friction distributions, drag coefficients, and integral parameters which characterize the viscous flow over a body or surface subjected to a particular pressure distribution. Because of the familiarity of the direct method, we will concentrate this discussion on the application of inverse methods.

Inverse methods, which apply to both attached and separated boundary layers, provide a pressure distribution when supplied with a displacement thickness or wall shear distribution. Inverse methods have several important applications when used alone, and can also be used in conjunction with direct boundary-layer methods and inviscid solution methods.

Used alone, inverse methods can be effective design tools. This is particularly true of the wall shear methods, where an optimal design for body shapes can be developed by prescribing the friction forces on a surface and determining the corresponding pressure distribution. Such methods could also be used for evaluating flow situations where the boundary layer maintains near zero wall shear values. An example of this situation is the Liebeck airfoils [18], which are designed for high lift characteristics.

An important application of inverse methods is interacting boundary-layer methods or viscous/inviscid interaction schemes. When the boundary-layer thickness remains of order $(Re)^{-1/2}$, the flow behavior downstream has negligible effect on the upstream flow. If the boundary-layer thickness becomes order unity, however, the upstream pressure effect is significant and the boundary-layer equations no longer adequately describe the flow. In these situations, the boundary-layer solution is usually coupled to an inviscid outer solution. Although this approach is useful for regions of weak interaction, with minor pressure effects, it is particularly appropriate for regions of strong interaction with boundary-layer separation. This is a satisfactory alternative to solving the full Navier-Stokes equations.

This area of computational fluid dynamics is too complex to be thoroughly discussed here, with many variations in the application of boundary-layer solutions, both direct and inverse. For our purpose, it is sufficient to make the reader aware of the use of boundary-layer solutions in this manner. For a more complete discussion refer of Veldman [19] or Vatsa and Verdon [20].

1.3 The Present Method

This study presents a unified approach to the numerical solution of the direct and inverse formulations of the boundary-layer equations using an implicit spline/finite difference discretization scheme. The method is formulated to allow the specification of transformed wall shear, skin friction coefficients, or displacement thickness distributions by simply switching the appropriate boundary conditions. This idea is similar to the work of Cebeci [15]. The current study goes beyond that of Cebeci by also allowing direct or inverse solutions to be

obtained with a similar technique. Thus the present work is truly unified in handling direct as well as shear or displacement thickness inverse solutions with the same formulation, requiring only minor changes in the boundary conditions depending upon the desired solution.

The present scheme applies fourth order splines, as derived by Rubin and Khosla [21], to approximate the normal derivatives in the boundary-layer equations, with two-and three-point backward differences to discretize the streamwise derivatives. The differencing scheme was chosen to yield a fully implicit solution method. The splines also provide increased accuracy for a given number of mesh points.

The mechul function method, originally devised for inverse methods by Cebeci and Keller [22], is used in a modified form described by Kaufman and Hoffman [23]. This modified form is necessary due to the use of the spline discretization. The FLARE approximation is employed in separation zones to prevent the development of instabilities inherent in marching downstream through regions of backflow.

To treat turbulent boundary layers, a two-piece algebraic eddy viscosity model, developed by Baldwin and Lomax [24], is incorporated in the formulation. The modified Levy-Lees transformation is used to capture the boundary-layer growth for laminar and turbulent flows. A modified version of the adaptive normal coordinate developed by Carter, Edwards, and Werle [25] is used to resolve the wall region of the turbulent boundary layer.

Following discretization, the nonlinear spline/finite difference equations are linearized and solved using Newton's method. The resulting linear block tridiagonal matrix system for the solution vector corrections at each streamwise station is solved using L-U

decomposition. Partial pivoting is necessary in the block tridiagonal solution process to prevent the buildup of roundoff errors.

Chapter 2

ANALYSIS

2.1 Governing Equations

The governing equations for steady, incompressible, two-dimensional boundary-layers in dimensionless, Reynolds number scaled form are

$$\text{continuity} \quad \frac{\partial u}{\partial x} + \frac{\partial V}{\partial Y} = 0 \tag{1}$$

$$\text{x-momentum} \quad \rho u \frac{\partial u}{\partial x} + \rho V \frac{\partial u}{\partial Y} = - \frac{\partial p}{\partial x} + \frac{\partial}{\partial Y} \left(\mu_t \frac{\partial u}{\partial Y} \right) \tag{2}$$

$$\text{y-momentum} \quad \frac{\partial p}{\partial Y} = 0 \tag{3}$$

where, $\mu_t = \mu + \rho\varepsilon$

and the Euler equation applied at the body surface gives

$$- \frac{dp_e}{dx} = \rho_e u_e \frac{du_e}{dx}$$

The non-dimensional, scaled variables are given by

$$x = x^*/L^*_{ref} \ , \ Y = y^* \sqrt{Re}/L^*_{ref}$$

$$u = u^*/u^*_{ref} \ , \ V = v \sqrt{Re}/u^*_{ref} \tag{4}$$

$$\rho = \rho^*/\rho^*_{ref}, \ \mu = \mu^*/\mu^*_{ref}$$

$$Re = \frac{\rho^*_{ref} u^*_{ref} L^*_{ref}}{\mu^*_{ref}} \tag{5}$$

(See any standard text on boundary-layer theory, such as Schlichting [26] for a discussion of Reynolds number scaling.)

The usual boundary conditions are

impervious wall $\psi(x,o) = 0$ (6a)

no-slip $u(x,o) = 0$ (6b)

far field $u(x,Y) = 1$ as $Y \to \infty$ (7)

where the stream function is defined by

$$u = \frac{\partial \psi}{\partial Y} \ , \ V = - \frac{\partial \psi}{\partial x} \tag{8}$$

The introduction of the stream function identically satisfies continuity, Eq. (1).

For a direct solution of the boundary-layer equations, an edge velocity or pressure coefficient distribution is typically specified. Inverse solutions of the boundary-layer equations can be obtained by specifying either a wall shear (or function of the wall shear) or a displacement thickness distribution. The form of the resulting boundary conditions will be discussed later.

2.2 Transformation of the Boundary-Layer Equations

The governing equations (1) - (3) and the boundary conditions (6) - (8) are transformed using the modified Levy-Lees pseudo-self-similar transformation. Once the equations are in similarity form, the FLARE approximation of Reyhner and Flugge-Lotz [5] can be introduced to handle thin regions of separation. A composite coordinate transformation is then introduced to resolve the two length scales present in turbulent boundary layers. The advantages and disadvantages of these transformations are also discussed later.

2.2.1 Modified Levy-Lees Transformation

The Levy-Lees transformation is well known and has proven to be very useful for capturing the growth of laminar boundary-layers. The standard Levy-Lees transformation (intended for laminar boundary layers) is not suited for capturing the growth of turbulent boundary layers because the laminar viscosity is so much smaller than its turbulent counterpart. For turbulent layers, a transformation which captures the rapid growth of the turbulent boundary layer and properly resolves the wall and wake regions of the layer is needed. Carter, et al. [25] have developed such a transformation. This transformation

(1) captures the growth of the turbulent boundary layer by modifying the form of the Levy-Lees transformation, and

(2) automatically scales the inner and outer regions of the boundary layer using a composite, adaptive coordinate transformation. (This coordinate is discussed in Section 2.2.3)

The modified Levy-Lees variables are given by

$$\xi(x) = \int_0^x \rho_e \mu_{t_e} u_e \, dx \tag{9a}$$

$$\eta(x,Y) = \frac{\rho_e u_e}{\sqrt{2\xi}} \int_0^Y \frac{\rho}{\rho_e} \, dY \tag{9b}$$

where

$$\mu_{t_e} = \mu_e + (\rho\varepsilon)_{ref}$$

For a laminar boundary layer, $\varepsilon_{ref} = 0$ and the modified transformation reverts to the standard Levy-Lees form. For a turbulent layer, $\varepsilon_{ref} = \varepsilon_{max}$ and typically, $\varepsilon_{ref} = \varepsilon_{outer}$, assuming a constant value of the eddy viscosity in the wake region.

A pseudo-self-similar stream function is defined as

$$\psi(x,y) = \sqrt{2\xi}\, f(\xi,\eta) \tag{10}$$

The introduction of Eq. (10) also removes the leading edge singularity and allows a self-starting solution, where the governing equations reduce to a system of ordinary differential equations.

The velocity components of the x-momentum equation are transformed first, yielding

$$u = u_e f_\eta \tag{11a}$$

$$V = - u_e \mu_{t_e} \sqrt{2\xi}\, [f_\xi + \frac{f}{2\xi} + (\frac{\partial \eta}{\partial \xi}|_Y) f_\eta] \tag{11b}$$

Transforming the x and y derivatives, Eq. (2) becomes

$$(b\, f_{\eta\eta})_\eta + f f_{\eta\eta} + \beta(1 - f_\eta^2) = 2\xi[f_\eta f_{\xi\eta} - f_\xi f_{\eta\eta}] \tag{12}$$

where β is the streamwise pressure gradient parameter defined as

$$\beta(\xi) = \frac{2\xi}{u_e} \frac{du_e}{d\xi}$$

and

$$b = \mu_t/\mu_{t_e} \tag{13}$$

By setting $\xi = 0$, Eq. (12) reduces to the Falkner-Skan equation, with no dependence on ξ. The ODE may be solved for any Falkner-Skan solution, or a starting solution may be obtained for a non-similar flow.

Using Eqs. (9b) and (13), the relation for $(\frac{\partial \eta}{\partial \xi}\,|_Y)$ appearing in normal velocity component can be obtained. For incompressible flow, Eq. (9b) becomes

$$\eta = \frac{u_e}{\sqrt{2\xi}}\, Y$$

and

$$\frac{\partial \eta}{\partial \xi}\Big|_Y = \left(\frac{1}{u_e}\frac{du_e}{d\xi} - \frac{1}{u_e}\right)\eta$$

Using the definition of β, this yields

$$\frac{\partial \eta}{\partial \xi}\Big|_Y = \frac{\eta}{2\xi}(\beta - 1) \tag{14}$$

The transformed boundary conditions are obtained from Eqs. (6) and (7), yielding

$$f(\xi,0) = f_\eta(\xi,0) = 0 \tag{15a}$$

$$f_\eta(\xi,\eta) = 1 \text{ as } \eta \to \eta_\infty \tag{15b}$$

2.2.2 FLARE

When solving regions of separated flow with the boundary-layer equations using a marching technique, stability problems are encountered because of the parabolic nature of the equations. To prevent the solution method from becoming unstable, the equations must be modified inside the separated region. A standard procedure to stabilize the solution in thin separated zones was given by Reyhner and Flugge-Lotz [5] and is known as the FLARE approximation. In the FLARE approach, the streamwise convection term in the boundary-layer equations is neglected inside the separated region. This stabilizes the marching procedure, and since the convection term is small in thin regions of separation, introduces only minor errors into the solution. More complicated procedures, such as that devised by Williams [6], require several iterations downstream and upstream through the separation bubble. While being more accurate, these procedures can only be used when the boundary layer reattaches or the separated region reaches an asymptotic state. Since only thin regions of separation (backward flow velocities no more

than 10% of the edge velocity), are considered, some of which do not close, the FLARE approach was chosen here.

To apply the FLARE approximation to the untransformed x-momentum equation (2), a FLARE coefficient Θ is defined so that

where $$\Theta u \frac{\partial u}{\partial x} + V \frac{\partial u}{\partial Y} = u_e \frac{du_e}{dx} + \frac{\partial}{\partial Y}\left(\nu_t \frac{\partial u}{\partial Y}\right)$$

$$\Theta = \begin{cases} 1, & u \geq 0 \\ 0, & u < 0 \end{cases}$$

Horton [11], however, notes that when using pseudo-self-similar variables, this approach is too restrictive, since it affects the self-similar as well as the non-similar solutions.

To devise a less restrictive approximation, the following substitutions are defined after noting the form of the convection terms on the right-hand side of Eq. (12):

$$f_\eta = \frac{u}{u_e} = U$$

$$f_\xi = - V$$

Substituting these definitions into Eq. (12), the right-hand side becomes

$$2\xi \left[U \frac{\partial U}{\partial \xi} + V \frac{\partial U}{\partial \eta}\right] .$$

This result parallels the form of the convection terms in the untransformed equation, (2), with ξ and η replacing x and Y respectively. Since the streamwise convection term introduces the instabilities in regions of backflow, only the analogous transformed term needs to be removed. The FLARE variable is applied only to the $U \frac{\partial U}{\partial \xi}$ term, and Eq. (12) becomes

$$(bf_{\eta\eta})_\eta + ff_{\eta\eta} + \beta(1 - f_\eta^2) = 2\xi[\Theta f_\eta f_{\xi\eta} - f_\xi f_{\eta\eta}] \qquad (16)$$

where

$$\Theta = \begin{cases} 1, & f_\eta \geq 0 \\ 0, & f_\eta < 0. \end{cases}$$

Here, when ξ is set to zero for a Falkner-Skan or starting solution, no Θ-terms remain which would interfere with obtaining the self-similar solution that is sought.

2.2.3 Adaptive Composite Coordinate

The modified Levy-Lees transformation captures the growth of the boundary layer for both laminar and turbulent flows, but two length scales still exist for the turbulent case and the wall region must be adequately resolved. To accomplish this, a new normal coordinate is introduced for the inner region,

$$N_i = \frac{\sqrt{C_{f_e}/2}}{a} \tan^{-1}\left(a\sqrt{R_e C_{f_e}}\,\xi\ \eta\right) \tag{17}$$

This inner coordinate is based on an approximate analytical velocity profile given by Whitfield [27].

The composite coordinate is formed by matching N_i to an outer normal coordinate which is derived from the universal coordinate work of Clauser [28]. The outer coordinate has the form

$$N_o = (1 - b)\tanh^{1/\alpha}\{\, d[(1 - b)\,\eta\ /\ \tilde{\delta}^*]^\alpha\} + b \tag{18}$$

where b is a slip velocity at $\eta = 0$, allowing for the presence of the inner layer.

The composite is given by

$$N = N_i + N_o - N_{i/o}$$

where $N_{i/o}$ is the outer limit of the inner coordinate. This is matched to the inner limit of the outer coordinate, giving the result

$$N_{i/o} = b = \frac{\pi}{2a}\sqrt{\frac{C_{f_e}}{2}} \tag{19}$$

The composite coordinate maps the semi-infinite line $0 \leq \eta < \infty$ to $0 \leq N \leq 1$.

Carter et al. [25] test the composite coordinate in this form, using a noniterative finite-difference scheme, with satisfactory results. The coordinate in this form applied to the present scheme has several problems. These problems are due mainly to the asymptotic form of the outer coordinate. As η approaches infinity, N approaches unity and the metric coefficient

$$\frac{\partial N}{\partial \eta} \rightarrow 0 \quad .$$

This metric appears in the denominator of the coefficients resulting from the spline discretization (See section 2.7). Even when the coordinate N is taken to be slightly less than unity, as discussed by Edwards et al. [29], the division by small metrics remains a problem. To correct this problem, the outer coordinate, Eq. (18) as given by Carter et al. [25], is modified so that η does not asymptotically approach infinity as N approaches unity.

After attempting a linear and quadratic distribution for N_o, a coordinate based on the inverse hyperbolic sine was adopted. This coordinate, while maintaining close similarity with the hyperbolic tangent, does not approach an asymptote and so does not create problems with the metric coefficients.

The inner coordinate is kept as before,

$$N_i = a_1 \tan^{-1}(a_2\eta)$$

where $$a_1 = \sqrt{C_{f_e}/2} \quad /a \tag{20}$$

$$a_2 = a\sqrt{R_e\, C_{f_e}\, \xi}$$

The new outer coordinate is chosen to be

$$N_o = (1 - b)\, a_3 \sinh^{-1}(a_4\eta) + b \tag{21}$$

and the following conditions are enforced:

1) $N_o = b$ at $\eta = 0$,

2) $N_o = 1$ at $\eta = \eta_\infty$,

3) $\left.\frac{\partial N}{\partial \eta}\right|_o = (1 - b)\, d^{1/\alpha}/\hat{\delta}^*$

Condition (3) is prescribed by forcing the slope of the new outer coordinate to match the slope of the original outer coordinate at $\eta = 0$.

Condition (1) is automatically satisfied by the form chosen for N_o. Condition (2) yields the result

$$\eta_\infty\, a_4 = \sinh(1/a_3) \tag{22}$$

and condition (3) yields

$$a_3 a_4 = (1 - b)\, d^{1/\alpha}/\hat{\delta}^* \tag{23}$$

These equations result in a transcendental relation for a_3, which is solved using the Newton-Raphson technique, after which a_4 may be found from Eq. (22) or (23). The modified composite coordinate is then given by

$$N = a_1 \tan^{-1}(a_2\eta) + (1 - b)\, a_3 \sinh^{-1}(a_4\eta) \tag{24}$$

where $$b = \frac{\pi}{2}\, a_1$$

$$a_1 = \sqrt{\frac{C_{f_e}}{2}} \; / a$$

$$a_2 = a \sqrt{R_e \, C_{f_e}} \; \xi$$

a_3, a_4 = determined by Newton-Raphson iteration

$a = 0.09$

$d = 0.45$

$\alpha = 1.25$

With the composite distribution specified, the corresponding η distribution can be determined by again using Newton-Raphson iteration. The first and second order metrics, to be used later, are given by

$$\frac{\partial N}{\partial \eta} \quad \frac{a_1 a_2}{1 + (a_2 \eta)^2} + \frac{(1 - b)\, a_3 a_4}{\sqrt{1 + (a_4 \eta)^2}} \tag{25a}$$

$$\frac{\partial^2 N}{\partial \eta^2} = - \frac{2 a_1 a_2^3 \eta}{[1 + (a_2 \eta)^2]^2} - \frac{(1 - b)\, a_3 a_4^3 \eta}{[1 + (a_4 \eta)^2]^{3/2}} \tag{25b}$$

With the adaptive composite coordinate fully defined, the x-momentum equation in (ξ,η) coordinates can be transformed to (ξ,N) coordinates. The derivatives transform according to

$$\left(\frac{\partial}{\partial \eta}\right)_\xi = N_\eta \left(\frac{\partial}{\partial N}\right)_\xi \tag{26a}$$

$$\left(\frac{\partial}{\partial \xi}\right)_\eta = N_\xi \left(\frac{\partial}{\partial N}\right)_\xi + \left(\frac{\partial}{\partial \xi}\right)_N \tag{26b}$$

and

$$\left(\frac{\partial^2}{\partial \eta^2}\right)_\xi = N_{\eta\eta} \left(\frac{\partial}{\partial N}\right)_\xi + N_\eta^2 \left(\frac{\partial^2}{\partial N^2}\right)_\xi \tag{26c}$$

The transformed x-momentum equation is put into first order form, yielding

$$f_\eta = u \tag{27a}$$

$$u_\eta = \tau \tag{27b}$$

$$(b\tau)_\eta + f\tau + \beta(1 - u^2) = 2\xi(\Theta u u_\xi - \tau f_\xi). \tag{27c}$$

Transforming to the (ξ, N) plane, Eqs. (27) become

$$N_\eta f_N = u \tag{28a}$$

$$N_\eta u_N = \tau \tag{28b}$$

$$N_\eta (b\tau)_N + f\tau + \beta(1 - u^2) = 2\xi[\Theta u(N_\xi u_N + u_\xi) - \tau(N_\xi f_N + f_\xi)]. \tag{28c}$$

Substituting from Eqs. (28a) and (28b), Eq. (28c) is written as

$$N_\eta (b\tau)_N + f\tau + \beta(1 - u^2) = 2\xi[\Theta u(\frac{N_\xi}{N_\eta}\tau + u_\xi) - \tau(\frac{N_\xi}{N_\eta} u + f_\xi)].$$

The term $\Theta \frac{N_\xi}{N_\eta} u\tau$ never appears, regardless of the value of Θ, since it cancels with the term of opposite sign when Θ is set to unity, and when the flow is separated, $\Theta = 0$. Thus the above equation may be simplified to

$$N_\eta (b\tau)_N + f\tau + \beta(1 - u^2) = 2\xi[\Theta u u_\xi - \tau f_\xi + (\Theta - 1)\, ru\tau] \tag{29}$$

where

$$r = N_\xi / N_\eta$$

To avoid taking the derivative of the eddy viscosity ratio b, a new variable is introduced as

$$\tau = b^* G$$

where

$$b^* = b^{-1} = \mu_{t_e} / \mu_t.$$

Then, the final form of the governing equations is

$$N_\eta f_n = u \tag{30a}$$

$$N_\eta u_\eta = b^* G \tag{30b}$$

$$N_\eta G_N + b^* fG + \beta(1 - u^2) + (1 - \theta)2\xi r b^* uG = \xi[\theta(u^2)_\xi - 2b^* G f_\xi] \tag{30c}$$

Here, three important items can be noted:

(1) The governing equations in (ξ,N) coordinates can easily be reduced to (ξ,η) coordinates by setting

$$N_\eta = 1$$
$$N_\xi = 0$$

(2) The composite coordinate must be simplified for laminar flow. The inner coordinate N_i and the slip velocity are set to zero, since these allow for the presence of the turbulent wall layer. For flows transitioning from laminar to turbulent, the inner coordinate should be "switched on" at the beginning of transition to allow the coordinate to grow with the changing boundary layer.

(3) The term $(1 - \theta)\, 2\xi r b^* uG$ does not appear unless (ξ,N) coordinates are used and the flow separates. Since the adaptive composite coordinate is only intended for use with attached boundary layers, this term never actually contributes in the problem considered here. It is included for completeness, however, in the event that an adaptive coordinate is developed for both separated and attached flow. This would involve modifying the inner coordinate N_i to account for regions of backflow (see Swafford [30] and Whitfield [31]).

2.3 Mechul Function Method

The final form of the governing equations in first-order form is given in the previous section by Eqs. (30), with the boundary conditions

$$f(\xi,0) = u(\xi,0) = 0 \tag{31a}$$

$$u(\xi,\eta) = 1 \text{ as } \eta \to \eta_\infty \tag{31b}$$

where η_∞ is chosen as a suitably large constant. In this system, there are three first-order equations, three variables f, u, and G, and three boundary conditions. If β is given, as in a direct case, then the system of equations is complete.

For an inverse solution, however, an additional boundary condition is added, which consists of specifying wall shear, displacement thickness, or another quantity. The streamwise pressure gradient parameter is unknown, and the system is overdetermined.

To close the system, Cebeci and Keller [22] introduce an additional differential equation. The form of this auxiliary equation is determined by letting

$$\beta(\xi) = \beta(\xi,\eta)$$

and requiring

$$\frac{\partial \beta}{\partial \eta} = 0 \tag{32}$$

This provides the additional relation needed to close the system of equations for an inverse solution.

While this formulation of the mechul function method was applied in Reference 22, Kaufman and Hoffman [23] discovered that, when applying a spline finite-difference scheme (particularly spline $S^1(4,0)$, [21]) to the mechul function method, Eq. (32) resulted in a singular matrix. This singularity was due totally to the form of the spline relations. To prevent this problem, the auxiliary equation is changed to

$$\frac{\partial^2 \beta}{\partial \eta^2} = 0 \tag{33}$$

with Eq. (32) enforced through the boundary conditions.

Transforming Eq. (33) with Eq. (26c), the resulting system of equations is given by

$$N_\eta f_N = u \tag{34a}$$

$$N_\eta u_N = b^* G \tag{34b}$$

$$N_\eta G_N + b^* fG + \beta(1 - u^2) + (1 - \theta)\, \bar{r}\, b^* uG = \xi[\theta(u^2)_\xi - 2b^* G f_\xi] \tag{34c}$$

$$\beta_{NN} = 0 \tag{34d}$$

with boundary conditions given by Eqs. (31), (33), and the specified inverse condition, to be discussed in the following section. These relations close the system so that it can be solved.

2.4 Inverse Formulations

The system of equations, including the momentum equation in first order form and the auxiliary equation obtained through the mechul function method, is given by Eqs. (34). Three of the necessary boundary conditions are given by

$$f(\xi, 0) = 0 \tag{35a}$$

$$u(\xi, 0) = 0 \tag{35b}$$

$$u(\xi, \eta_\infty) = 1 \tag{35c}$$

with Eq. (32) to be applied either at the wall or far field, as needed. For an inverse solution, an additional equation is needed which specifies the wall shear, displacement thickness or similar quantity. This section discusses four possible boundary conditions which are

considered in this study. Two conditions specify a function of the wall shear, while the remaining two specify the displacement thickness.

2.4.1 Transformed Wall Shear Method

The inverse solutions of Keller and Cebeci [8], Cebeci and Keller [22], where the mechul function is introduced, Horton [10], and Kaufman and Hoffman [23] specify the self-similar form of the wall shear, given by f_w'' (where primes denote differentiation with respect to η). This is by far the simplest of the inverse boundary conditions when the equations are cast in similarity form. The boundary condition takes the form

$$f_w'' = S(\xi)$$

In first order form, in terms of the variable G, this becomes

$$b_w^* G_w = S(\xi) \tag{36}$$

This condition with Eqs. (32) and (35) closes the system of equations in differential equation form. When the equations are discretized, numerical boundary conditions are needed to complete the resulting block tridiagonal system. These additional conditions are discussed in Section 2.7.

2.4.2 Skin Friction Coefficient Method

Although Eq. (36) is the simplest condition to apply, it is not the most useful. From a physical standpoint, specification of a skin friction coefficient is more plausible. Here, a skin friction coefficient with one of two possible definitions is specified:

(1) Skin friction coefficient based on the reference velocity or the velocity in the freestream,

$$C_{f_\infty} = \frac{\tau_w^*}{\frac{1}{2}\rho^*(u_\infty^*)^2},$$

(2) Skin friction coefficient based on the boundary-layer edge velocity,

$$C_{f_e} = \frac{\tau_w^*}{\frac{1}{2}\rho^*(u_e^*)^2} .$$

Transforming these definitions yields

$$C_{f_\infty}\sqrt{Re} = \frac{2u_e^2}{\sqrt{2\xi}} f_w'' \tag{37a}$$

$$C_{f_e}\sqrt{Re} = \frac{2}{\sqrt{2\xi}} f_w'' . \tag{37b}$$

When a skin friction coefficient is specified, however, f_w'' no longer remains constant. To obtain a boundary condition, f_w'' is specified as a function of C_{f_e} or C_{f_∞}, u_e and ξ, so that

$$f_w'' = F(C_f, u_e, \xi)$$

where, for C_{f_e}

$$F = \frac{1}{2}\sqrt{2\xi}\,(C_{f_e}\sqrt{Re}\quad), \tag{38a}$$

and for C_{f_∞}

$$F = \frac{1}{2}\frac{\sqrt{2\xi}}{u_e^2}(C_{f_\infty}\sqrt{Re}). \tag{38b}$$

The boundary condition takes the form

$$b_w^* G_w - F = 0. \tag{39}$$

This boundary condition also closes the system of equations in differential equation form, and as discussed in the previous section, additional conditions are required to complete the system in discretized form.

2.4.3 Hybrid Method

The hybrid formulation was developed as a possible method for specifying the displacement thickness while still making use of the shear boundary condition at the wall. This hybrid condition is implemented through the integral momentum equation, in similarity form, as a wall boundary condition.

The x-momentum equation (12), with b set to unity for laminar flow only, is integrated across the boundary layer, yielding

$$f_w'' = (\beta + 1)\,\hat{\Theta} + \beta\hat{\delta}^* + 2\,\xi\,\frac{d\hat{\theta}}{d\xi} \tag{40}$$

where

$$\hat{\Theta} = \int_0^{\eta_\infty} f'(1 - f')\,d\eta \tag{41a}$$

$$\hat{\delta}^* = \int_0^{\eta_\infty} (1 - f')\,d\eta \tag{41b}$$

and

$$H = \hat{\delta}^*/\hat{\Theta} \tag{41c}$$

The similarity form of the momentum thickness, $\hat{\Theta}$ is eliminated from Eq. (40) in favor of the shape factor H, which tends to vary at a slower rate. The resulting equation is given by

$$f_w'' = \hat{\delta}^* \left(\frac{\beta + 1}{H} + \beta\right) + 2\xi\,\frac{d}{d\xi}\left(\hat{\delta}^*/H\right) \tag{42}$$

Eq. (42) permits the specification of $\hat{\delta}^*$ while maintaining the

inverse shear condition at the wall. This condition introduces β dependence as well as the shape factor, H, which varies with ξ. To handle this problem, the shape factor is assumed to be a function of β alone. This is strictly true for self-similar solutions only, but is a better approximation than simply neglecting the dependence on the shape factor in Eq. (42).

2.4.4 Displacement Thickness Method

A more direct method of specifying the displacement thickness, in contrast to the hybrid method, involves obtaining a boundary condition containing $\hat{\delta}^*$ to be enforced at the far field. The standard definition of displacement thickness is given as

$$\delta^* = \int_0^\infty \left(1 - \frac{u}{u_e} \right) dy. \tag{43}$$

Stretching the normal coordinate and transforming to similarity variables, Eq. (43) becomes

$$\delta^* \sqrt{Re} = \frac{\sqrt{2\xi}}{u_e} \int_0^{\eta_\infty} (1 - f') \, d\eta \tag{44}$$

The transformed displacement thickness has been previously defined to be

$$\hat{\delta}^* = \int_0^{\eta_\infty} (1 - f') \, d\eta \tag{41b}$$

Integrating across the boundary layer, Eq. (41b) becomes

$$\left.\begin{aligned} &\hat{\delta}^* = \eta - f \\ \text{or} \quad &\\ &f = \eta - \hat{\delta}^* \end{aligned}\right\} \quad \text{as } \eta \to \eta_\infty \tag{45}$$

If the untransformed displacement thickness is specified, the substitution from Eq. (44) yields

$$f = \eta - \frac{u_e}{\sqrt{2\xi}} \left(\delta^* \sqrt{Re}\right) \tag{46}$$

This condition, as opposed to the conditions obtained in the previous three subsections, is applied at the far field, where $\eta = \eta_\infty$.

2.5 Direct Formulation

The system of equations for obtaining an inverse solution of the boundary-layer equations, as discussed in this study, Eqs. (34), can also be used to solve for a direct boundary-layer solution. For a standard direct boundary-layer solution, the streamwise pressure gradient is given, either directly or indirectly by specifying u_e or C_p, and β is treated as a fixed parameter at each streamwise station.

For the system of equations considered here, β is considered as a variable to be obtained during the solution process. Thus, to solve a direct case using this system, an additional boundary condition must be specified which sets β at each streamwise station. The boundary conditions to be set are then

$$f(\xi, 0) = 0 \tag{47a}$$

$$u(\xi, 0) = 0 \tag{47b}$$

$$u(\xi, \eta_\infty) = 1 \tag{47c}$$

$$\beta(\xi, \eta_\infty) = \beta(\xi) \tag{47d}$$

Here, Eq. (47d) takes the place of the inverse boundary condition discussed in the previous section.

A direct solution is typically obtained by specifying the edge velocity or the pressure coefficient, C_p, given by

$$C_p = 1 - \frac{(u_e^*)^2}{(u_\infty^*)^2} = 1 - u_e^2$$

Given C_p, the normalized edge velocity is easily determined from the above relation. To obtain a β distribution, Lagrange polynomials are used to form backward differences (See Appendix A). For laminar flows, the ξ and β distributions can be determined prior to beginning the solution iteration process. For turbulent flows, however, ξ and β must be updated after each iteration because of the presence of μ_{t_e} in the integral for ξ. Thus, these quantities can only be computed as the solution proceeds downstream.

2.6 Eddy Viscosity Model

An algebraic, two-piece eddy viscosity is chosen as the turbulence model for the present study. This type of model is based on the original assumption of Boussinesq that the apparent turbulent shearing stresses might be related to the rate of mean strain through a scalar turbulent viscosity. Algebraic models, while simple in form and application, have been shown to yield satisfactory results for most boundary-layer problems [32]. The eddy viscosity is also compatible with the modified Levy-Lees transformation. The eddy viscosity is calculated in kinematic form, so that the effective turbulent viscosity is given by

$$\mu_t = \mu_m + \rho\varepsilon$$

where μ_m = dimensionless molecular viscosity

ε = dimensionless kinematic eddy viscosity

The eddy viscosity model used here was developed by Baldwin and Lomax [24]. This model, while using the standard Prandtl-van Driest formulation of Cebeci and Smith [33] for the inner region, replaces the usual Clauser formulation with an outer equation which does not require the determination of the displacement thickness. Baldwin and Lomax maintain that this is advantageous for computation of separated flows.

The two-piece model is given by

$$\varepsilon_i = \begin{cases} \varepsilon_i, & y \le y_c \\ \varepsilon_o, & y_c \le y \end{cases}$$

with y_c as the crossover value of y where ε_i is matched to ε_o. For the inner region, the Prandtl-van Driest formulation is

$$\varepsilon_i = \ell^2 |\omega| \tag{48a}$$

with the Prandtl mixing length

$$\ell = ky\,[1 - \exp(-y^+/A^+)], \tag{48b}$$

$$y^+ = \rho_w u_\tau y/\mu_w \tag{48c}$$

and the magnitude of the vorticity is

$$|\omega| = \left[\left(\frac{\partial u}{\partial y} - \frac{\partial v}{\partial x}\right)^2 + \left(\frac{\partial v}{\partial z} - \frac{\partial w}{\partial y}\right)^2 + \left(\frac{\partial w}{\partial x} - \frac{\partial u}{\partial z}\right)^2\right]^{1/2} . \tag{48d}$$

For two-dimensional boundary-layer theory, Eq. (48d) reduces to

$$|\omega| = \left|\frac{\partial u}{\partial y}\right| . \tag{48e}$$

The necessary constants are

k = 0.4 von Karman's constant

A^+ = 26 van Driest damping factor.

For the outer region, Baldwin and Lomax [24] replace the Clauser formulation

$$\varepsilon_o = \alpha\, u_c\, \delta^*,$$

with the following expression:

$$\varepsilon_o = K\, C_{CP}\, F_{WAKE}\, F_{KLEB}\,(y), \tag{49}$$

where

$$F_{WAKE} = \left\{ \begin{array}{l} Y_{MAX} \ F_{MAX} \\ C_{WK} \ Y_{MAX} \ u_{DIF}^2/F_{MAX} \end{array} \right\} \text{ the smaller.} \qquad (50a)$$

In Eqs. (50), F_{MAX} is obtained from

$$F(y) = y|\omega|[1 - \exp(-y^+/A^+)] \qquad (51a)$$

where y_{MAX} is the y value at the maximum F(y). The velocity difference u_{DIF} is defined as

$$u_{DIF} = (\sqrt{u^2 + v^2 + w^2})_{MAX} - (\sqrt{u^2 + v^2 + w^2})_{MIN} .$$

In two dimensions, with the second term taken as zero, this reduces to

$$u_{DIF} = (\sqrt{u^2 + v^2})_{MAX} . \qquad (51b)$$

Also in Eq. (49), the Klebanoff intermittency factor is given by

$$F_{KLEB}(y) = [1 + 5.5 (\frac{C_{KLEB}\, y}{y_{MAX}})^6]^{-1} . \qquad (51c)$$

The required constants are

$K = 0.0168$

$C_{CP} = 1.6$

$C_{KLEB} = 0.3$

$C_{WK} = 0.25.$

For simplicity in this study, the Klebanoff intermittency factor is taken to be unity across the layer. The above equations then yield an algebraic eddy viscosity with a constant value, ε_o, in the outer region. This value is taken as ε_{ref}.

To apply this turbulence model to the present problem, Eqs. (48)-(51) must be nondimensionalized and transformed to the modified Levy-Lees variables. See Appendix B for a complete list of all transformed quantities related to the turbulence model.

2.7 Discretization

With the analytical form of the governing equations, boundary conditions, and turbulence model fully defined, the discrete form of the equations is next considered. The equations are discretized using fourth-order accurate splines to approximate the normal derivatives and backward differences to approximate streamwise derivatives. This yields a fully implicit scheme, which is desirable for stability and accuracy.

2.7.1 Backward Differences

The system of equations, Eqs. (34), is first written in index form at a nodal point as

$$N_{\eta ij}\ f'_{ij} = u_{ij} \tag{52a}$$

$$N_{\eta ij}\ u'_{ij} = b^{*}_{ij}\ G_{ij} \tag{52b}$$

$$N_{\eta ij}\ G'_{ij} + b^{*}_{ij}\ f_{ij}\ G_{ij} + \beta_{ij}(1 - u^{2}_{ij}) + (1 - \Theta_{ij})\ \bar{r}_{ij}\ b^{*}_{ij}\ u_{ij}\ G_{ij} = \varepsilon_{i}\ [\Theta_{ij}\ (u^{2}_{ij})_{\xi} - 2\ b^{*}_{ij}\ G_{ij}\ f_{\xi ij}] \tag{52c}$$

$$\beta''_{ij} = 0 \tag{52d}$$

where primes refer to derivatives with respect to N, and i and j are the indices referring to streamwise and normal location of the node, respectively, in the computational domain. The final discretized system of equations will be solved over a domain where $1 \leq i \leq M+1$ and $1 \leq j \leq K+1$.

The ξ-derivatives occurring in Eq. (52c) are discretized using variable stepsize backward (upwind) differences derived from Lagrange polynomials. In general, the backward difference expression has the form

$$\left(\frac{\partial g}{\partial \xi_i}\right) = a g_i + b g_{i-1} + c\, g_{i-2} \tag{53}$$

where $a = -(b + c)$

$$b = A_1' / B_1$$

$$c = A_2' / B_2$$

and

1) for 3-point backward differences:

$$A_1' = \xi_i - \xi_{i-2}, \qquad B_1 = (\xi_{i-1} - \xi_i)(\xi_{i-1} - \xi_{i-2}),$$

$$A_2' = \xi_i - \xi_{i-1}, \qquad B_2 = (\xi_{i-2} - \xi_i)(\xi_{i-2} - \xi_{i-1}),$$

2) for 2-point backward differences:

$$A_1' = 1, \qquad B_1 = \xi_{i-1} - \xi_i ,$$

$$c = 0.$$

Applying Eq. (53) to the ξ-derivatives, Eq. (52c) becomes

$$N_{\eta ij} G_{ij}' + b_{ij}^{*} f_{ij} G_{ij} + \beta_{ij} (1 - u_{ij}^2) + (1 - \Theta_{ij}) \bar{r}_{ij} b_{ij}^{*} u_{ij} G_{ij} = \xi_i [\Theta_{ij} (a u_i^2 + b u_{i-1}^2 + c u_{i-2}^2)_j - 2 b_{ij}^{*} G_{ij} (a f_i + b f_{i-1} + c f_{i-2})_j]. \tag{54}$$

With all ξ-derivatives eliminated in the momentum equation, the system is ready to be discretized in the normal direction.

2.7.2 Splines

The normal derivatives in Eqs. (52a), (52b), (52d) and (54) are approximated using two fourth order spline formulas, $S^1(4,0)$ and $S^2(4,0)$, derived by Rubin and Khosla [21]. To begin, the following spline derivative approximations are introduced:

$$\left.\begin{aligned} \ell^f &= f_N \\ \ell^u &= u_N \\ \ell^G &= G_N \\ \ell^\beta &= \beta_N \\ L^\beta &= \beta_{NN} \end{aligned}\right\} \quad . \tag{55}$$

Then Eqs. (52a), (52b), (54) and (52d) are written as

$$N'_{ij}\, \ell^f_{ij} = u_{ij} \tag{56a}$$

$$N'_{ij}\, \ell^u_{ij} = b^*_{ij}\, G_{ij} \tag{56b}$$

$$\begin{aligned} N'_{ij}\, \ell^G_{ij} &= \beta_{ij}(u^2_{ij} - 1) - b^*_{ij}\, f_{ij}\, G_{ij} + (\Theta_{ij} - 1)\bar{r}_{ij}\, b^*_{ij}\, u_{ij}\, G_{ij} \\ &+ \xi_i\, [\Theta_{ij}\, (au^2_i + bu^2_{i-1} + cu^2_{i-2})_j - 2\, b^*_{ij}\, G_{ij}\, (af_i + bf_{i-1} + cf_{i-2})_j] \end{aligned} \tag{56c}$$

$$L^\beta_{ij} = 0 \tag{56d}$$

where primes now denote differentiation with respect to η. Collecting terms, Eq. (56c) becomes

$$\begin{aligned} N'_{ij}\, \ell^G_{ij} &= \Theta_{ij}\, C_{1_{ij}}\, u^2_{ij} + C_{2_{ij}}\, b^*_{ij}\, f_{ij}\, G_{ij} + \beta_{ij}\, (u^2_{ij} - 1) \\ &+ (\Theta_{ij} - 1)\bar{r}_{ij}\, b^*_{ij}\, u_{ij}\, G_{ij} + C_{3_{ij}}\, b^*_{ij}\, G_{ij} + \Theta_{ij}\, C_{4_{ij}} \end{aligned} \tag{57}$$

where

$$C_{1_{ij}} = a\xi_i$$

$$C_{2_{ij}} = -\,(2a\xi_i + 1)$$

$$C_{3_{ij}} = -2\xi_i(bf_{i-1} + cf_{i-2})_j$$

$$C_{4_{ij}} = \xi_i(bu^2_{i-1} + cu^2_{i-2})_j.$$

Spline S (4,0), defined by,

$$\ell^g_{j+1} + (1 + \sigma)^2\, \ell^g_j + \sigma^2\, \ell^g_{j-1}$$

$$= \frac{2}{1 + \sigma}\frac{1}{h_j}\left[\frac{1 + 2\sigma}{\sigma}\, g_{j+1} + \frac{\sigma - 1}{\sigma}\,(1 + \sigma)^3 g_j - \sigma^2(2 + \sigma)g_{j-1}\right] \tag{58}$$

with

$$h_j = \Delta N_j$$

and

$$\sigma = \sigma_j = h_{j+1}/h_j$$

is introduced to eliminate the spline derivative approximations ℓ^f, ℓ^u, and ℓ^G from Eqs. (56a), (56b) and (57). Considering each of these equations in turn yields (with i subscript understood)

$$\sigma_2\left(\frac{u}{N'}\right)_{j-1} + \sigma_1\left(\frac{u}{N'}\right)_j + \left(\frac{u}{N'}\right)_{j+1} = \sigma_3\, f_{j-1} + \sigma_4 f_j + \sigma_5\, f_{j+1}, \tag{59a}$$

$$\sigma_2\left(\frac{b^*G}{N'}\right)_{j-1} + \sigma_1\left(\frac{b^*G}{N'}\right)_j + \left(\frac{b^*G}{N'}\right)_{j+1} = \sigma_3 u_{j-1} + \sigma_4 u_j + \sigma_5\, u_{j+1}, \tag{59b}$$

and, defining the right-hand-side of Eq. (57) as RHS_{ij}.

$$N'_{ij}\, \ell^G_{ij} = RHS_{ij},$$

the final first-order spline relation is,

$$\sigma_2\left(\frac{RHS}{N'}\right)_{j-1} + \sigma_1\left(\frac{RHS}{N'}\right)_j + \left(\frac{RHS}{N'}\right)_{j+1} = \sigma_3\, G_{j-1} + \sigma_4\, G_j + \sigma_5\, G_{j+1}. \tag{59c}$$

See Appendix C for a list of all spline coefficients.

Spline $S^2(4,0)$, defined by,

$$\frac{\sigma^2 + \sigma - 1}{12\sigma} L^g_{j+1} + \frac{\sigma^3 + 4\sigma^2 + 4\sigma + 1}{12\sigma} L^g_j + \frac{1 + \sigma - \sigma^2}{12} L^g_{j-1}$$
$$= \frac{1}{h_j^2} \left[\frac{1}{\sigma} g_{j+1} - \frac{1 + \sigma}{\sigma} g_j + g_{j-1}\right] \tag{60}$$

is introduced to eliminate the spline derivative approximation L^β from Eq. (56d), yielding

$$\beta_{j-1} + \sigma_7 \beta_j + \sigma_6 \beta_{j+1} = 0. \tag{61}$$

Eqs. (59) and (60) form a nonlinear 4 X 4 block tridiagonal system for each streamwise station, i. The boundary conditions to complete the system are discussed in the following section.

2.8 Boundary Conditions

The system of equations obtained above, Eqs. (59) and (60), apply to the interior points of the 4 X 4 block tridiagonal system. To close the system, four boundary conditions must be supplied for both the wall and far field. When an insufficient number of physical conditions is provided, numerical conditions obtained from two-point spline relations are added to close the system. In the following subsections, the boundary conditions for the shear/hybrid methods, displacement thickness method and direct method are discussed.

2.8.1 Shear and Hybrid Method Conditions

The follcwing Dirichlet boundary conditions have been specified from physical constraints (with i subscript understood):

$$f_i = 0 \tag{47a}$$

$$u_i = 0 \tag{47b}$$

$$u_{K+1} = 1 . \tag{47c}$$

For the transformed wall shear case, the condition given by Eq. (36)

$$b_1^* G_1 - S = 0$$

is also specified. When a $(C_{f_e} \sqrt{Re})$ distribution is specified, Eq. (36) is replaced by Eq. (39), so that (with i subscripts understood),

$$b_i^* G_i - \frac{1}{2} \sqrt{2\xi} \, (C_{f_e} \sqrt{Re}) = 0 \quad .$$

To specify $(C_{f_\infty} \sqrt{Re})$, Eq. (39) is again used, but with F given by Eq. (38b), yielding

$$b_1^* G_1 - \frac{1}{2} \frac{\sqrt{2\xi}}{u_e^2} (C_{f_\infty} \sqrt{Re}) = 0 \quad .$$

Finally, for the hybrid method, Eq. (36) is replaced by Eq. (42), so that

$$b_1^* G_1 - \hat{\delta}^* \left(\frac{\beta_1 + 1}{H} + \beta_1\right) + 2\xi \frac{d}{d\xi} \left(\frac{\hat{\delta}^*}{H}\right) = 0.$$

For any of the shear conditions together with the derivative condition on β, Eq. (32),

$$\beta_N (\xi, N) = 0$$

specified, the system is complete at the wall. To implement Eq. (32), a two-point spline relation, given by Rubin and Khosla [21], is used.

The fourth-order accurate two-point spline relation to be used throughout this investigation is given by

$$g_2 - g_1 - \frac{h_2}{2} (\ell_2^g + \ell_1^g) + \frac{h_2^2}{12} (L_2^g - L_1^g) = 0. \qquad (62)$$

When $g = \beta$, Eq. (62) becomes

$$\beta_2 - \beta_1 - \frac{h_2}{2}(\beta_2' + \beta_1') + \frac{h_2^2}{12}(\beta_2'' - \beta_1'') = 0.$$

Upon substitution of Eqs. (32) and (34d), the preceding relation reduces to

$$\beta_2 - \beta_1 = 0. \tag{63}$$

With regard to the far field conditions, the spline relation Eq. (62) must be used three times since only one physical constraint, Eq. (47c) exists. The numerical conditions used to close the system are

$$f_{K+1} - f_K - \frac{h_{K+1}}{2}(f_{K+1}' + f_K') + \frac{h_{K+1}^2}{12}(f_{K+1}'' - f_K'') = 0 \tag{64a}$$

$$u_{K+1} - u_K - \frac{h_{K+1}}{2}(u_{K+1}' + u_K') + \frac{h_{K+1}^2}{12}(u_{K+1}'' - u_K'') = 0 \tag{64b}$$

$$G_{K+1} - G_k - \frac{h_{K+1}}{2}(G_{K+1}' + G_K') + \frac{h_{K+1}^2}{12}(G_{K+1}'' - G_K'') = 0 \tag{64c}$$

where primes denote differentiation with respect to N. Since G and its normal derivatives approach zero exponentially rapidly near the boundary-layer edge, the difference $(G_{K+1}'' - G_K'')$ in Eq. (64c) is expected to be small and hence is neglected, leaving

$$G_{K+1} - G_K - \frac{h_{K+1}}{2}(G_{K+1}' + G_K') = 0. \tag{64d}$$

The first-order derivatives can be eliminated by substituting from Eqs. (28). To obtain the second derivative of f with respect to N, note that, from Eqs. (27),

$$f_{\eta\eta} \equiv \tau \equiv b^* G$$

Transforming to (ξ,N) coordinates with Eq. (26c) and substituting from Eq. (27a) yields

$$f'' = \frac{1}{N_\eta^2}\left(b^* G - \frac{N_{\eta\eta}}{N_\eta} u\right) \tag{65}$$

Similarly, for the second derivative of u with respect to N, we begin with the following identity in (ξ, η) variables:

$$u_{\eta\eta} \equiv \tau_\eta \equiv (b^* G)_\eta$$

Normally, this relation would have to be expanded using the product rule, but since Eq. (64b) is applied at the far field, b^* equals unity because the eddy viscosity is constant in the wake region of the turbulent boundary layer. The relation for u then becomes

$$u'' = \frac{1}{N_\eta^2}\left(N_\eta G' - \frac{N_{\eta\eta}}{N_\eta} G\right)$$

Here, and in Eq. (64d), the momentum equation is used to eliminate G'.

Upon making all necessary substitutions, Eqs. (64) become

$$f_{K+1} - f_K - \rho_{K+1} u_{K+1} + \rho_K u_K + \frac{h_{K+1}^2}{12}\left(\frac{G_{K+1}}{N'^2_{K+1}} - \frac{G_K}{N'^2_K}\right) = 0 \tag{66a}$$

$$u_{K+1} - u_K - \frac{h_{K+1}}{2}\left(\frac{G_{K+1}}{N'_{K+1}} + \frac{G_K}{N'_K}\right) + \frac{h_{K+1}^2}{12}\left[\frac{1}{N'^2_{K+1}}\left(\mathrm{RHS} - \frac{N''}{N'} G\right)_{K+1}\right. \tag{66b}$$

$$\left. - \frac{1}{N'^2_K}\left(\mathrm{RHS} - \frac{N''}{N'} G\right)_K\right] = 0$$

$$G_{K+1} - G_K - \frac{h_{K+1}}{2}\left(\frac{RHS_{K+1}}{N'_{K+1}} + \frac{RHS_K}{N'_K}\right) = 0 \qquad (66c)$$

where,

$$\rho_K = \frac{1}{N'_K}\left(\frac{h^2_{K+1}}{12}\frac{N''_K}{N'^2_K} - \frac{h_{K+1}}{2}\right)$$

$$\rho_{K+1} = \frac{1}{N'_{K+1}}\left(\frac{h^2_{K+1}}{12}\frac{N''_{K+1}}{N'^2_{K+1}} + \frac{h_{K+1}}{2}\right) .$$

Summarizing, the wall boundary conditions used are

$$f_1 = 0 \qquad (67a)$$

$$u_1 = 0 \qquad (67b)$$

$$\beta_2 - \beta_1 = 0 \qquad (67c)$$

and, for f''_w specified,

$$b^*_1 G_1 - S = 0 \qquad (67d)$$

or, for C_{f_e} specified,

$$b^*_1 G_1 - \frac{1}{2}\sqrt{2\xi}\,(C_{f_e}\sqrt{Re}) \qquad (67e)$$

or, for C_{f_∞} specified,

$$b^*_1 G_1 - \frac{1}{2}\frac{\sqrt{2\xi}}{u_e^2}\,(C_{f_\infty}\sqrt{Re}) . \qquad (67f)$$

The far field boundary conditions are

$$u_{K+1} = 1 \qquad (67g)$$

$$f_{K+1} - f_K - \rho_{K+1} u_{K+1} + \rho_K u_K + \frac{h_{K+1}^2}{12} \left(\frac{G_{K+1}}{N'^2_{K+1}} - \frac{G_K}{N'^2_K} \right) = 0 \tag{67h}$$

$$u_{K+1} - u_K - \frac{h_{K+1}}{2} \left(\frac{G_{K+1}}{N'_{K+1}} + \frac{G_K}{N'_K} \right) + \frac{h_{K+1}^2}{12} \left[\frac{1}{N'^2_{K+1}} \left(RHS - \frac{N''}{N'} G \right)_{K+1} \right.$$
$$\left. - \frac{1}{N'^2_K} \left(RHS - \frac{N''}{N'} G \right)_K \right] = 0 \tag{67i}$$

$$G_{K+1} - G_K - \frac{h_{K+1}}{2} \left(\frac{RHS_{K+1}}{N'_{K+1}} + \frac{RHS_K}{N'_K} \right) = 0 \tag{67j}$$

These are the conditions used when a form of the wall shear is specified, or the hybrid method is used with the displacement thickness specified. For the displacement thickness method or a direct solution, other modifications must be made.

2.8.2 Displacement Thickness Method Conditions

When the displacement thickness method is used, the boundary conditions described in the previous subsection must be altered, both at the wall and far field. The inverse condition for the displacement thickness method is implemented at the boundary-layer edge. Thus, Eq. (36) must be replaced by a two-point spline relation and one spline condition at the wall must be discarded to allow for the condition on δ^*.

The two-point spline relation chosen for the wall condition is

$$f_2 - f_1 - \frac{h_2}{2} (f'_2 + f'_1) + \frac{h_2^2}{12} (f''_2 - f''_1) = 0 \tag{68}$$

This condition is identical to Eq. (64a) applied at the far field for

the shear case. After making the appropriate substitutions, the conditions are given by

$$f_2 - f_1 - \rho_2 u_2 + \rho_1 u_1 + \frac{h_2^2}{12}\left(\frac{b_2^* G_2}{N_2'^2} - \frac{b_1^* G_1}{N_1'^2}\right) = 0 \qquad (69)$$

where

$$\rho_1 = \frac{1}{N_1'}\left(\frac{h_2^2}{12}\frac{N_1''}{N_1'^2} - \frac{h_2}{2}\right)$$

$$\rho_2 = \frac{1}{N_2'}\left(\frac{h_2^2}{12}\frac{N_2''}{N_2'^2} + \frac{h_2}{2}\right)$$

In the far field, Eq. (64a) is replaced by Eq. (45),

$$f_{K+1} - \eta_{K+1} + \hat{\delta}^* = 0 \qquad (45)$$

or Eq. (46),

$$f_{K+1} - \eta_{K+1} + \frac{u_e}{\sqrt{2\xi}}\left(\delta^*\sqrt{Re}\right) = 0 \qquad (46)$$

depending upon whether the transformed or untransformed displacement thickness is specified.

2.8.3 Direct Method Boundary Conditions

For the direct case, a slightly different set of boundary conditions is used. At the wall, the conditions are identical to those used for the displacement thickness method. These conditions are Eqs. (47a), (47b), (63), and (69).

At the boundary-layer edge, two physical conditions are given, Eq. (47c) which is always specified regardless of method, and Eq. (47d),

$$\beta(\xi_1 N_{K+1}) = \beta(\xi) \quad . \qquad (47d)$$

Two-point spline relations are required to close the system. The obvious choices are Eqs. (66a) and (66b), since these complete the system and do not neglect any terms, as was done in Eq. (66c).

It is apparent, considering the boundary conditions discussed in the previous subsections, that only minor modifications need to be made to the boundary conditions even though a range of methods is treated here. This is quite surprising and also very helpful, since it allows the various methods to be combined into a single computer code with little difficulty.

It should also be noted, however, that while only minor changes to the boundary conditions are required, very few other possibilities exist when using the two-point spline relations. The conditions obtained in the above sections consist of all available conditions for the current problem without further differentiating the momentum equation, which would greatly increase the complexity of the boundary conditions.

2.9 Linearization

The system of block tridiagonal equations and boundary conditions discussed in the above sections is nonlinear. The system is linearized and solved using Newton's method, where a variable at the most recent iteration, (n+1), is equal to the variable at the last iteration, (n), plus a small correction. Then, the variables at the (n+1) iteration can be written as

$$\left.\begin{aligned} f^{(n+1)} &= f^{(n)} + \delta f^{(n)} \\ u^{(n+1)} &= u^{(n)} + \delta u^{(n)} \\ G^{(n+1)} &= G^{(n)} + \delta G^{(n)} \\ \beta^{(n+1)} &= \beta^{(n)} + \delta\beta^{(n)} \quad . \end{aligned}\right\} \tag{70}$$

These relations are substituted into the nonlinear equations at the (n+1) iteration and all terms which are quadratic in the corrections are neglected. This yields a linear system of equations which can be solved for the corrections δf, δu, δG, and $\delta\beta$ using a lower-upper (L-U) decomposition method. The following subsections describe the linearization of the eddy viscosity, the interior spline relations and the boundary conditions.

2.9.1 Eddy Viscosity

Before beginning the linearization of the equations, we considered the turbulence model formulas. In simplified form, the eddy-viscosity relations can be written as

$$\varepsilon_i = C_1(\eta)\,|f''|, \tag{71a}$$

$$\varepsilon_o = C_2. \tag{71b}$$

Here, the inner equation is a function of η and f'' (primes denoting η-derivatives), while the outer equation is a constant when the Klebanoff intermittency factor is set to unity. Thus, to maintain consistency in the solution, it is obvious that the eddy-viscosity equation must also be linearized.

Upon substituting for f'', Eq. (71a) becomes

$$\varepsilon_i = C_1(\eta)\, b^*\, |G| \quad , \tag{72}$$

where b^* can be taken outside the absolute value sign since its value is always positive. Since b^* is also a function of ε_i, the value of ε_i is determined by solving a quadratic equation, yielding

$$\varepsilon_i = \frac{1}{2}\left[(1 + 4C_1(\eta)\,(1 + \varepsilon_o)\,|G|)^{1/2} - 1\right] .$$

To eliminate the absolute value of G, Eq. (72) is recast as

$$\varepsilon_i = (-1)^s C_1(\eta) b^* G, \tag{73}$$

where $s = 1$ for $G < 0$, and

$s = 2$ for $G > 0$.

Writing ε_i in Newton iterate form,

$$\varepsilon_i^{(n+1)} = \varepsilon_i^{(n)} + \delta\varepsilon_i^{(n)}, \tag{74}$$

Eq. (73) may be substituted at (n) and (n+1) iterations and the result solved for $\delta\varepsilon_i^{(n)}$.

$$\delta\varepsilon_i^{(n)} = (-1)^s C_1(\eta) (b^* G)^{(n+1)} - (-1)^s C_1(\eta) (b^* G)^{(n)}.$$

Upon substitution for the (n+1) Newton iterates, as in Eq. (70), the above equation may be solved for the correction of the solution variable G, yielding

$$\delta\varepsilon_i^{(n)} = \frac{(-1)^s C_1(\eta) (1 + \varepsilon_o)}{(2\varepsilon_i^{(n)} + 1)} \delta G^{(n)} \tag{75a}$$

or, in a more convenient form,

$$\delta\varepsilon_i^{(n)} = \frac{(-1)^s C_1(\eta) b^{*(n)}}{1 + \left(\frac{\varepsilon_i}{1 + \varepsilon_i}\right)^{(n)}} \delta G^{(n)}. \tag{75b}$$

2.9.2 Interior Equations

The interior block tridiagonal equations are given by Eqs. (59) and (61). Two of these equations contain nonlinear terms, Eqs. (59b) and (59c). Each of the nonlinear terms is linearized separately, then substituted into the appropriate equations. The remaining equations are then linearized and put into correction form.

A recurring term in both nonlinear equations is $b_j^* G_j$. First, b_j^*, is linearized using the binomial expansion theorem, yielding

$$b_j^{*(n+1)} = b_j^{*(n)} \left(1 - \frac{\delta\varepsilon^{(n)}}{1 + \varepsilon^{(n)}}\right) \tag{76}$$

For the inner region, $\delta\varepsilon$ is given by Eq. (75) and for the outer region, $\delta\varepsilon$ us equal to zero. Upon linearization and substitution of Eqs. (73), (75b) and (76), the term $(b_j^* G_j)$ becomes (with n iterate superscripts understood),

$$(b_j^* G_j)^{(n+1)} = b_j^* [G_j + (1 - e_j)\ \delta G_j] \tag{77}$$

with

$$e_j = \begin{cases} \dfrac{\varepsilon_i}{2\varepsilon_i + 1} & \text{for inner region} \\ 0 & \text{for outer region .} \end{cases}$$

The remaining terms in linearized form are:

$$(b_j^* f_j G_j)^{(n+1)} = b_j^* f_j\ [G_j + (1 - e_j)\ \delta G_j] + b_j^*\ G_j\ \delta f_j \tag{78a}$$

$$(b_j^*\ u_j\ G_j)^{(n+1)} = b_j^* u_j\ [G_j + (1 - e_j)\ \delta G_j] + b_j^* G_j \delta u_j \tag{78b}$$

$$(u_j^2)^{(n+1)} = u_j^2 + 2u_j \delta u_j \tag{78c}$$

$$[\beta_j (u_j^2 - 1)]^{(n+1)} = \beta_j (u_j^2 - 1) + 2\beta_j u_j\ \delta u_j + (u_j^2 - 1)\ \delta\beta_j \tag{78d}$$

Upon substitution of these terms into Eq. (59c), the equation is solved for all correction terms, with all known quantities moved to the right-hand-side. The final, linear tridiagonal result is given by

$$\frac{\sigma_2}{N_{j-1}'} [\hat{A}\delta f + \hat{B}\delta u + \hat{D}\delta G + \hat{G}\delta\beta]_{j-1}$$

$$+ \quad \frac{\sigma_1}{N_j'} [\hat{A}\delta f + \hat{B}\delta u + \hat{E}\delta G + \hat{G}\delta\beta]_j$$

$$+ \quad \frac{1}{N_{j+1}'} [\hat{A}\delta f + \hat{B}\delta u + \hat{F}\delta G + \hat{G}\delta\beta]_{j+1}$$

$$= - \frac{\sigma_2}{N'_{j-1}} [T_1 + (T_2 - \frac{N'}{h_j} \frac{\sigma_3}{\sigma_2}) G + \Theta C_4]_{j-1}$$

$$- \frac{\sigma_1}{N'_j} [T_1 + (T_2 - \frac{N'}{h_j} \frac{\sigma_4}{\sigma_1}) G + \Theta C_4]_j \qquad (79)$$

$$- \frac{1}{N'_{j+1}} [T_1 + (T_2 - \frac{N'}{h_j} \sigma_5) G + \Theta C_4]_{j+1}$$

See Appendix C for a list of all block tridiagonal coefficients.

The remaining three tridiagonal spline relations in linearized form are

$$(\frac{\sigma_3}{h_j} \delta f - \frac{\sigma_2}{N'} \delta u)_{j-1} + (\frac{\sigma_4}{h_j} \delta f - \frac{\sigma_1}{N'} \delta u)_j + (\frac{\sigma_5}{h_j} \delta f - \frac{1}{N'} \delta u)_{j+1}$$

$$= (\frac{\sigma_2}{N'} u - \frac{\sigma_3}{h_j} f)_{j-1} + (\frac{\sigma_1}{N'} u - \frac{\sigma_4}{h_j} f)_j + (\frac{u}{N'} - \frac{\sigma_5}{h_j} f)_{j+1}, \qquad (81a)$$

$$(\frac{\sigma_3}{h_j} \delta u - \frac{\sigma_2}{N'} b^* (1 - e) \delta G)_{j-1} + (\frac{\sigma_4}{h_j} \delta u - \frac{\sigma_1}{N'} b^* (1 - e) \delta G)_j$$

$$+ (\frac{\sigma_5}{h_j} \delta u - \frac{b^*}{N'} (1 - e) \delta G)_{j+1} = (\frac{\sigma_2}{N'} b^* G - \frac{\sigma_3}{h_j} u)_{j-1}$$

$$+ (\frac{\sigma_1}{N'} b^* G - \frac{\sigma_4}{h_j} u)_j + (\frac{b^*}{N'} G - \frac{\sigma_5}{h_j} u)_{j+1}, \qquad (81b)$$

and

$$\delta\beta_{j-1} + \sigma_7 \delta\beta_j + \sigma_6 \delta\beta_{j+1} = - (\beta_{j-1} + \sigma_7 \beta_j + \sigma_6 \beta_{j+1}). \qquad (81c)$$

(See Appendix C for a summary of all spline coefficients.)

2.9.3 Boundary Conditions

Since in general, the boundary conditions are linearized by the same procedure discussed in the previous subsections, a detailed

linearization of the boundary conditions is not provided here. Several special cases do exist, however, for the various "inverse" conditions. These special cases are examined here, followed by a brief summary of all boundary conditions in linearized correction form.

(1) Skin friction and displacement thickness methods

For the transformed wall shear case, the correction form of Eq. (36) is

$$(1 - e_1)\, b_1^*\, \delta G_1 = 0 \ ,$$

since $S(\xi)$ is a given constant at each streamwise station. When either C_{f_e} or C_{f_∞} is specified, however, the function F in Eq. (39) varies as the solution converges, since it is dependent upon ξ and u_e (for C_{f_∞} case only). Thus, F must be put into linearized form. Upon linearization, Eq. (39) becomes

$$(1 - e_1)\, b_1^*\, \delta G_1 - (F_{C_f}\, \delta C_f + F u_e\, \delta u_e + F_\xi\, \delta_\xi) = 0, \qquad (82)$$

where we set δC_f to zero since C_f is specified. The partial derivatives of F are easily found to be:

(a) for C_{f_e}

$$F_{u_e} = 0 \ , \qquad (83a)$$

$$F_\xi = \frac{1}{2}\,\frac{1}{\sqrt{2\xi}}\,(C_{f_e}\ \sqrt{Re}) \ , \qquad (83b)$$

b) and for C_{f_∞}

$$F_{u_e} = -\,\frac{\sqrt{2\xi}}{u_e^3}\,(C_{f_\infty}\ \sqrt{Re}), \qquad (83c)$$

$$F_\xi = \frac{1}{\sqrt{2\xi}\ u_e^2}\,(\tfrac{1}{2} - \beta)\,(C_{f_\infty}\ \sqrt{Re}). \qquad (83d)$$

The corrections δu_e and $\delta\xi$ must be related to the actual solution variables. Using the definition of ξ, Eq. (9a), $\delta\xi$ is found to be

$$\delta\xi_i = \frac{\Delta x}{2} \left[\mu_{t_e} \delta u_e + u_e \delta\mu_{t_e}\right]_i \quad .$$

For the present analysis, the contribution of the correction $\delta\mu_{t_e}$ is ignored, thereby greatly simplifying the linearization procedure. The above equation then reduces to

$$\delta\xi_i = \frac{\Delta x}{2} \mu_{t_{e_i}} \delta u_{e_i} \tag{84}$$

Similarly, δu_e is obtained using the relation for updating u_e after each iteration (See Eq. 101 in Section 2.12). After lengthy algebraic manipulation, the final result is

$$\delta u_{e_i} = \{\frac{1}{4} \left[\left(\frac{\beta_{i-j} + \beta_i}{\xi_i}\right) \delta\xi_i + \left(\ell n \frac{\xi_i}{\xi_{i-1}}\right) \delta\beta_i\right]\} \quad . \tag{85}$$

Equations (84) and (85) are simultaneously solved for $\delta\xi_i$ and δu_{e_i}, yielding

$$\delta\xi_i = \left(\frac{t_1 t_3}{(1 - t_1 t_2)}\right) \delta\beta_i \tag{86a}$$

$$\delta u_{e_i} = \frac{u_{e_i} t_3}{4(1 - t_1 t_2)} \delta\beta_i \tag{86b}$$

where

$$t_1 = \frac{\Delta x}{8} u_{e_i} \mu_{t_{e_i}} \tag{86c}$$

$$t_2 = \frac{1}{\xi_i} (\beta_{i-1} + \beta_i) \tag{86d}$$

$$t_3 = \ell n \left(\frac{\xi_i}{\xi_{i-1}}\right) \tag{86e}$$

Returning to Eq. (82) and substituting the previous results for $\delta\xi$ and δu_e, the boundary condition takes the general form,

$$(1 - e_1)\, b_1^*\, \delta G_1 - \lambda_1\, \delta\beta_1 = 0 \tag{87}$$

where

$$\lambda_1 = \frac{t_1\, t_3}{(1 - t_1\, t_2)}\, F_\xi + \frac{u_e\, t_3}{4(1 - t_1\, t_2)}\, F_{u_e}$$

For the displacement thickness method, a similar procedure is followed, except that the resulting boundary condition contains δf and $\delta\beta$ insteady of δG and $\delta\beta$. The final form is given by

$$\delta f_{K+1} + \lambda_1\, \delta\beta_{K+1} = \eta_{K+1} - f_{K+1} - \frac{u_e}{\sqrt{2\xi}}\,(\delta^*\sqrt{Re}) \tag{88a}$$

where

$$F_\xi = \left(\frac{\partial f}{\partial \xi}\right) + u_e\,(2\xi)^{-3/2}\,(\beta - 1)\,(\delta^*\sqrt{Re}), \tag{88b}$$

$$F_{u_e} = (2\xi)^{-1/2}\,(\delta^*\sqrt{Re}), \tag{88c}$$

the ξ-derivative is found by backward differences, and λ_1 is given above. If $\hat{\delta}^*$ is specified, Eq. (88a) is replaced by

$$\delta f_{K+1} = \eta_{K+1} - f_{K+1} - \hat{\delta}^* \tag{89}$$

(2) Hybrid method

Upon discretizing the ξ-derivative, Eq. (47) becomes at $j = 1$

$$b_i^* G_i - \hat{\delta}_i^*\left(\frac{\beta_i + 1}{H_i} + \beta_i\right) - 2\xi_i\left[a\left(\frac{\hat{\delta}_i^*}{H_i}\right) + b\left(\frac{\hat{\delta}_{i-1}^*}{H_{i-1}}\right) + c\left(\frac{\hat{\delta}_{i-2}^*}{H_{i-2}}\right)\right] = 0 \tag{90}$$

Here, the shape factor must be linearized along with the solution

variables. To accomplish this, H is assumed to be a function of β alone, so that

$$H^{(n+1)} = H^{(n)} + \delta H^{(n)} = H^{(n)} + \left(\frac{dH}{d\beta}\right)^{(n)} \delta\beta^{(n)}$$

Strictly, this is true only for self-similar flows, but the approximation is used here to include, at least partially, the dependence of the boundary condition on the variation of H.

Introducing the Newton iterates into Eq. (90) and linearizing yields, in correction form,

$$(1 - e_1)\, b_1^*\, \delta\, G_1 + \lambda_2\, \delta\beta_1 = P_1 \tag{91a}$$

where, with j=1 understood,

$$\lambda_2 = -\hat{\delta}_i^* \left[\frac{H_i + 1}{H_i} - \frac{1}{H_i^2}\,(\beta_i + 2\xi_i a + 1)\left(\frac{dH}{d\beta}\right)_i\right] \tag{91b}$$

$$P_1 = \hat{\delta}_i^* \left[\frac{\beta_i + 2\xi_i\, a + 1}{H_i} + \beta_i\right] + 2\xi_i \left[b\left(\frac{\hat{\delta}_{i-1}^*}{H_{i-1}}\right) + c\left(\frac{\hat{\delta}_{i-2}^*}{H_{i-2}}\right)\right] - b_i^* G_i \tag{91c}$$

The derivative $\left(\frac{dH}{d\beta}\right)_i$ is obtained by Lagrange backward differences past the second streamwise station. For $1 \leq i \leq 2$, the derivative is given its self-similar value based on the current value of β.

(3) Summary of boundary conditions

The wall conditions are:

$$\delta f_1 = 0 \tag{92a}$$

$$\delta u_1 = 0 \tag{92b}$$

$$\delta\beta_1 - \delta\beta_2 = 0 \tag{92c}$$

and,

(a) for the transformed wall shear method

$$\delta G_1 = 0 \tag{92d}$$

(b) for the skin friction coefficient method

$$(1 - c_1) b_1^* \delta G_1 - \lambda_1 \delta\beta_1 = 0, \tag{92e}$$

(c) for the hybrid method

$$(1 - e_1)\, b_1^*\, \delta G_1 + \lambda_2\, \delta\beta_1 = P_1 \tag{92f}$$

(d) and for the displacement thickness or direct method

$$\delta f_2 - \delta f_1 - \rho_2 \delta u_2 + \rho_1 \delta u_1 + \frac{h_2^2}{12} \left[\frac{b_2^*}{N_2'^2} (1 - e_2)\, \delta G_2 - \frac{b_1^*}{N_1'^2} (1 - e_1)\, \delta G_1 \right] \tag{92g}$$

$$= f_1 - f_2 - \rho_1 u_1 + \rho_2 u_2 - \frac{h_2^2}{12} \left[\frac{b_2^*}{N_2'^2}\, G_2 - \frac{b_1^*}{N_1'^2}\, G_1 \right] .$$

The far field boundary conditions are:

$$\delta u_{K+1} = 0 \tag{93a}$$

and, from the two-point spline conditions,

$$B11\delta f_K + B12\delta u_K + B13\delta G_K + B14\delta\beta_K + A11\delta f_{K+1} + A12\delta u_{K+1} + A13\delta G_{K+1} + A14\delta\beta_{K+1} = T_{K+1}, \tag{93b}$$

$$B31\delta f_K + B32\delta u_K + B33\delta G_K + B34\delta\beta_K + A31\delta f_{K+1} + A32\delta u_{K+1} + A33\delta G_{K+1} + A34\delta\beta_{K+1} = P_{K+1}, \tag{93c}$$

$$B41\delta f_K + B42\delta u_K + B43\delta G_K + B44\delta\beta_K + A41\delta f_{K+1} + A42\delta u_{K+1} + A43\delta G_{K+1} + A44\delta\beta_{K+1} = Q_{K+1}. \tag{93d}$$

For the displacement thickness method, Eq. (93b) is replaced by

$$\delta f_{K+1} + \lambda_1 \delta\beta_{K+1} = \eta_{K+1} - f_{K+1} - \frac{u_e}{\sqrt{2\xi}} (\delta^* \sqrt{Re}). \tag{93e}$$

For the direct method, the final boundary condition reduces to

$$\delta\beta_{K+1} = 0. \tag{93f}$$

2.10 Block Tridiagonal Solver

The linearized interior spline equations, Eqs. (79) and (81), together with the wall and far field boundary conditions, Eqs. (92) and (93), can be put into the following block matrix form:

$$\begin{aligned} A_1 Z_1 + C_1 Z_2 &= R_1 \\ B_j Z_{j-1} + A_j Z_j + C_j Z_{j+1} &= R_j, \quad 2 \le j \le K, \\ B_{K+1} Z_K + A_{K+1} Z_{K+1} &= R_{K+1}, \end{aligned} \tag{94}$$

with the solution vector

$$Z_j = \begin{bmatrix} \\ \delta f \\ \delta u \\ \delta G \\ \delta\beta \\ \\ \end{bmatrix}_j ,$$

and the right-hand-side vector

$$R_j = \begin{bmatrix} \\ T \\ L \\ P \\ Q \\ \\ \end{bmatrix}_j .$$

This is a 4 X 4 block tridiagonal system which can be accurately and efficiently solved by lower-upper (L-U) decomposition. A block tridiagonal solver, using subroutines developed by Blottner [34] which perform partial pivoting, is used to solve the matrix equation for the correction vectors at each iteration. Partial pivoting is employed to prevent the buildup of roundoff errors.

The tridiagonal system of Eq. (94) can be written as

$$\mathbb{A}\,\underline{Z} = \underline{R}$$

where $\mathbb{A}$ can be decomposed as

$$\mathbb{A} = \mathbb{L}\,\mathbb{U}$$

with

$$\mathbb{A} = [B_j,\ A_j,\ C_j]$$

$$\mathbb{L} = [\beta_j,\ \delta_j,\ \underline{0}]$$

$$\mathbb{U} = [\underline{0},\ \alpha_j,\ \gamma_j].$$

The forward and backward substitution equations are then

$$\mathbb{L}\,\underline{y} = \underline{R}$$

$$\mathbb{U}\,\underline{Z} = \underline{y}$$

Since the factorization is not uniquely determined by the decomposition as given, α_j in $\mathbb{U}$ is set to the identity matrix (This is Keller's case (ii). See Ref. [35]). The resulting recursion formulas are

$$\delta_1 = A_1, \tag{95a}$$

$$\beta_j = B_j, \qquad 2 \le j \le K+1 \tag{95b}$$

$$\delta_j = A_j - \beta_j\,\gamma_{j-1}, \tag{95c}$$

$$\delta_j\,\gamma_j = C_j, \qquad 1 \le j \le K \tag{95d}$$

and the forward and backward substitution formulas are

$$\delta_1 y_1 = R_1, \tag{96a}$$

$$\delta_j y_j = R_j - \beta_j\,y_{j-1}, \qquad 2 \le j \le K+1 \tag{96b}$$

$$Z_{K+1} = y_{K+1}, \tag{96c}$$

$$Z_j = y_j - \gamma_j\,Z_{j-1}, \qquad K \ge j \ge 1 \tag{96d}$$

The block tridiagonal solution process is repeated at a streamwise station i, updating the solution variables with each iteration, until

convergence for the vector of solution corrections is achieved. The convergence criterion, applied to each correction at each η nodal point for station i, is

$$|g_j^{(n+1)} - g_j^{(n)}| = |\delta g_j^{(n)}| \leq 10^{-8}, \quad 1 \leq j \leq K+1 \ .$$

Upon convergence of the solution at a streamwise station, the iteration process is repeated at the next streamwise station, and the solution is marched progressively downstream.

2.11 Starting Solution

The transformed pseudo-self-similar form of the equations allows the solution procedure to be self-starting since, in most cases, the solution can be started from either a flat plate or stagnation point flow. Both of these flows are self-similar in nature, and the transformed governing equations reduce to ordinary differential equations with no dependence on ξ.

As an initial guess for the starting solution, a fourth-order Pohlhausen polynomial is used to approximate the self-similar profiles of $(f,u,G,\beta)_{ij}$. The Pohlhausen polynomial has the form

$$\frac{u}{u_e} = f_\eta = b\zeta + c\zeta^2 + d\zeta^3 + e\zeta^4 \tag{97}$$

where $\zeta = \eta/r_\infty$. The constants b,c,d, and e are found by applying the boundary conditions and the Falkner-Skan equation

$$f_{\eta\eta\eta} + ff_{\eta\eta} + \beta(1 - f_\eta^2) = 0 \ . \tag{98}$$

The polynomials for the other required profiles can be found by integrating Eq. (97), for f, and differentiating Eq. (97), for G.

An initial guess for β can be found by substituting the previous results into the Falkner-Skan differential equation, yielding

$$\beta = \frac{6}{\eta_\infty^2}\,(b - 2) \tag{99a}$$

with $$b = \eta_\infty\, f_w'' \tag{99b}$$

This result can be reversed to find f_w'', with β given, for the direct method so that

$$f_w'' = b/\eta_\infty \tag{100a}$$

$$b = \frac{\eta_\infty^2\,\beta + 12}{6} \tag{100b}$$

With the initial conditions provided by the Pohlhausen polynomial, the starting solution is obtained by solving the ODE system with the standard block tridiagonal method. This procedure can also be used to obtain any Falkner-Skan self-similar solution.

If a non-similar solution is to be obtained, the starting solution is found using the fourth-order polynomial approximation, followed by marching the solution in the downstream direction. For the second streamwise station, two-point backward differences, instead of the usual three-point differences, are used to approximate the ξ-derivatives. Once past the second streamwise station, the three-point differences are ordinarily used.

2.12 Determination of the Edge Velocity

The boundary-layer edge velocity, u_e, is required to obtain the eddy viscosity distribution. It is also an important parameter of the boundary-layer flow and, should the present method be extended to a viscous-inviscid procedure, would be necessary for the outer iteration. For these reasons, an accurate method of determining the edge velocity

is most important. The edge velocity cannot, however, be determined directly from the solution procedure, since the pseudo-self-similar transformation eliminates u_e from appearing explicitly in the governing equations. For this formulation, u_e must be obtained through an integration of the solution variable.

The pressure gradient parameter is defined as

$$\beta = \frac{2\xi}{u_e} \frac{du_e}{d\xi} \tag{13}$$

Noting that this is a double logarithmic derivative, Eq. (13) can be recast as

$$\frac{1}{2} \beta = \frac{d(\ell n u_e)}{d(\ell n\ \xi)} \tag{101}$$

Rearranging and integrating over the numerical interval i-1 to i, Eq. (101) becomes

$$\ell n \frac{u_{e_i}}{u_{e_{i-1}}} = \frac{1}{2} \int_{i-1}^{i} \beta d\ell n\xi$$

The right-hand-side of the previous equation may be approximated using the trapezoidal integration rule. The edge velocity at station i is then obtained from

$$u_{e_i} = u_{e_{i-1}} e^{\Gamma} \tag{102a}$$

where

$$\Gamma = \frac{1}{4} (\beta_i^{(n)} + \beta_{i-1}) \ell n \frac{\xi_i^{(n)}}{\xi_{i-1}} \tag{102b}$$

As the iteration process proceeds, Eq. (102) must be updated with new values of β_i and ξ_i.

This method of determining u_e presents a problem when solving a nonsimilar flow beginning with a stagnation point. At the stagnation point, i=1, the edge velocity is zero. To calculate subsequent edge velocity values, the value of u_e at i=2 must be input directly or estimated. This anamolous behavior at the second streamwise station is due to the double logarithmic form of the pressure gradient parameter definition.

The reason for this behavior is apparent if the flow near the stagnation point is assumed to behave like a wedge flow [36]. Then, the edge velocity is an exponential function of x such that ($\beta = 1$)

$$u_e = cx^{\frac{\beta}{2-\beta}} = cx$$

The constant c can not be determined without specifying the body shape because of the psuedo-self-similar character of the flow. A similar observation is made by Bradshaw, Cebeci, and Whitelaw, [37], who note that it is necessary to specify the slope c near a stagnation point.

2.13 Normal Coordinate Distributions

Although the governing equations are formulated to allow the use of the adaptive normal coordinate, the use of this coordinate is not always practical for all flows, particularly flows which are entirely laminar. For laminar flows, the system is returned to (ξ, η) coordinates and a more straightforward distribution of the normal coordinate is used.

For entirely laminar flows, either a constant η stepsize or a geometric progression in $\Delta\eta$ is computed. The geometric progression is obtained from

$$\Delta\eta_1 = \frac{1 - C_e}{1 - C_e^k} \eta_\infty$$

$$\Delta\eta_j = C_e \, \Delta\eta_{j-1}, \quad 2 \leq j \leq K+1$$

with the constant c_e set to 1.1.

As an alternative to the adaptive normal coordinate for turbulent boundary-layer computations, hyperbolic stretching functions are also installed in the computer code. This type of coordinate distribution is discussed at length by Vinokur [38] and Thompson, Warsi, and Mastin [39]. Here, one-sided hyperbolic tangent or hyperbolic sine functions are used to determine a coordinate distribution in η. The details of these stretching functions are not included here since they are adequately covered in the noted references.

Chapter 3

RESULTS

3.1 Laminar Results

The following subsections describe the seven laminar test cases which were run, including both inverse and direct solutions. The cases are summarized in Table 2, which displays pertinent information about each run. Geometric progressions were used for the normal coordinate distributions unless otherwise noted.

3.1.1 Linearly Decreasing Wall Shear

The linearly decreasing wall shear cases were originally devised by Keller and Cebeci [8], and were later repeated by Cebeci and Keller [22], Horton [10], and Kaufman and Hoffman [23]. The cases listed here are a review of those given in Reference 23 with several additions.

The cases were devised to specify a linearly decreasing transformed wall shear with one case beginning with a flat plate,

$$S(\xi) = 0.4696\ (1 - \xi),\ \xi \geq 0\ ,$$

and the second case beginning with a stagnation point,

$$S(\xi) = 1.23259\ (1 - \xi),\ \xi \geq 0\ ,$$

with both proceeding to separation at $\xi = 1$. For this case, comparisons are also made with the hybrid solution method, the displacement thickness method, and a direct solution.

Figure 1 gives a comparison of run (1a) and the computational results of Keller and Cebeci [8] and Cebeci and Keller [22]. This figure clearly shows the breakdown of the Cebeci and Keller mechul function near separation. The results from the present method compare

Table 2

Boundary Layer Test Cases

Run No.	Mode	B.D.	M	K	η_∞	Specifications
Case 1: Linearly Increasing Wall Shear						
1a	I-A	3 pt.	23	20	7	Flat Plate
1b	I-A	3 pt.	23	20	7	Stag. Point
1c	I-A	3 pt.	23	10	7	F.P.
1d	I-A	3 pt.	23	20	7	F.P., Const.$\Delta\eta$
1e	D	3 pt.	23	20	7	F.P.
1f	I-G	3 pt.	23	20	7	F.P.
1g	I-G	3 pt.	23	20	7	S.P.
1h	I-E	3 pt.	23	20	7	F.P.
1i	I-E	3 pt.	23	20	7	S.P.
Case 2: Howarth Flow						
2a	D	3 pt.	22	20	7	----
2b	I-B	3 pt.	20	20	7	----
2c	I-F	3 pt.	20	30	8	----
Case 3: Potential and Viscous Circular Cylinder						
3a	D	3 pt.	50	20	7	Potential
3b	I-A	3 pt.	47	20	7	Potential
3c	D	3 pt.	40	20	7	Hiemenz Fit
3d	I-A	3 pt.	36	20	7	Hiemenz Fit

Table 2 (Continued)

Run No.	Mode	B.D.	M	K	η_∞	Specifications
Case 4: Horton Parabolic Wall Shear Distribution						
4a	I-A	3 pt.	50	30	7	----
4b	I-B	3 pt.	50	30	7	----
4c	I-C	3 pt.	50	30	7	----
4d	I-F	2 pt.	50	30	8	----
4e	I-E	2 pt.	50	30	8	----
Case 5: Analytic $\delta^*\sqrt{Re}$ Distribution						
5a	I-F	3 pt.	50	30	8	$\delta^*_{max} = 5.6$
5b	I-F	3 pt.	50	30	14	$\delta^*_{max} = 8.6$
5c	I-F	3/2 pt.	50	30	14	$\delta^*_{max} = 8.6$
5d	I-F	2 pt.	50	30	14	$\delta^*_{max} = 8.6$
5e	I-C	3/2 pt.	50	30	8	$\delta^*_{max} = 5.6$
5f	I-F	3 pt.	100	30	8	$\delta^*_{max} = 5.6$
5g	I-F	3/2 pt.	100	30	14	$\delta^*_{max} = 8.6$
Case 6: Horton/Ntim $\delta^*\sqrt{Re}$ Distribution						
6a	D	3 pt.	76	30	7	----
6b	I-F	3 pt.	76	30	8	----
6c	I-F	3/2 pt.	76	30	8	----

Table 2 (Continued)

Run No.	Mode	B.D.	M	K	η_∞	Specifications
Case 7: Klineberg-Steger $\hat{\tau}$ Distribution						
7a	I-D	3 pt.	120	20	7	sep. 2-6
7b	I-D	3 pt.	120	20	7	sep. 2.5-5.5
7c	I-D	3 pt.	120	20	7	sep. 3-5

Modes: D-Direct
I-Inverse A - f_w'' specified

B - $C_{f_e}\sqrt{Re}$ specified

C - $C_{f_\infty}\sqrt{Re}$ specified

D - $\hat{\tau}$ specified

E - $\hat{\delta}^*$ specified

F - $\delta^*\sqrt{Re}$ specified

G - Hybrid Method

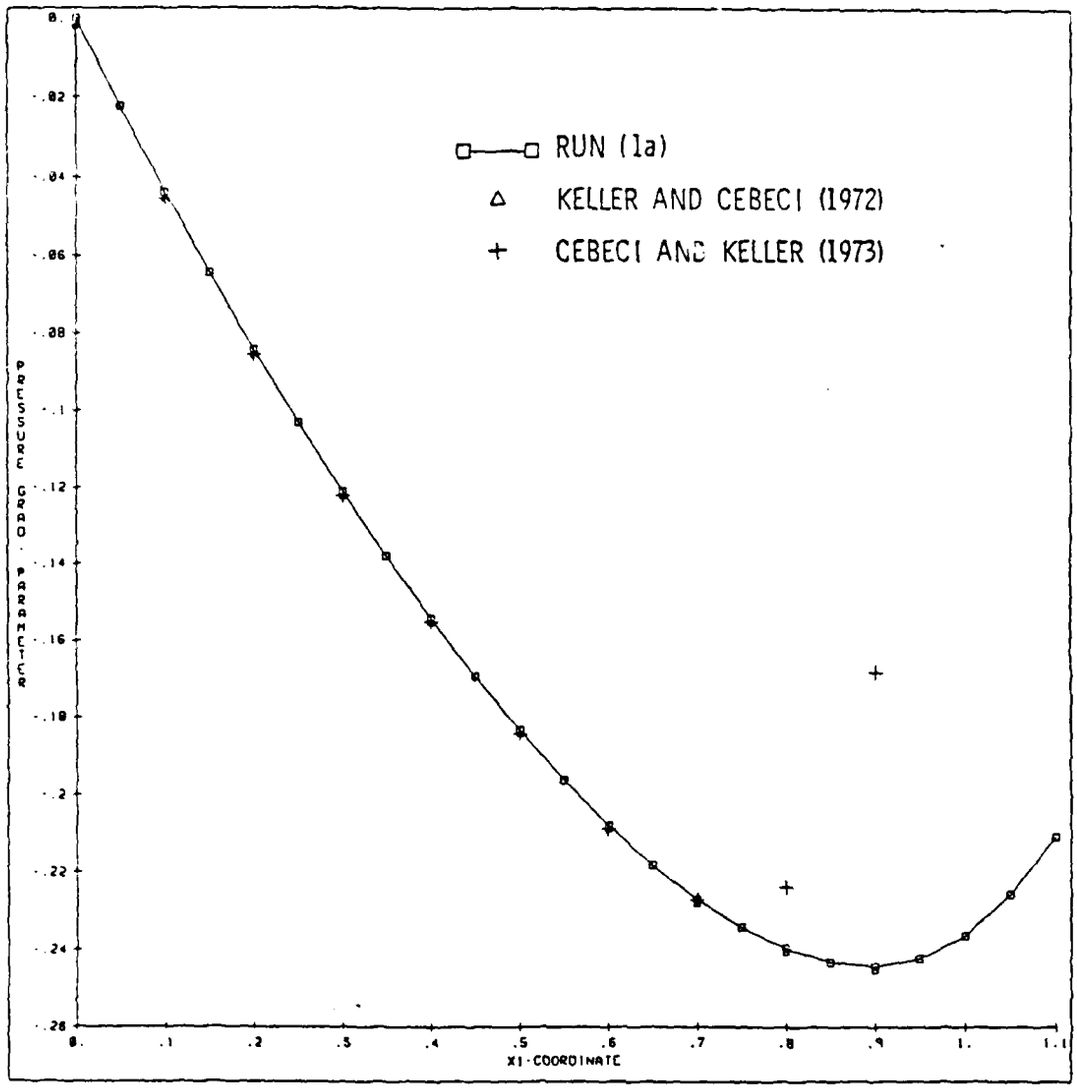

Figure 1. Comparison of β with References 8 and 22 for Case 1. Flat Plate to Separation.

well with those of the Keller and Cebeci eigenvalue method to $\xi = 0.9$, and proceed through separation while the other two methods fail.

Figure 2 gives a comparison of results for the transformed wall shear method, the hybrid method, and the displacement thickness method. All agree quite well up to separation, where the hybrid method fails to converge. The other methods continue through separation with excellent agreement. It should be noted that calculations are only shown slightly past the separation point since the flow separation is severe and the computation methods fail for large regions of backflow.

A study of the accuracy of the fourth-order splines for different normal coordinate distributions is displayed in Figure 3. Here, a comparison is made between a twenty-point geometric progression in η, a twenty-point constant increment in η, and a ten point geometric progression in η. All three resulting β distributions are identical, indicating the ability of the splines to yield accurate results with significantly fewer nodal points.

The direct method was tested on the flat plate to separation problem by using the u_e distribution obtained from run (1a). The transformed wall shear from this run is compared in Figure 4 with direct results for Reference 8 as well as with the exact value specified in run (1a). The comparison is quite good with only slight deviation of the present results from the exact distribution at separation, which is expected for a direct boundary-layer method.

The calculations of the various inverse methods for the stagnation point to separation case are shown in Figure 5, with comparison of computational results from Reference 8. Again, the agreement is quite

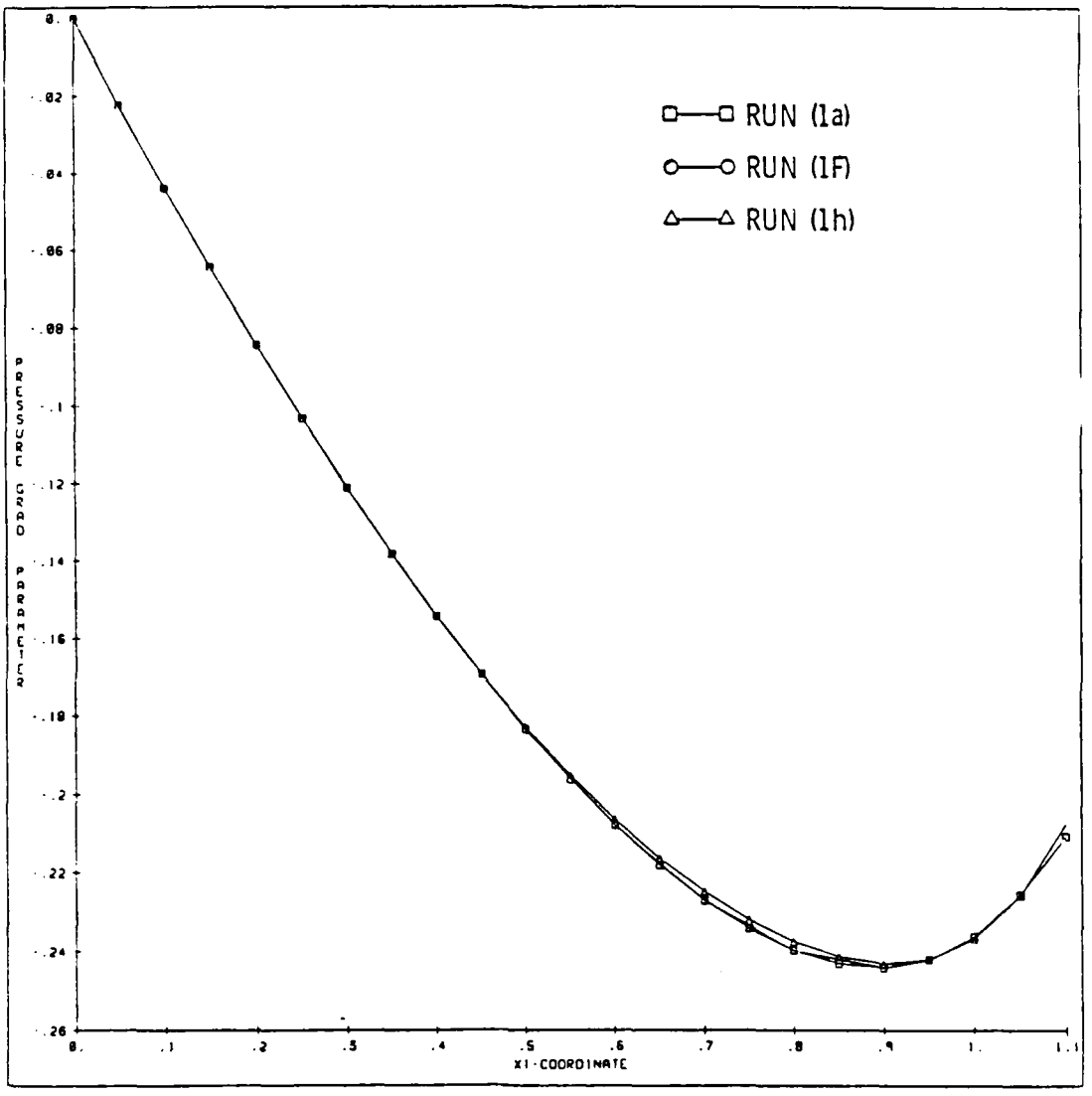

Figure 2. Comparison of β from Inverse Methods for Case 1. Flat Plate to Separation.

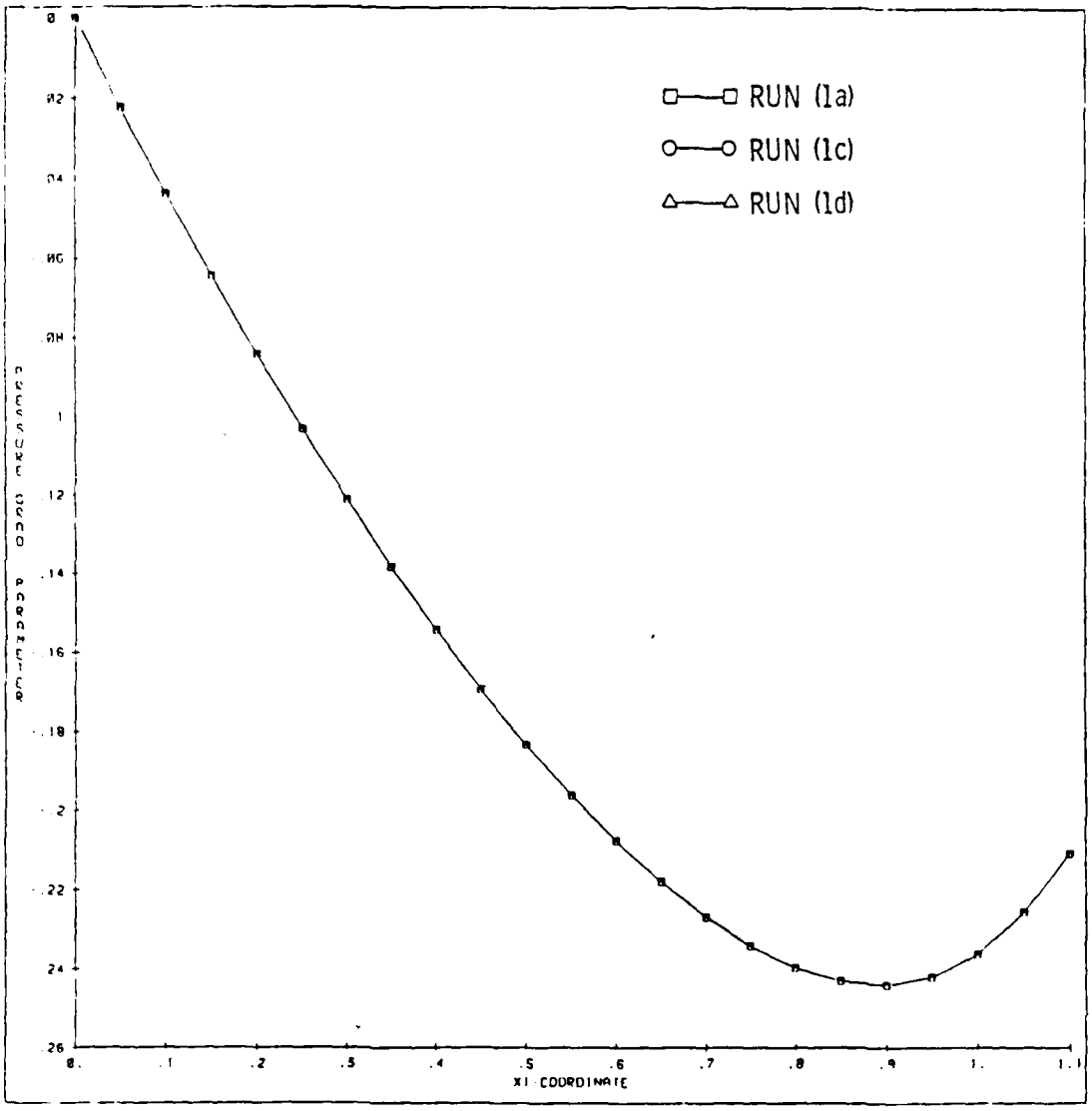

Figure 3. Comparison of δ for Normal Coordinate Distributions for Case 1. Flat Plate to Separation.

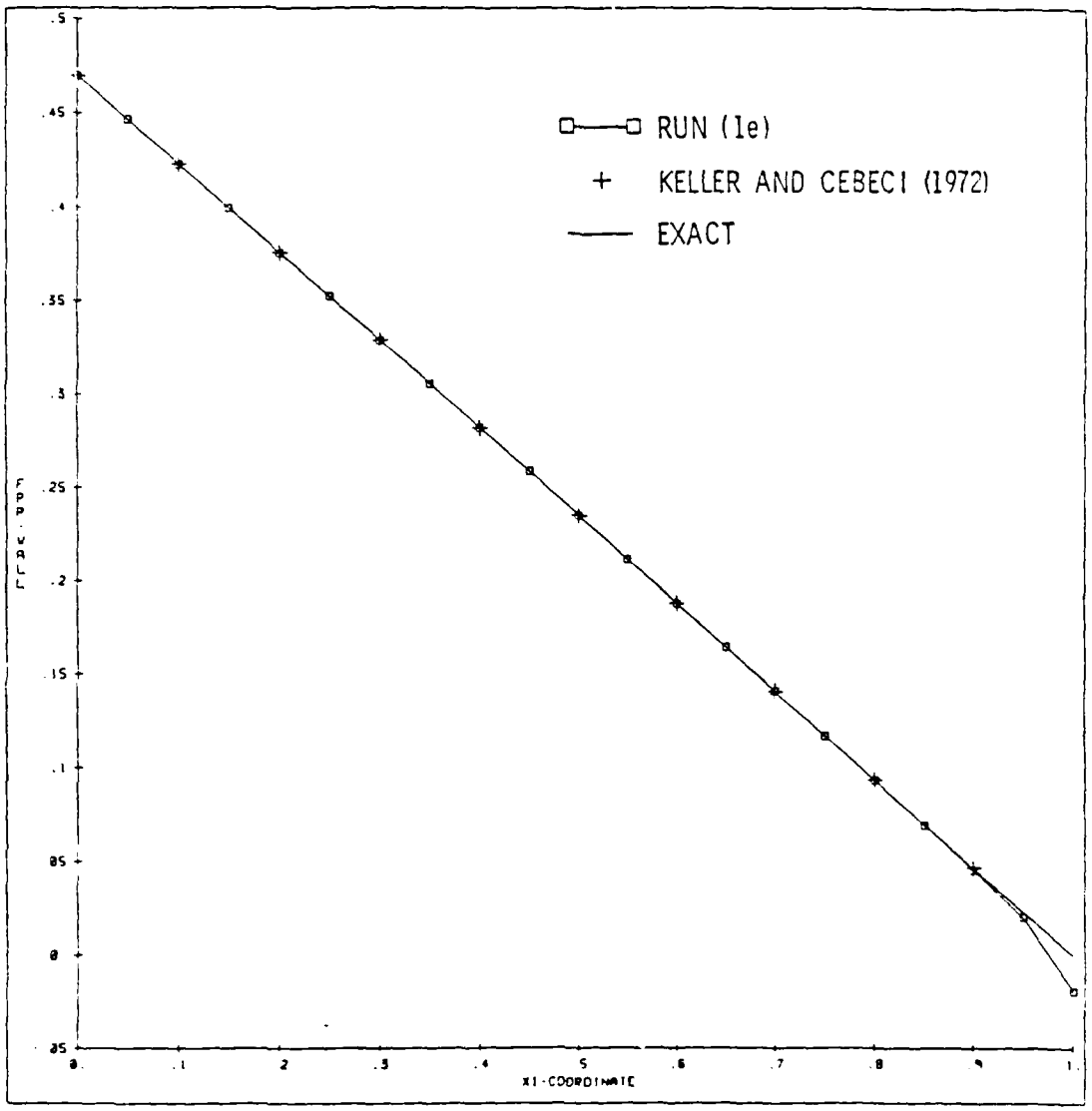

Figure 4. Comparison of f_w'' from Direct Method with Reference 8 for Case 1. Flat Plate to Separation.

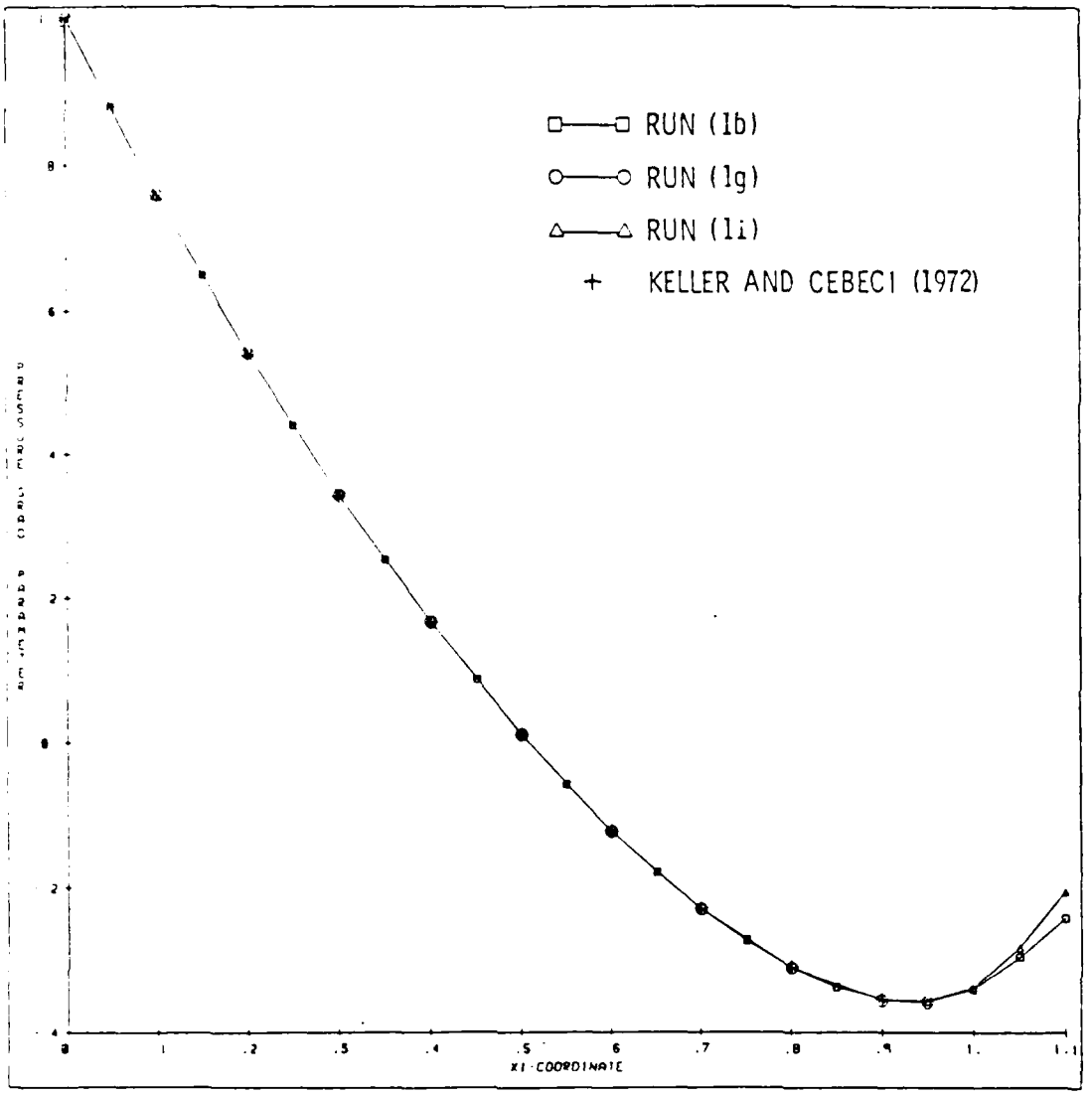

Figure 5. Comparison of β with Reference 8 for Case 1. Stagnation Point to Separation.

good, with both the wall shear and displacement thickness methods continuing through separation.

3.1.2 Howarth Flow

A boundary layer with a linearly decreasing edge velocity, the Howarth flow [1,40], has become a well-known test case for boundary-layer computations, and is included here mainly as a test for the direct method since no separation data is available. Two inverse runs are included for completeness.

Figure 6 shows both direct and inverse methods to have excellent agreement with both new (Edwards et al. [29]) and old (Smith and Clutter [1]) computational methods. A tabular comparison of dimensionless wall shear values obtained by the present method and results from Howarth [41], Cebeci and Smith [33], and Smith and Clutter [1] is presented in Table 3. Figures 7 and 8 compare the exact edge velocity and pressure gradient parameter distributions, respectively, with the inverse results. The agreement is excellent, with only slight deviation evident in β near separation. This discrepancy is most likely due to the direct solution being used as input for the inverse runs.

3.1.3 Circular Cylinder

As for the Howarth flow, the flow past a circular cylinder has also become a standard test case for boundary layer methods. Here direct solutions are computed using the edge velocity distribution from potential theory [40] as well as using the Hiemenz polynomial fit of the edge velocity for viscous flow. This case is included to test the ability of the direct and inverse methods to obtain a solution beginning with a stagnation point. Although Case 1 included a flow beginning

Table 3

Accuracy of Direct Method for Howarth Flows

Dimensionless Wall Shear $\tau_w / \rho U_e^2$

x	Present Method	Howarth [1938]	Smith [1966]	Cebeci-Smith [1974]
0.1	0.468454	0.468382		
0.2				
0.3	0.462782	0.462811		
0.4				
0.5				
0.6				
0.7				
0.8				
0.88				
0.9				
0.92				
0.94	0.029862			
x_{sep}	0.96	0.96	0.96	0.96

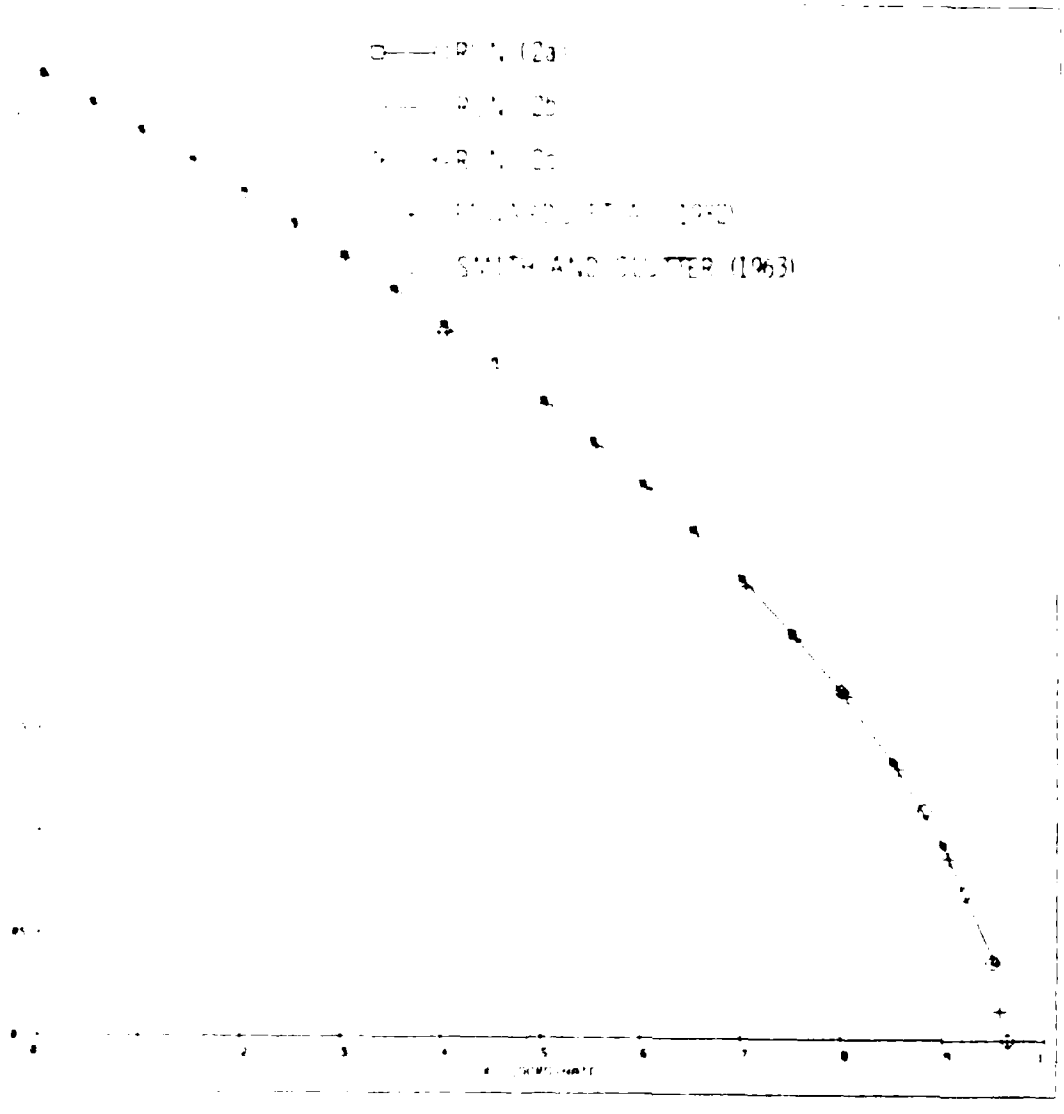

Figure [illegible] Pdf and Inverse Distributions of $E_{\gamma}^{\prime\prime}$ Compared with References 1 and 2[illegible] for Case 2.

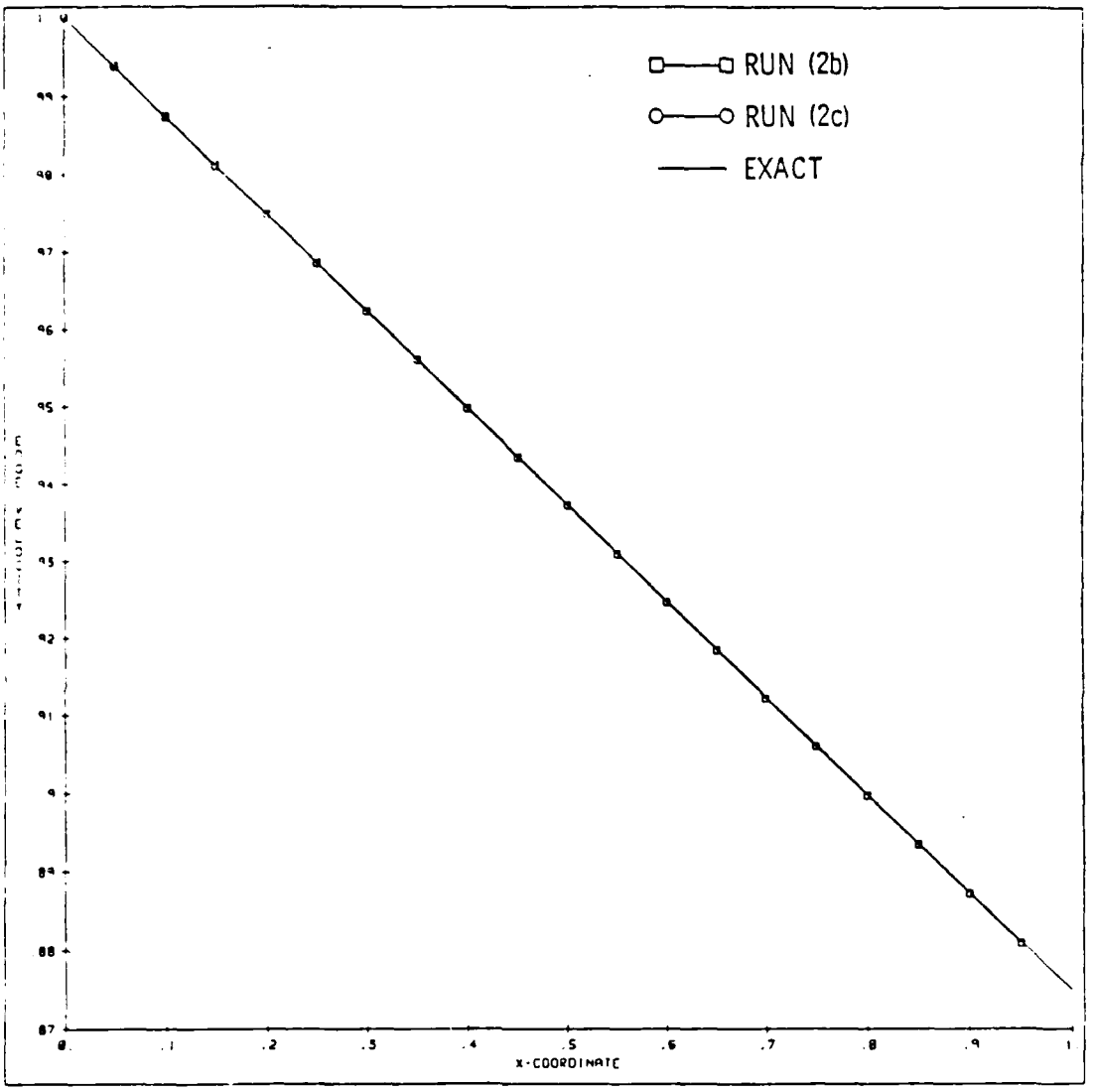

Figure 7. Comparison of u_e from Inverse Methods with Exact Distribution for Case 2.

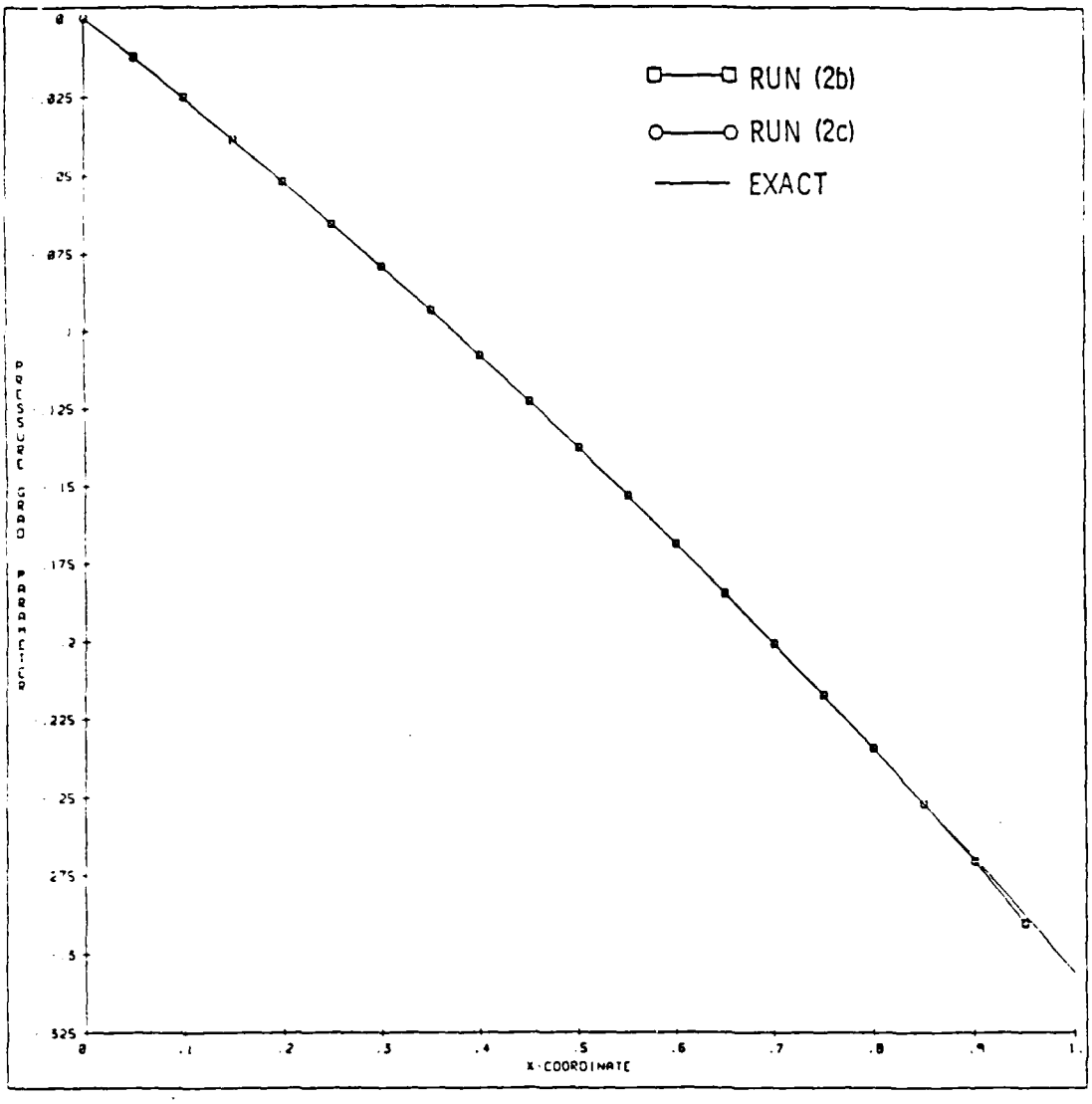

Figure 8. Comparison of $\bar{\beta}$ from Inverse Methods with Exact Distribution for Case 2.

with a stagnation point, the linearly decreasing wall shear problem is artificial, created only to test a solution procedure, and does not have a unique edge velocity distribution.

Figure 9 gives a comparison of transformed wall shear obtained by the present direct solution method with Terrill [42] for the potential flow, and Smith and Clutter [1] for the Hiemenz polynomial fit. The agreement is quite acceptable for both cases, with the present method yielding slightly larger values of f_w'' than References 1 and 42. A comparison of $C_{f_\infty}\sqrt{Re}$ distributions for the potential flow case is given in Figure 10. The values obtained by the direct and inverse runs (3a) and (3b) compare very well with results given by Cebeci and Bradshaw [43]. The direct solutions predict separation at approximately 109°, for the potential flow, and 80°, for the viscous flow. These values are generally accepted as the correct locations for separation [40].

The results of the inverse calculations are compared with the exact u_e distribution as given by White [40], and the analytically determined β distribution in Figures 11 and 12. Here, f_w'' distributions obtained from the direct solutions (3a) and (3c) are used as input for the inverse solution procedure. The match between the inverse solutions and the analytical curves is almost exact.

3.1.4 Horton's Parabolic Wall Shear Distribution

Horton [10] devised a parabolic distribution of f_w'' to test the ability of the boundary-layer equations to treat small regions of separation. The distribution of transformed wall shear is given by

$$S(\xi) = 0.4696\ (1 - \xi)\ (1 - 0.52649\xi),\ \xi \geq 0.$$

Separation occurs at $\xi = 1$, with reattachment at $\xi = 1.9$. Because of its simplicity and the existence of a small separation bubble, this case

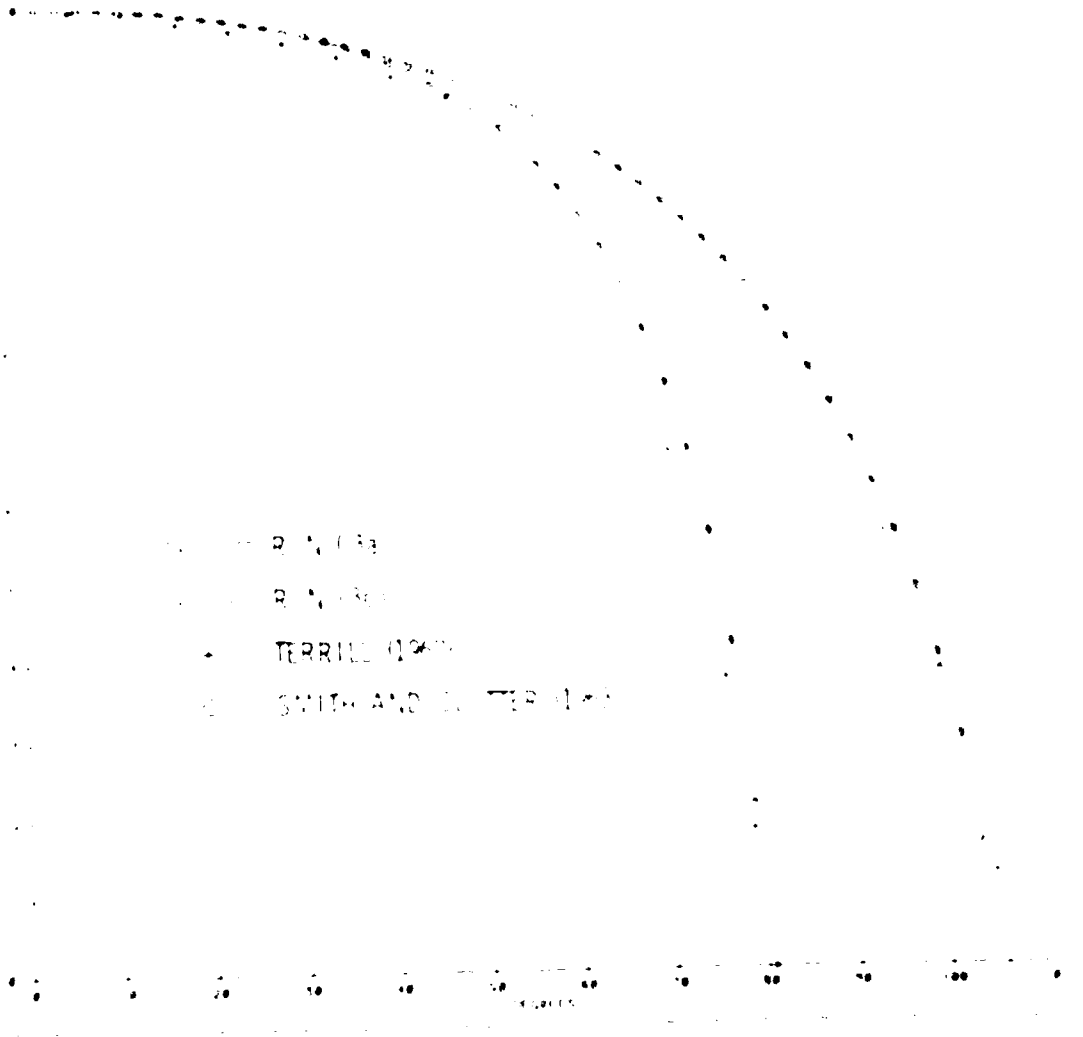
TERRILL
SMITH AND

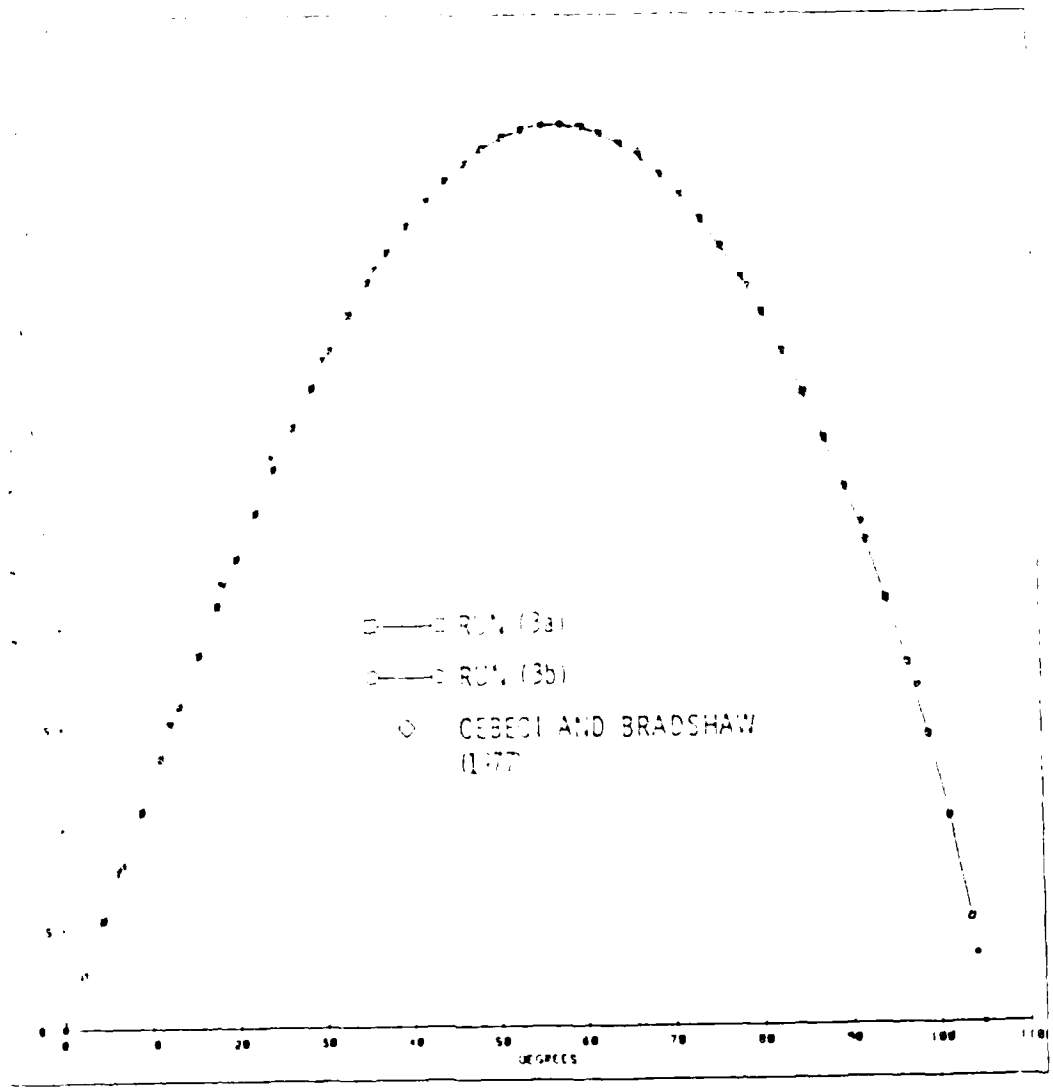

Figure 11. Direct and Inverse Distributions of $C_{f_\infty}\sqrt{Re}$ Compared with Reference 43 for Case 3.

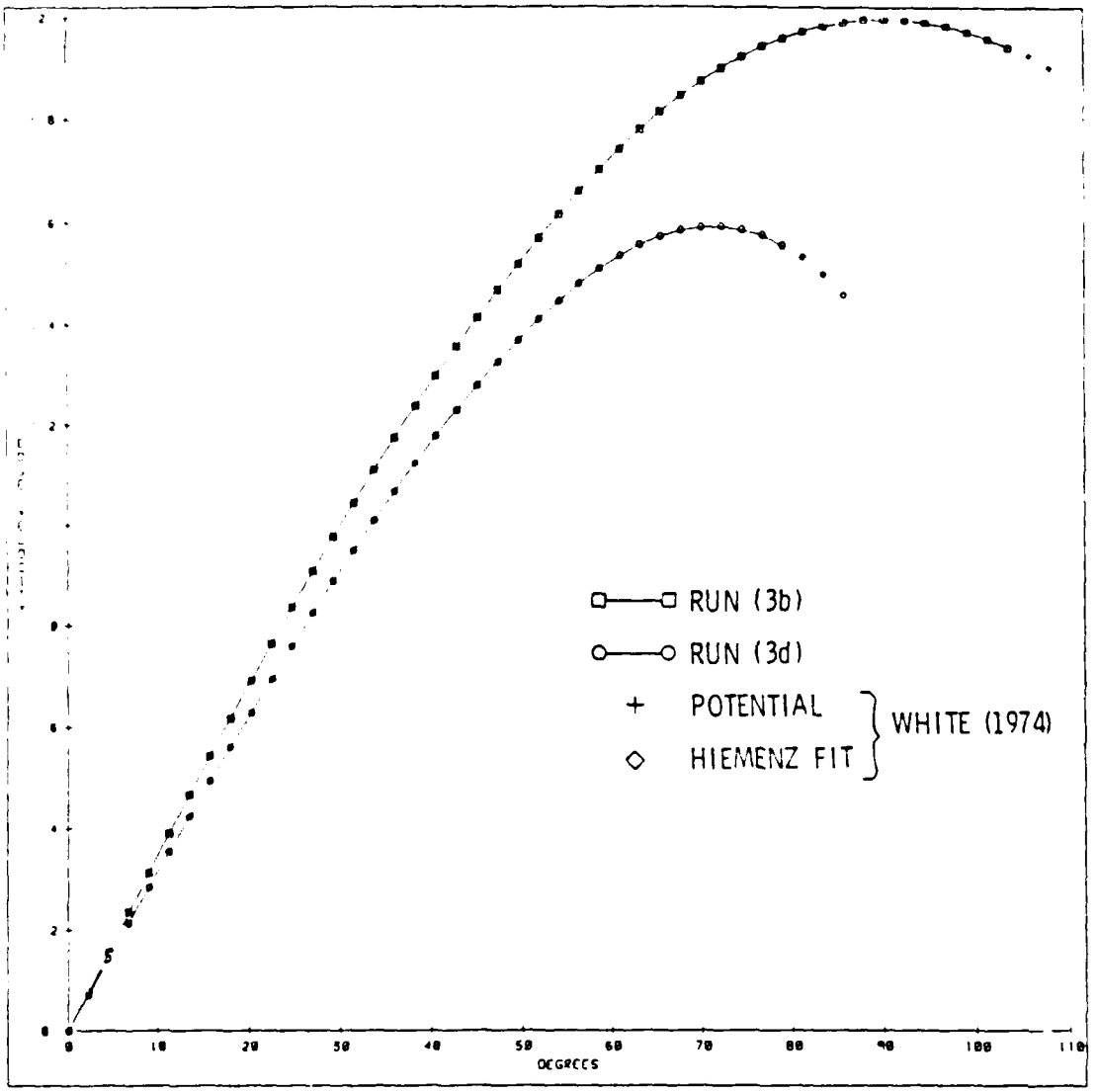

Figure 11. Comparison of u_e from Inverse Methods with Exact Distributions from Reference 40 for Case 3.

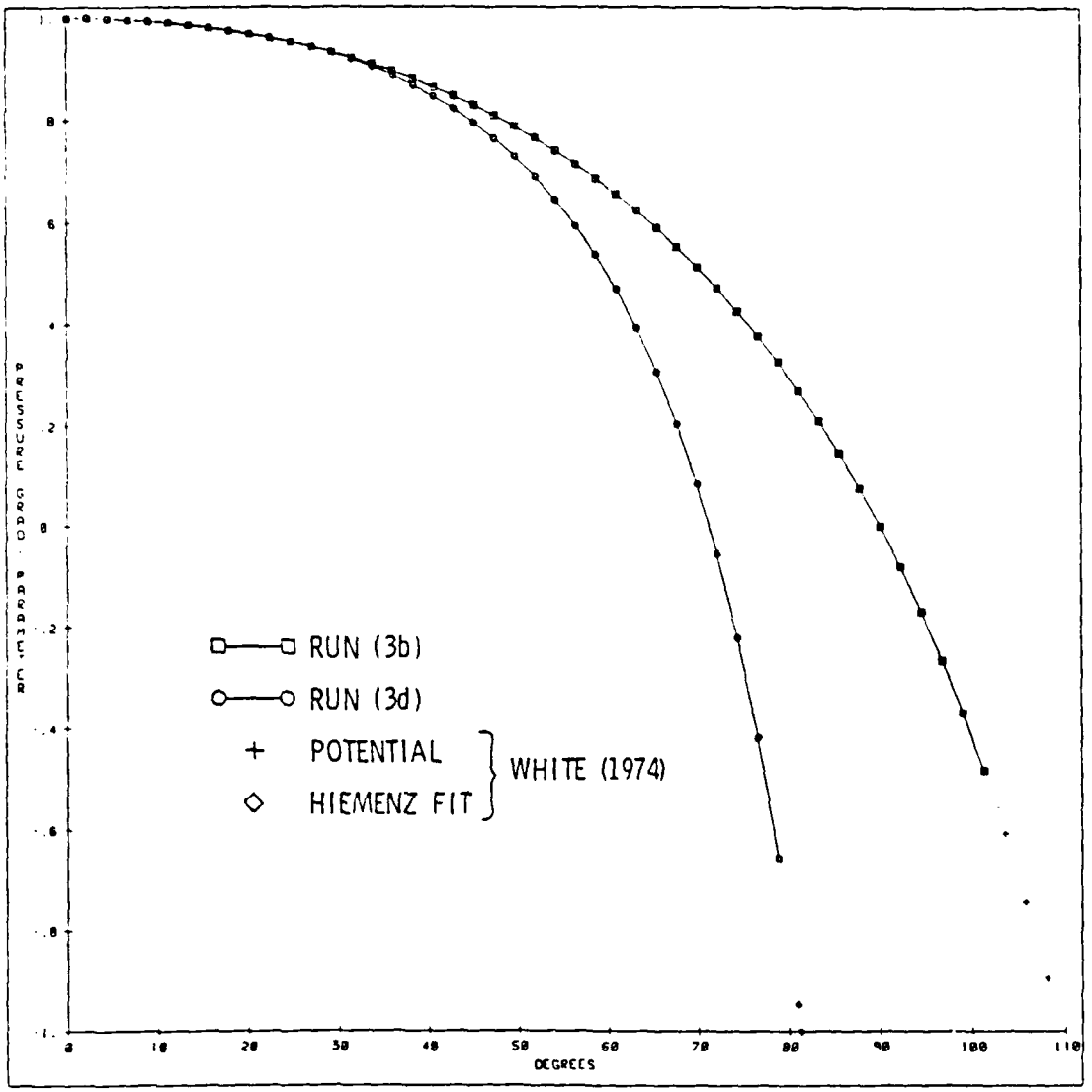

Figure 12. Comparison of β from Inverse Methods with Exact Distributions from Reference 40 for Case 3.

was used as a test for all five of the inverse options. The transformed wall shear run, (4a), was used to generate input data for the other four runs.

Figure 13 compares Horton's computational data with three inverse options, specifying f_w'', $C_{f_e}\sqrt{Re}$, and $\delta^*\sqrt{Re}$, from the present study. The agreement among all results is very good, although the displacement thickness run displays a slightly different trend from the other cases.

Two interesting discoveries were made while obtaining the displacement thickness runs. Accurate results could not be obtained without overestimating the value of η_∞ used for the wall shear cases by ten to fifteen percent, and using two-point backward differences, instead of the usual three-point differences, over the ξ-interval where the flow separates. Oscillations in the normal velocity, V, occurred when the case was run using three-point backward differences for the entire domain. The cases where wall shear or skin friction coefficient distributions were specified did not exhibit these oscillations.

Figure 14 compares runs (4b) and (4c), where $C_{f_e}\sqrt{Re}$ and $C_{f_\infty}\sqrt{Re}$ are specified, respectively. Figure 15 makes a similar comparison between the displacement thickness cases. For both figures, the compared curves are identical, with the exception of a small oscillation for the $C_{f_\infty}\sqrt{Re}$ run near the starting solution. This oscillation does not affect the solution downstream, and its origin is unclear.

Figure 16 compares the computed $\delta^*\sqrt{Re}$ distribution from run (4a) with the computational data of Horton [10]. The agreement is exceptionally good, with essentially no deviation between the two curves.

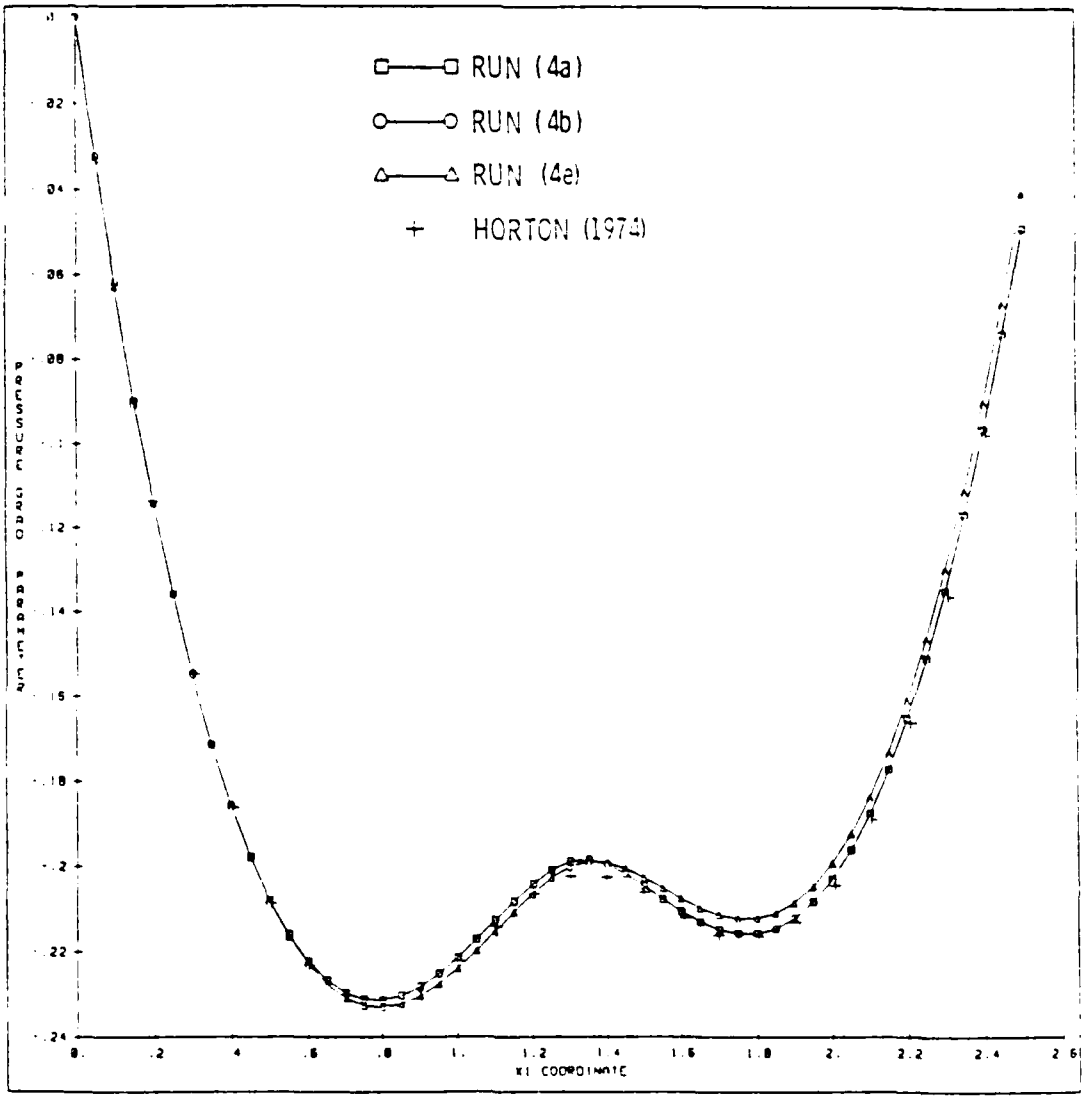

Figure 13. Comparison of β from Inverse Methods with Reference 10 for Case 4.

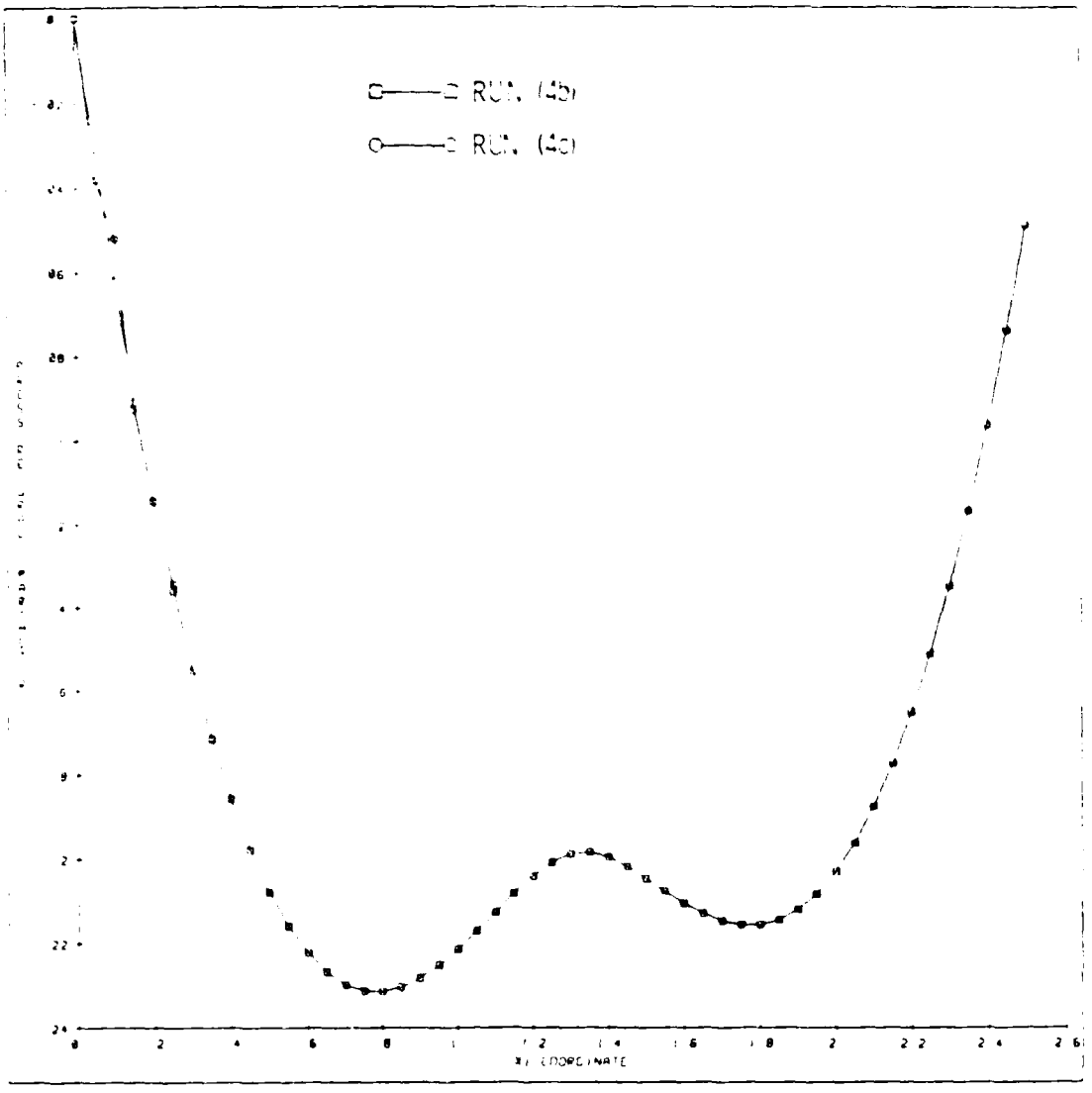

Figure 14. Comparison of I for Skin Friction Coefficient Options for Case 4.

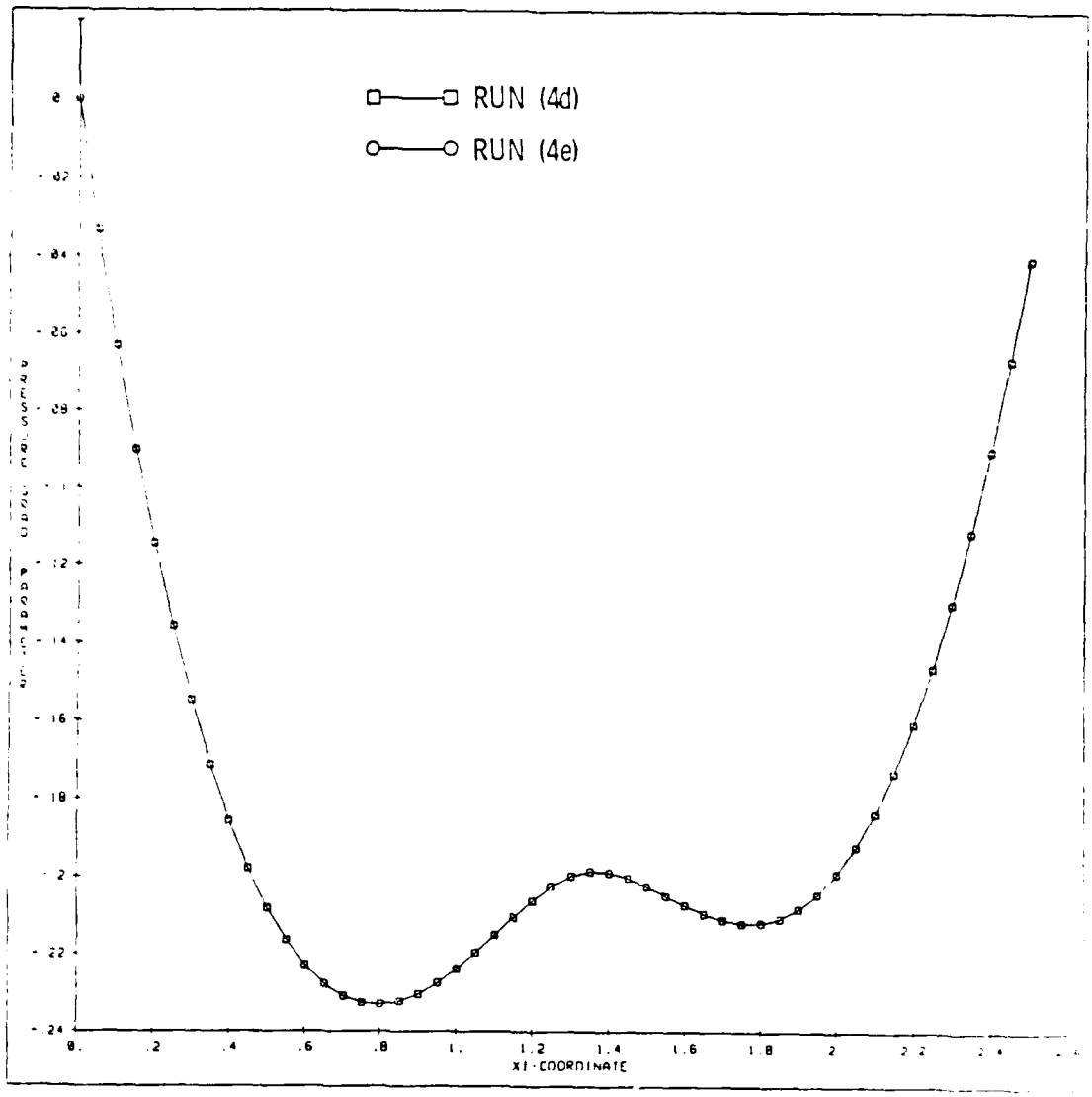

Figure 15. Comparison of β for Displacement Thickness Inverse [illegible] for Case 4.

AD-A178 223 A UNIFIED DIRECT-INVERSE PROCEDURE FOR TWO-DIMENSIONAL BOUNDARY LAYERS US (U) PENNSYLVANIA STATE UNIV STATE COLLEGE APPLIED RESEARCH LAB K C KAUFMAN ET AL FEB 87 2/2

UNCLASSIFIED TR-87-001 F/G 12/1 NL

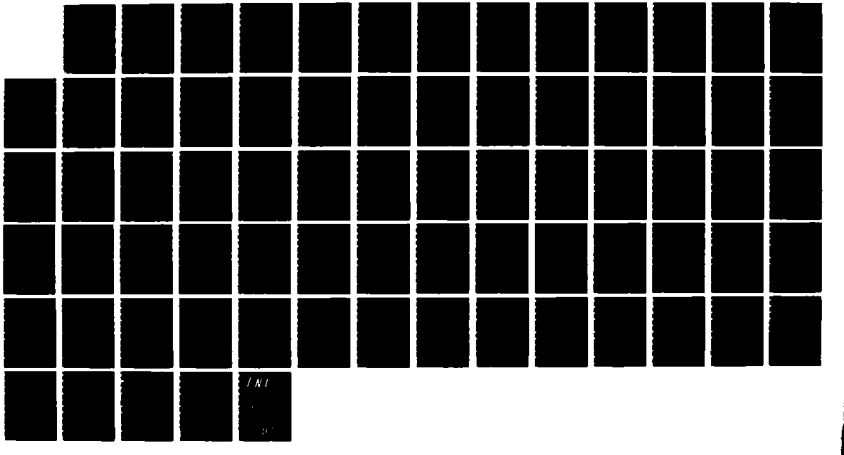

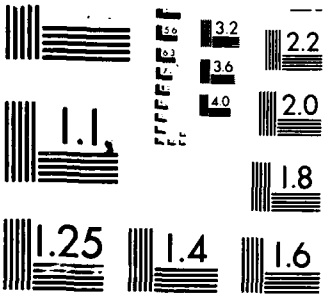

MICROCOPY RESOLUTION TEST CHART
NATIONAL BUREAU OF STANDARDS-1963-A

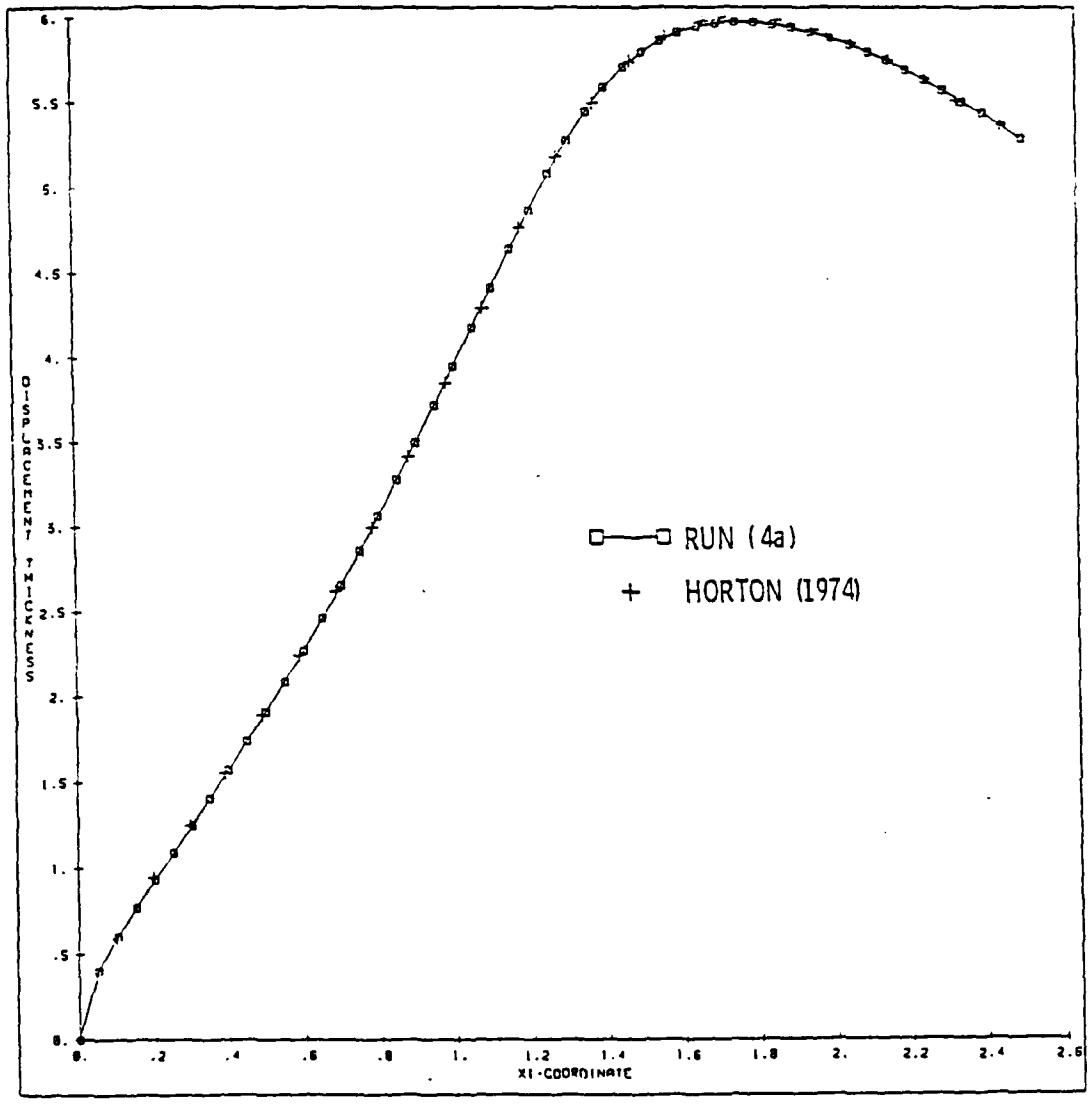

Figure 16. Comparison of $\delta^* \sqrt{Re}$ with Reference 10 for Case 4.

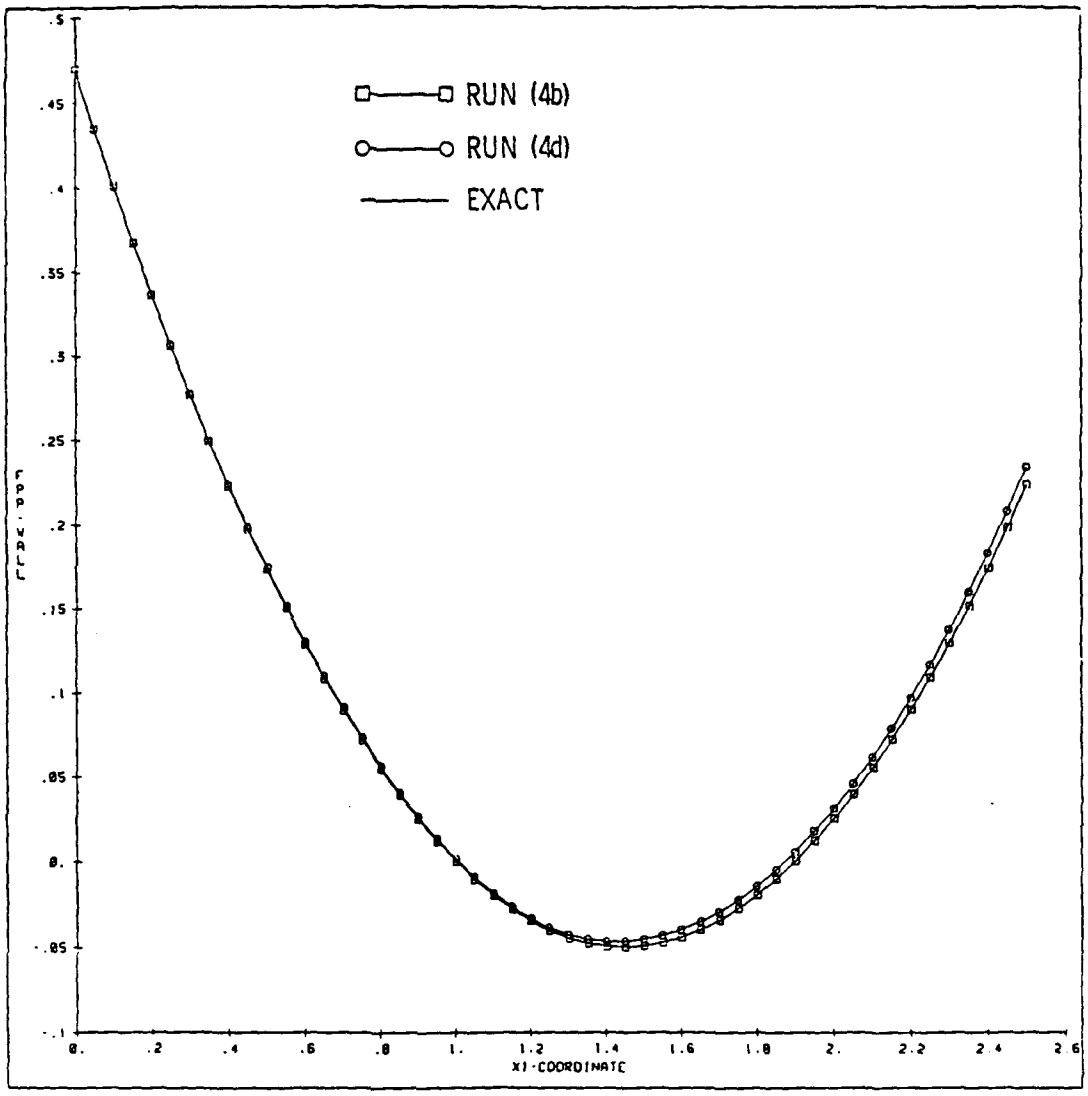

Figure 17. Comparison of f_w'' from Inverse Methods with Exact Distribution for Case 4.

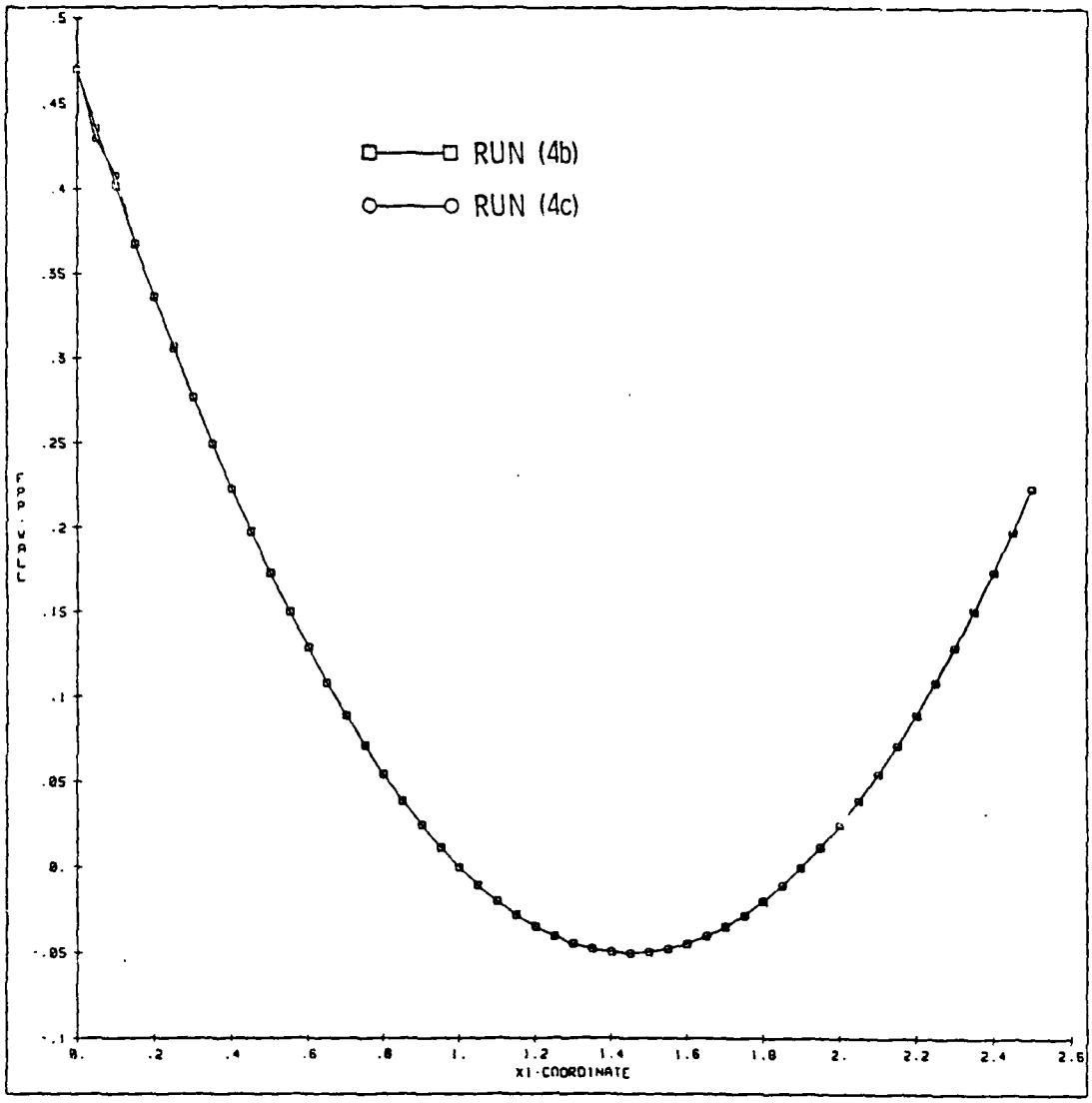

Figure 18. Comparison of f_w'' for Skin Friction Coefficient Options for Case 4.

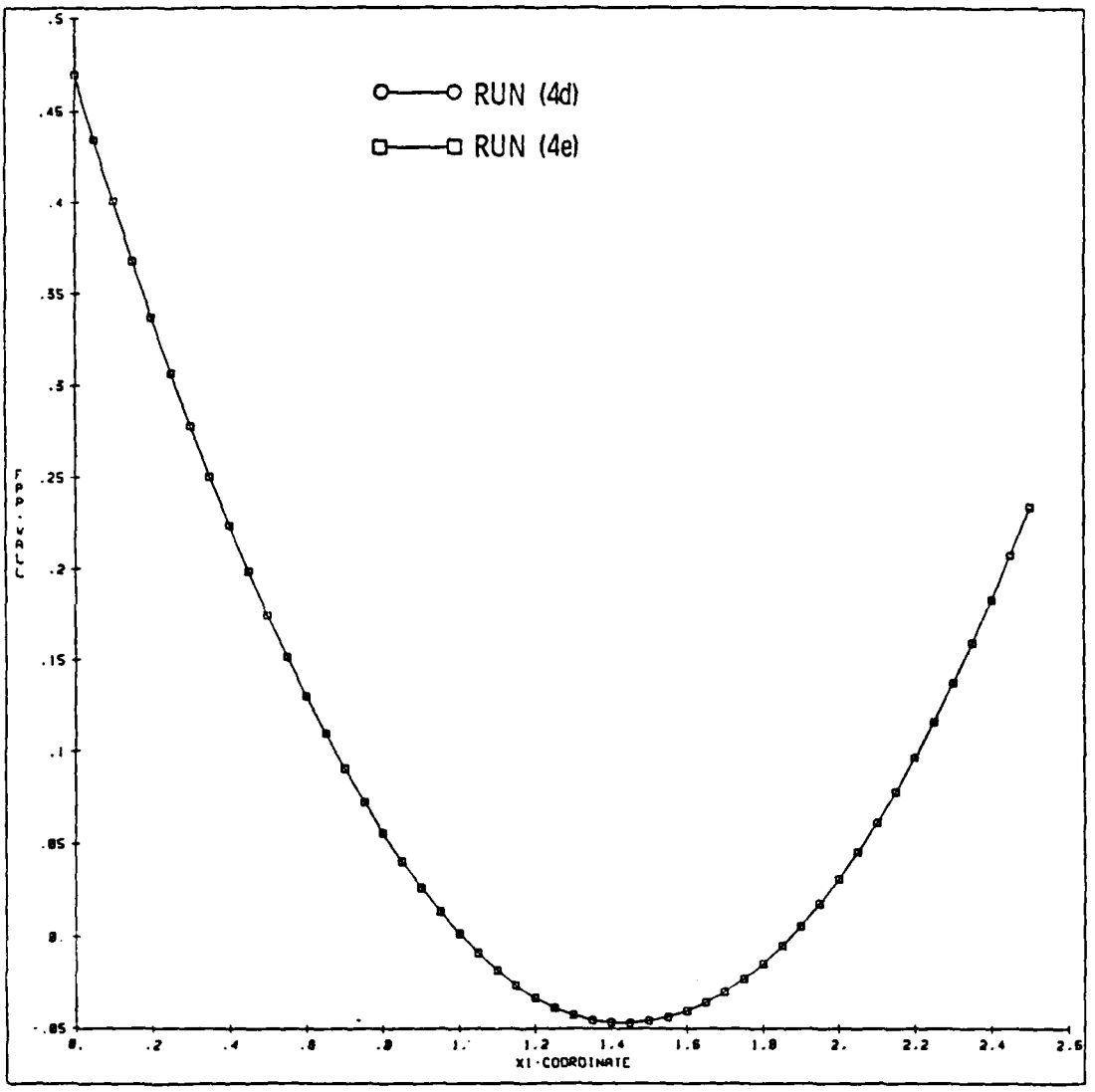

Figure 19. Comparison of f_w'' for Displacement Thickness Options for Case 4.

Computed values of f_w'' are compared in Figures 17, 18, and 19. In Figure 17, the skin friction coefficient and displacement thickness methods are compared. Again the curves show minor but acceptable differences between the methods, particularly in the latter half of the domain. The results of the skin friction coefficient method, however, exactly match the exact values of f_w'' as specified in run (4a). Figure 18 compares the skin friction coefficient runs, with no deviation between results, ignoring the small fluctuation near the starting solution. Figure 19 shows similar agreement for the displacement thickness runs.

3.1.5 Analytic Displacement Thickness Distribution

Carter [13] developed an algebraic distribution of the untransformed displacement thickness $\delta^*\sqrt{Re}$, which matches the flat plate displacement thickness at the start and end of the distribution and reaches a maximum value at a specified interior location. Carter uses this distribution to test a forward matching scheme with FLARE as well as a global iteration scheme. Cebeci, Keller, and Williams [7] use the same distribution to test the marching solution with the iterative DUIT procedure for separation bubbles. The distribution as given by Cebeci et al. [7] is (with errors corrected):

$$\bar{\delta}^*(x) = \sqrt{Re}\ \delta^*(x) = \begin{cases} 1.7208(x)^{1/2} & 1 \le x \le x_1 \\ a_1 + a_2(x-x_1) + a_3(x-x_1)^2 + a_4(x-x_1)^3, & x_1 \le x \le x_2 \\ \hat{a}_1 + \hat{a}_2(x-x_2)^2 + \hat{a}_3(x-x_2)^3, & x_2 \le x \le x_3 \end{cases}$$

where

$$a_1 = 1.7208(x_1)^{1/2} \quad , \quad a_2 = (0.5)\ (1.7208)/(x_1)^{1/2}$$

$$a_3 = \frac{1}{(2\Delta_1)} \left[\frac{6}{\Delta_1} (\bar{\delta}^*_{max} - a_o) - 4a_1\right]$$

$$a_4 = \frac{2}{(\Delta_1^3)} \left[\frac{a_2 \Delta_1}{2} - (\bar{\delta}^*_{max} - a_1)\right]$$

$$\bar{a}_1 = \bar{\delta}^*_{max}$$

$$\bar{a}_2 = -\left(\frac{1}{\Delta_2^2}\right) [3(\bar{\delta}^*_{max} - 2.25)]$$

$$\bar{a}_3 = \left(\frac{1}{\Delta_2^3}\right) [2(\bar{\delta}^*_{max} - 2.25)]$$

$$\Delta_1 = x_2 - x_1, \; \Delta_2 = x_3 - x_2$$

$$x_1 = 1.065, \; x_2 = 1.35, \; x_3 = 1.884 \; .$$

Figure 20 displays the resulting distributions for $\bar{\delta}^*_{max} = 5.6$ and $\bar{\delta}^*_{max} = 8.6$.

Figure 21 gives a comparison between the input displacement thickness distribution and the generated distribution from run (5a), specifying $\bar{\delta}^*$, and run (5e), specifying $C_{f_\infty} \sqrt{Re}$. The agreement between the displacement thickness solution and the exact distribution is quite good overall but overshoots where the distribution matches the flat plate value downstream. The skin friction case provides correct results while the flow remains attached, but degenerates rapidly upon separation and fails inside the separation bubble. The cause of this failure, in light of the apparent successful calculation for the Horton parabolic distribution [10], will be discussed in the following chapter.

The skin friction distribution resulting from run (5a) is compared with computational results of Carter [13] and Cebeci et al. [7] in Figure

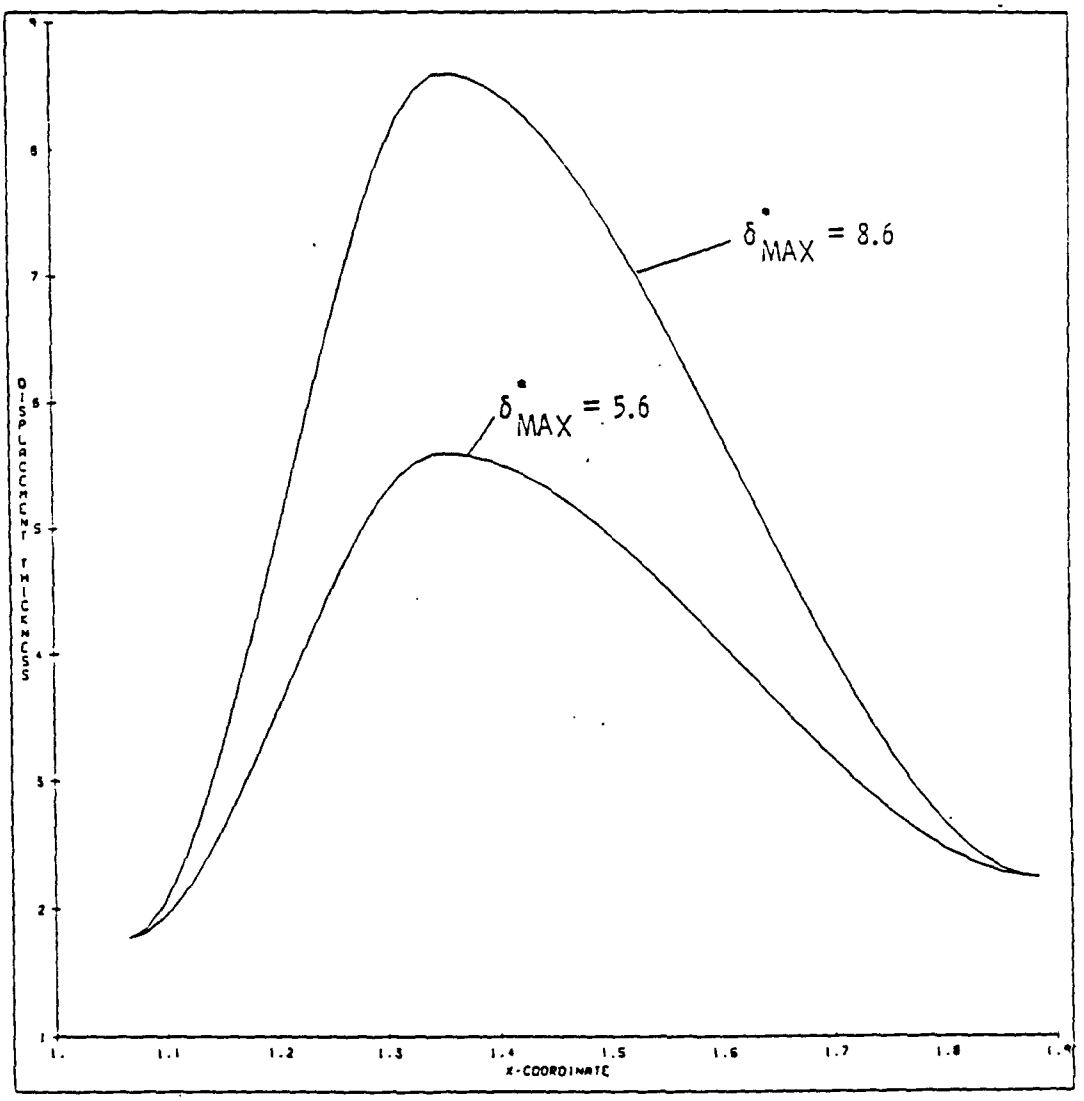

Figure 20. Analytic $\delta^* \sqrt{Re}$ Distributions for Case 5.

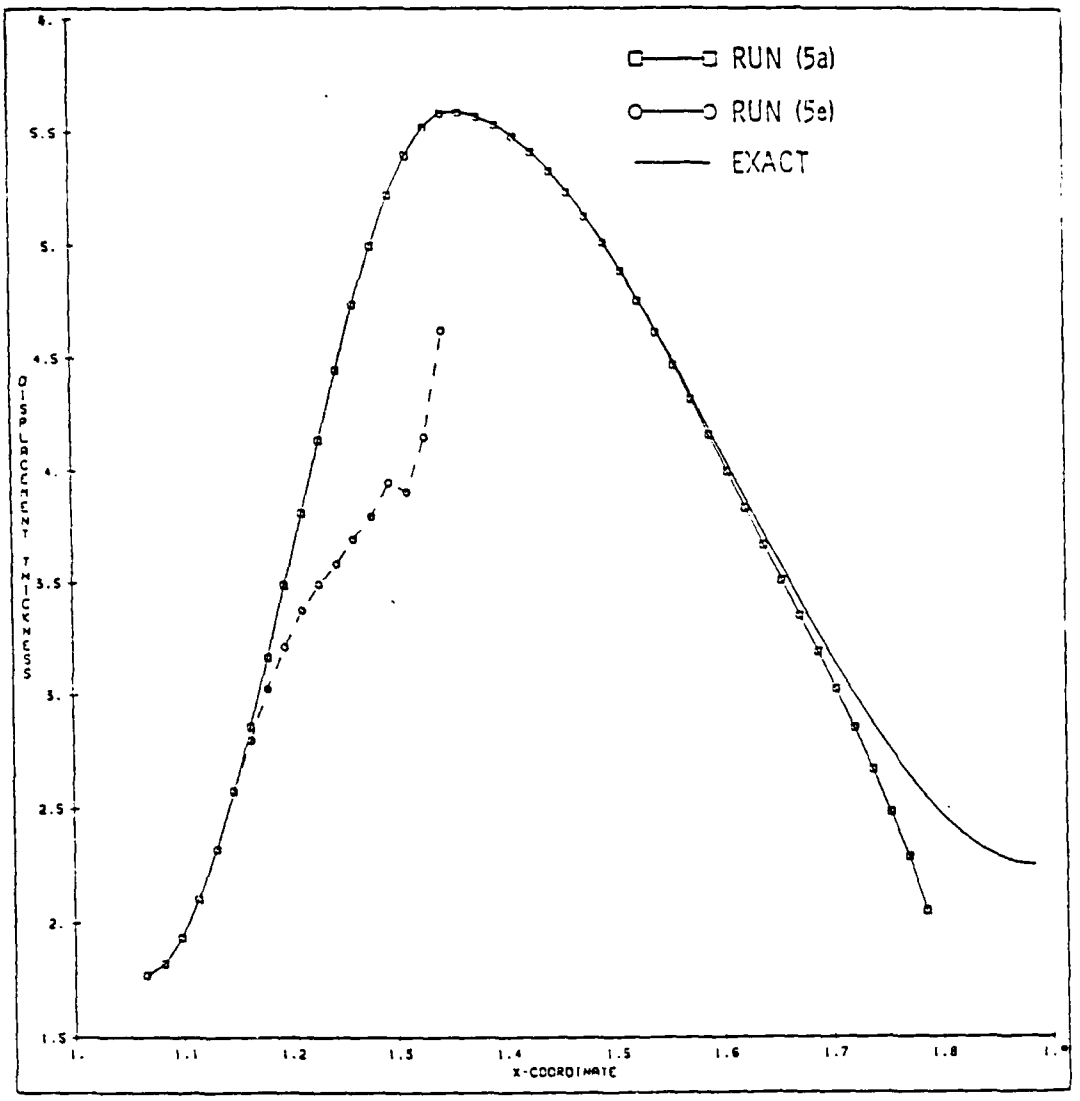

Figure 21. Comparison of δ^*, $\overline{Re}$ from Inverse Methods with Exact Distribution for Case 5 ($\delta^*_{max} = 5.6$).

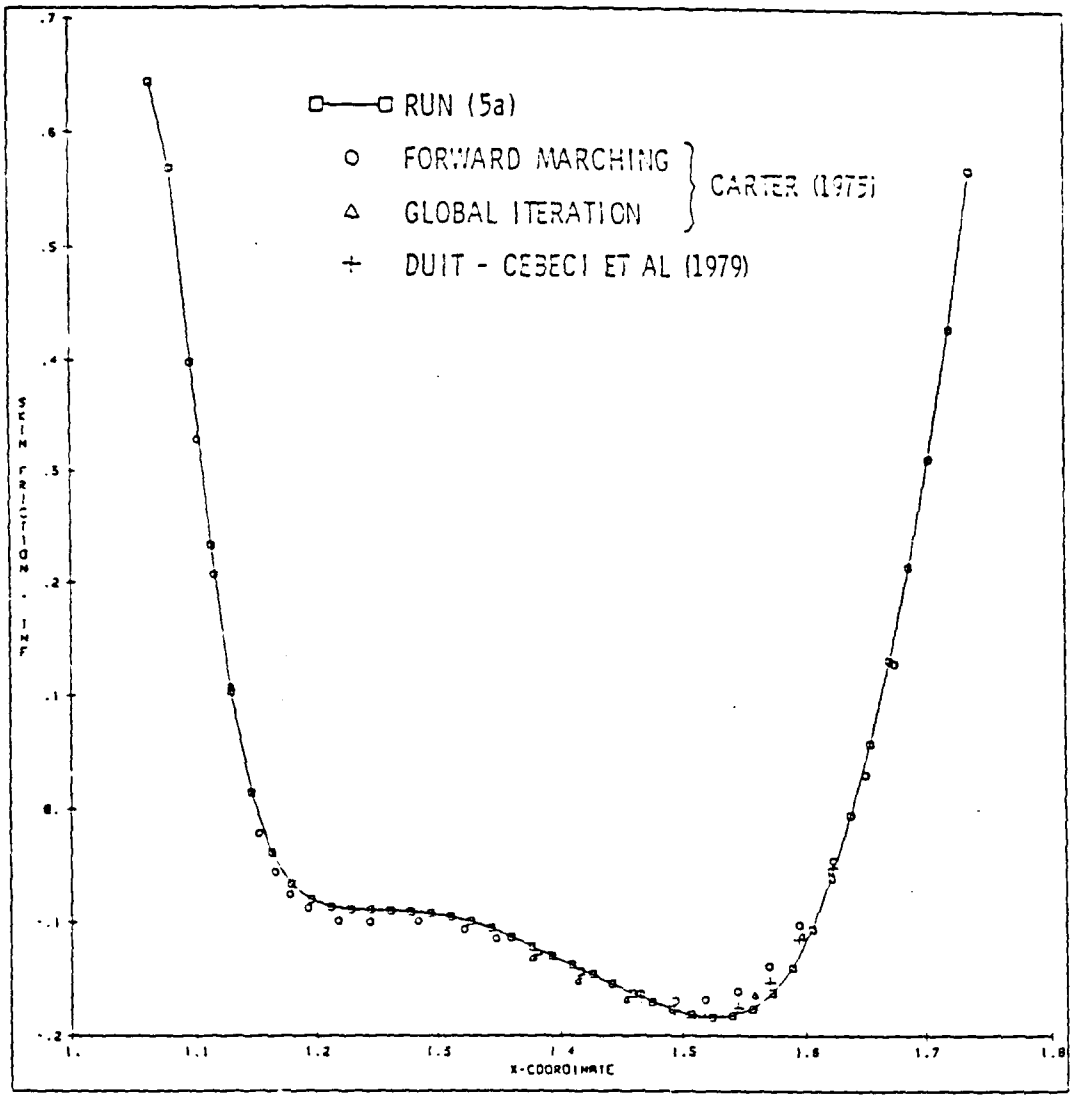

Figure 22. Comparison of $C_{f_\infty}\sqrt{Re}$ from Displacement Thickness Option with References 7 and 13 for Case 5 ($\delta^*_{max} = 5.6$).

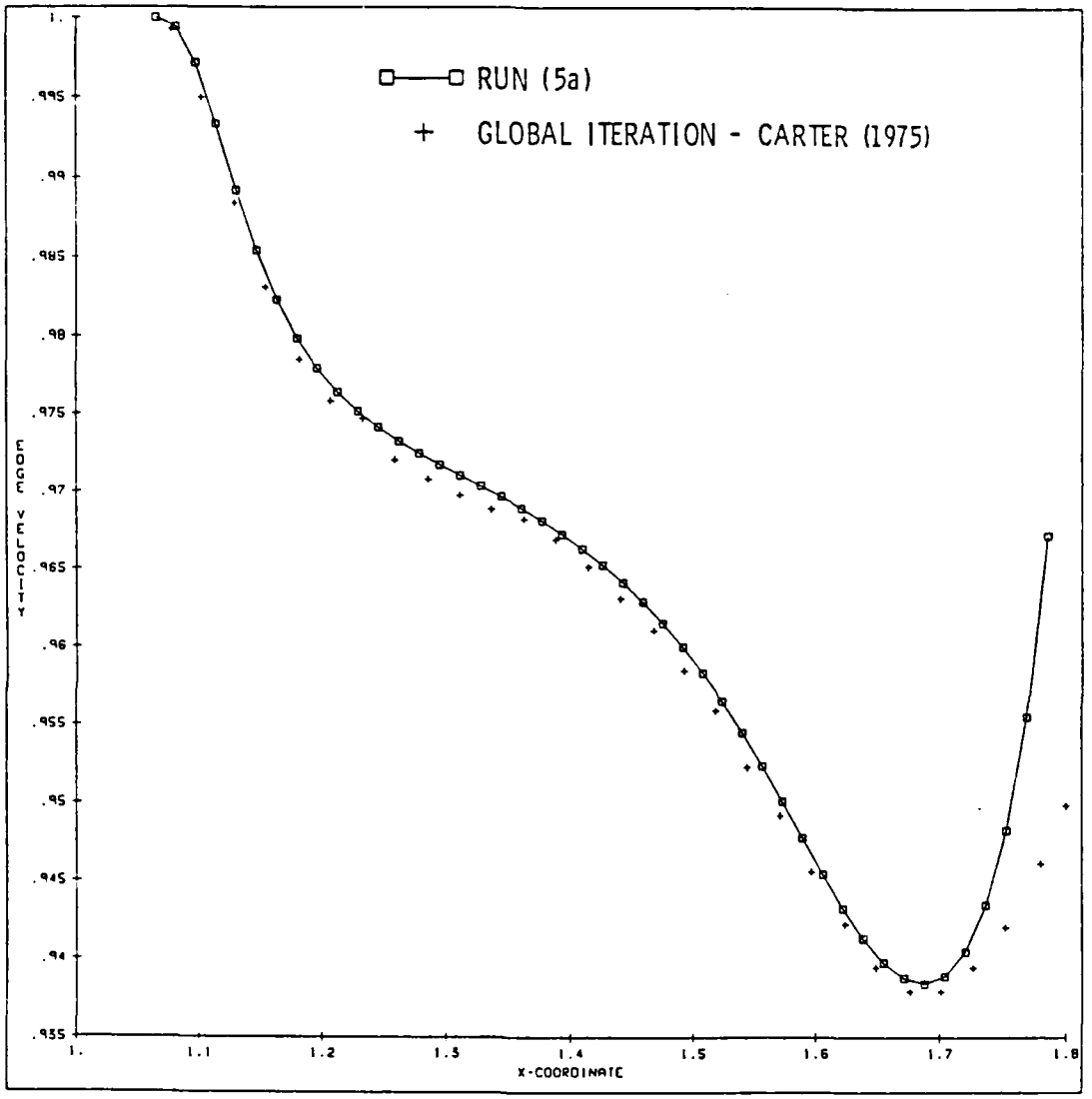

Figure 23. Comparison of u_e from Displacement Thickness Option with Reference 13 for Case 5 ($\delta^*_{max} = 5.6$).

22. The agreement within the region of separation is particularly good, with the present method matching the global iteration results of Carter and the DUIT procedure of Cebeci et al. more closely than the forward marching results of Carter. Figure 23 compares the edge velocity distribution for the same case with the global iteration results of Carter. Again, the comparison is quite good, although the region of overshoot is clearly identifiable following reattachment.

Figure 24 displays two computational runs, (5b) and (5c) for the analytic $\bar{\delta}^*$ distribution where $\bar{\delta}^*_{max} = 8.6$. Run (5b) was made with three-point backward differences, as was run (5a). For the larger displacement thickness case, however, it was necessary to switch to two-point backward differences upon separation to obtain an accurate solution. Using two-point backward differences, the solution matches the analytic $\bar{\delta}^*$ distribution very well, although the overshoot behavior is still apparent past x=1.7. For this case, the overshoot causes the solution to diverge near x=1.8. This behavior following reattachment is discussed later in this section and in Chapter 4.

A comparison of $C_{f_\infty}\sqrt{Re}$ distributions is made in Figure 25. From the present study, we compare displacement thickness method results with three-point, three/two-point combination, and two-point backward differences. The three-point backward difference result diverges rapidly following separation. The three/two-point combination and the two-point backward difference runs are essentially identical. These results are compared with forward marching and global iteration results from Carter [13] and forward marching results with DUIT from Cebeci et al. [7]. Again, the present results match the global iteration or DUIT results more closely than the forward marching results with FLARE provided by

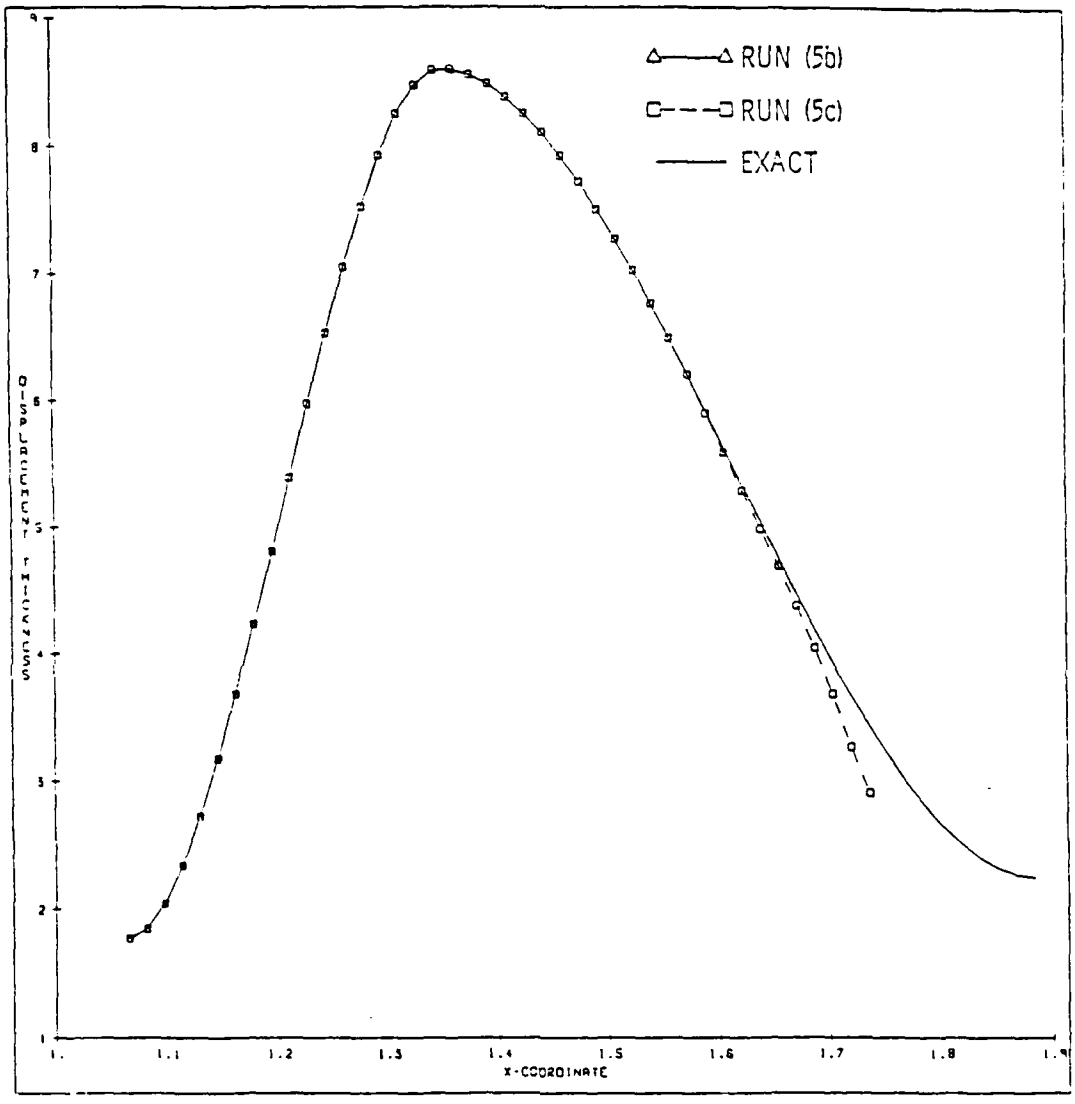

Figure 24. Comparison of $\delta^* \sqrt{Re}$ from Displacement Thickness Option with Exact Distribution for Case 5 ($\delta^*_{max} = 8.6$).

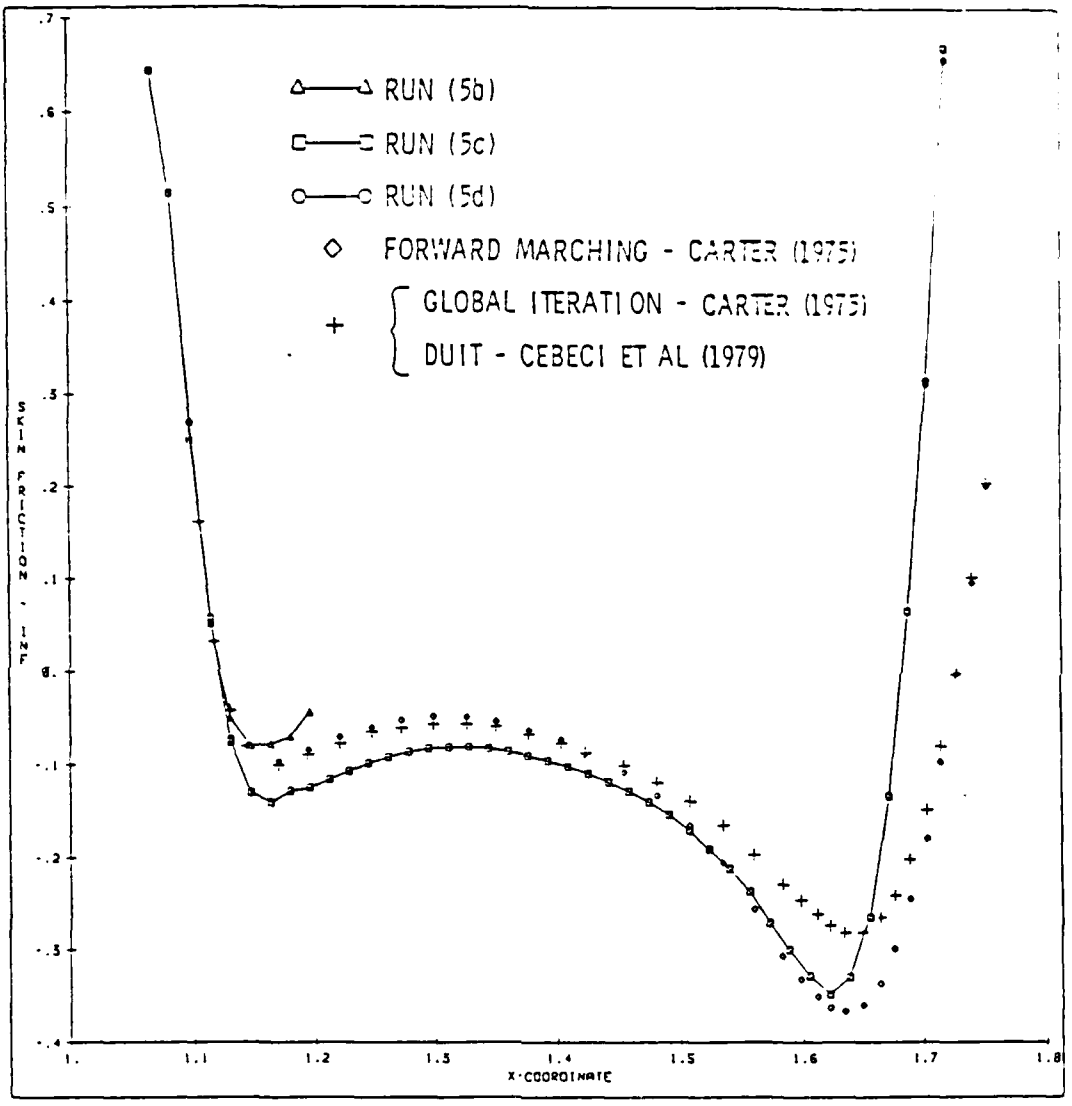

Figure 25. Comparison of $C_{f_\infty}\sqrt{Re}$ from Displacement Thickness Option with References 7 and 13 for Case 5 ($\delta^*_{max} = 8.6$).

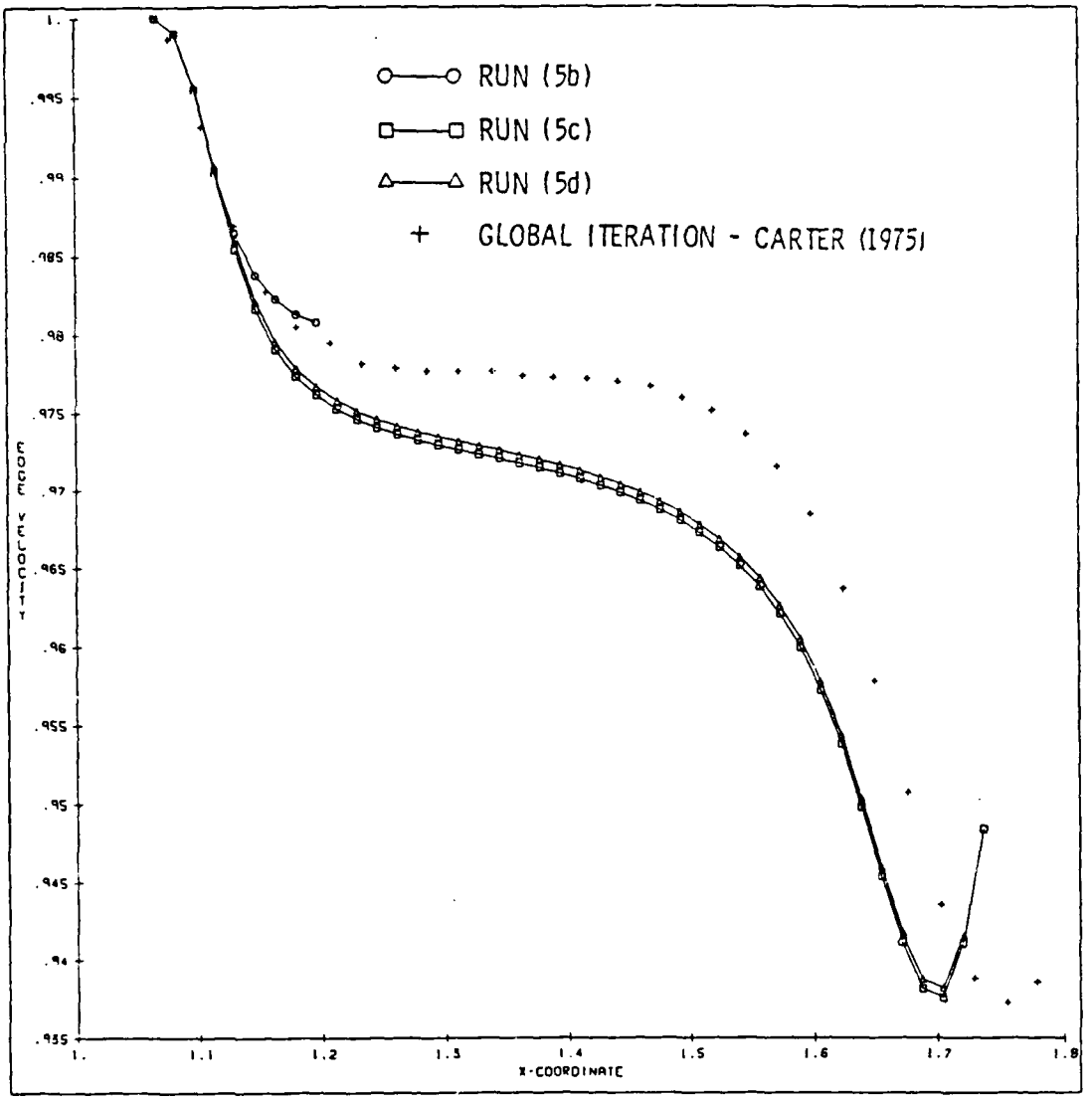

Figure 26. Comparison of u_e from Displacement Thickness Option with Reference 13 for Case 5 ($\delta^*_{max} = 8.6$).

Carter. The overshoot behavior is also more evident here than in run (5a). The edge velocity distribution from the same runs is compared with Carter's global iteration results in Figure 26. Here, the calculations of the present method fall slightly below the results of Carter, but only by approximately one percent. The overshoot behavior is very apparent downstream of x=1.6, shifting the minimum value of u_e upstream approximately 0.05 units.

The suspected cause of the overshoot behavior is streamwise discretization error. To study this effect, the number of streamwise points was doubled, and the cases rerun. Figures 27 and 28 display the results for the two maximum displacement thickness values. In both cases, and particularly for $\bar{\delta}^*_{max} = 8.6$, there is a marked improvement over the original results.

Figure 29 shows the remarkable improvement obtained with the decrease in streamwise stepsize for the skin friction results. The results of run (5g) match the global iteration and DUIT results much more closely than before, with only minor overshoot evident compared to the initial run with 50 streamwise grid points. Figures 30 and 31 show similar results for the edge velocity distribution, again with the most improvement shown for the case where $\bar{\delta}^*_{max} = 8.6$. Although there is still a slight upstream shift near reattachment evident in Figure 31, the decrease in stepsize dramatically effected the results throughout the domain.

A series of plots are also included here detailing the streamwise velocity profile as the solution marches downstream through separation for run (5a). Figures 32 a-c show velocity profiles from the separation

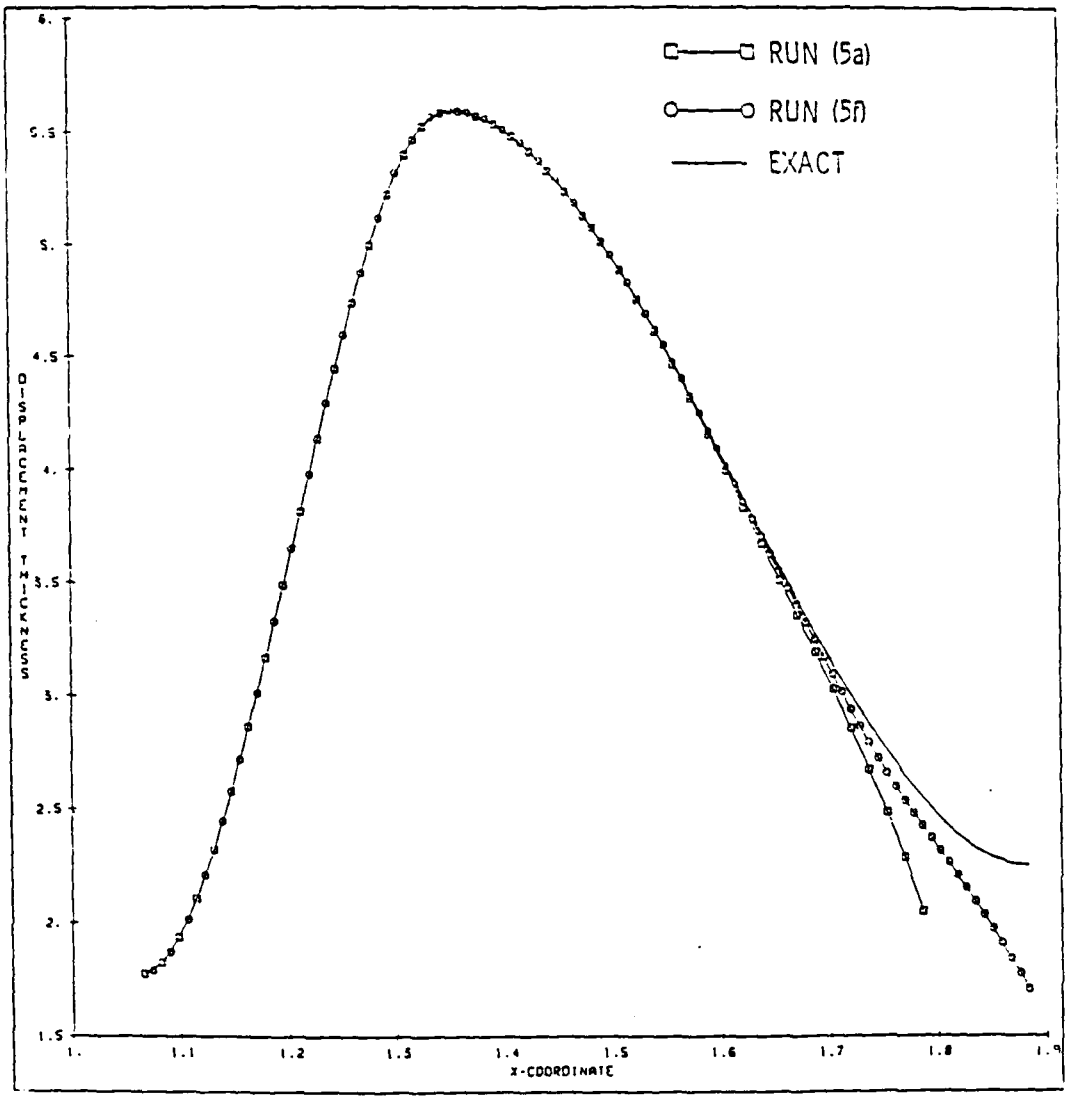

Figure 27. Effect of Streamwise Stepsize Reduction. Comparison of $\delta^* \sqrt{Re}$ for Case 5 ($\delta^*_{max} = 5.6$).

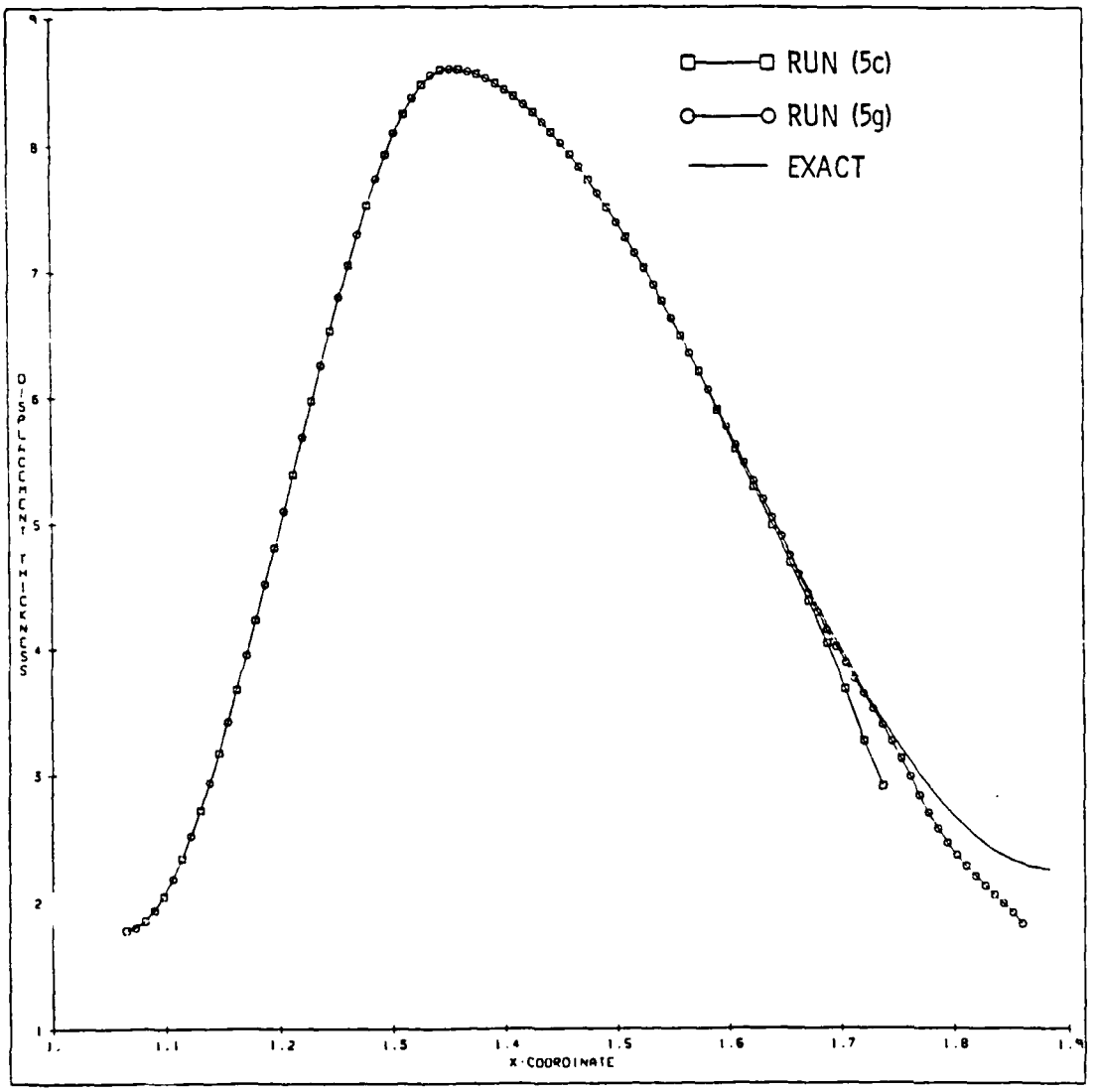

Figure 28. Effect of Streamwise Stepsize Reduction. Comparison of $\delta^* \sqrt{Re}$ for Case 5 ($\delta^*_{max} = 8.6$).

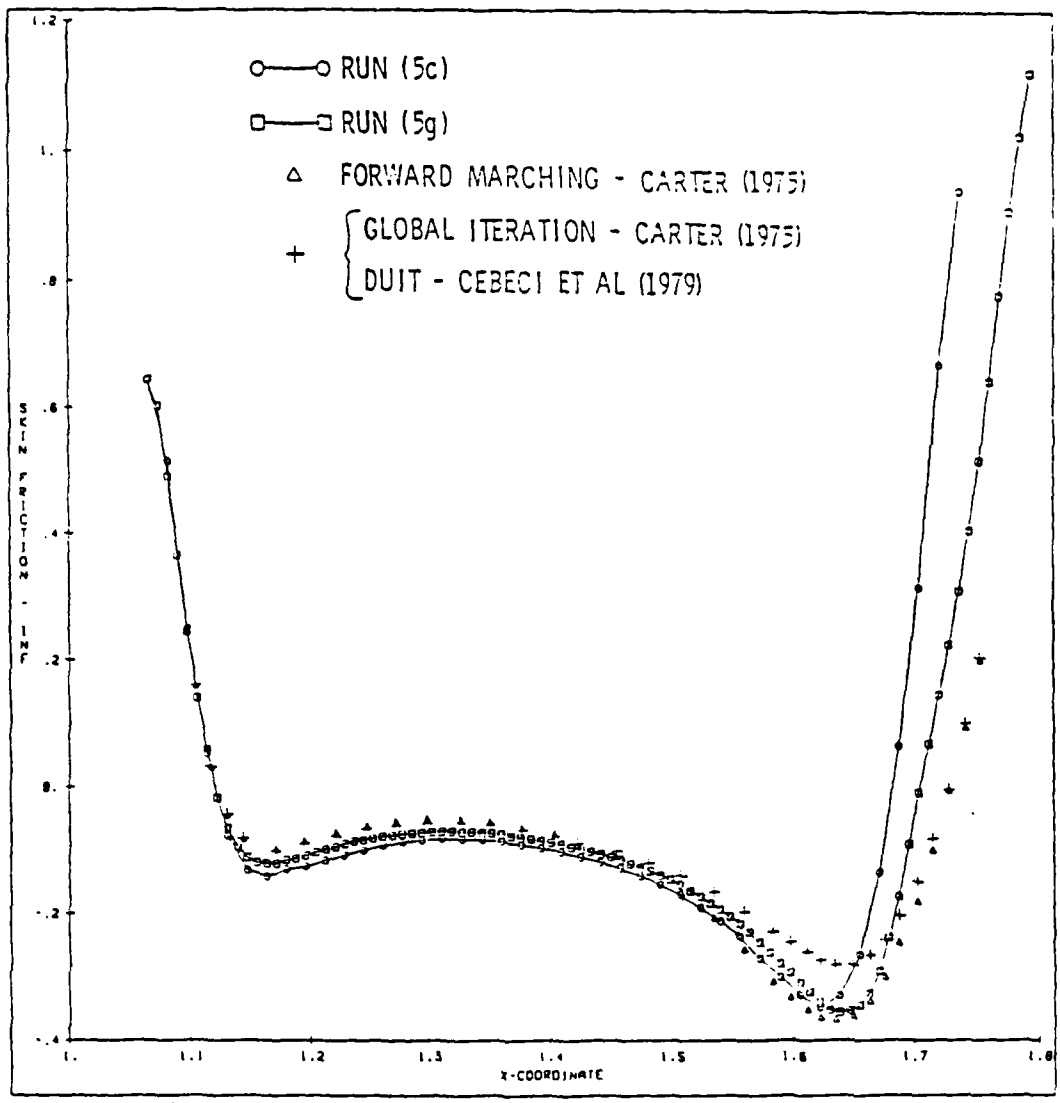

Figure 29. Effect of Streamwise Stepsize Reduction. Comparison of $C_{f_\infty}\sqrt{Re}$ for Case 5 ($\delta^*_{max} = 8.6$).

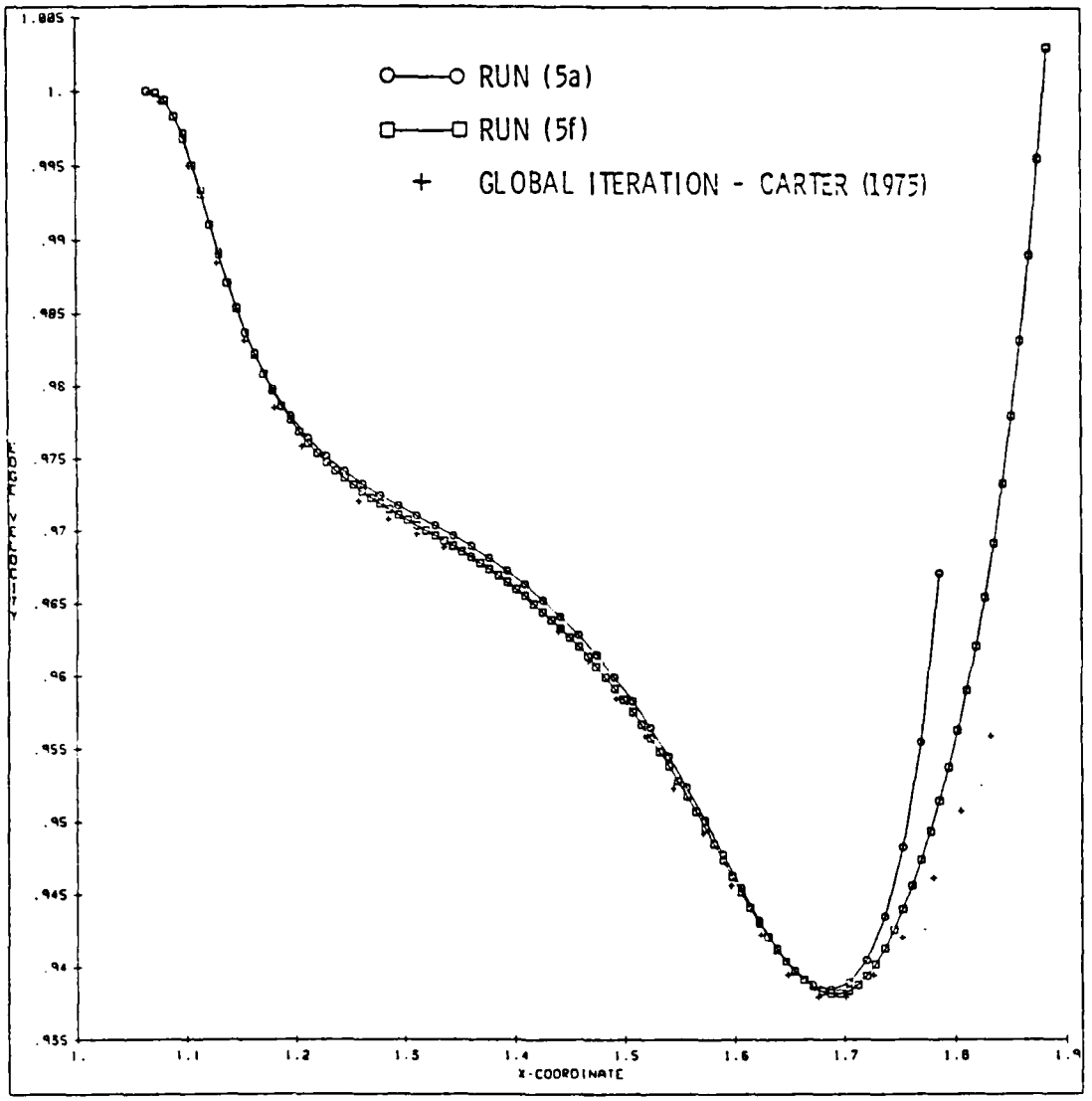

Figure 30. Effect of Streamwise Stepsize Reduction. Comparison of u_e for Case 5 (δ^*_{max} = 5.6).

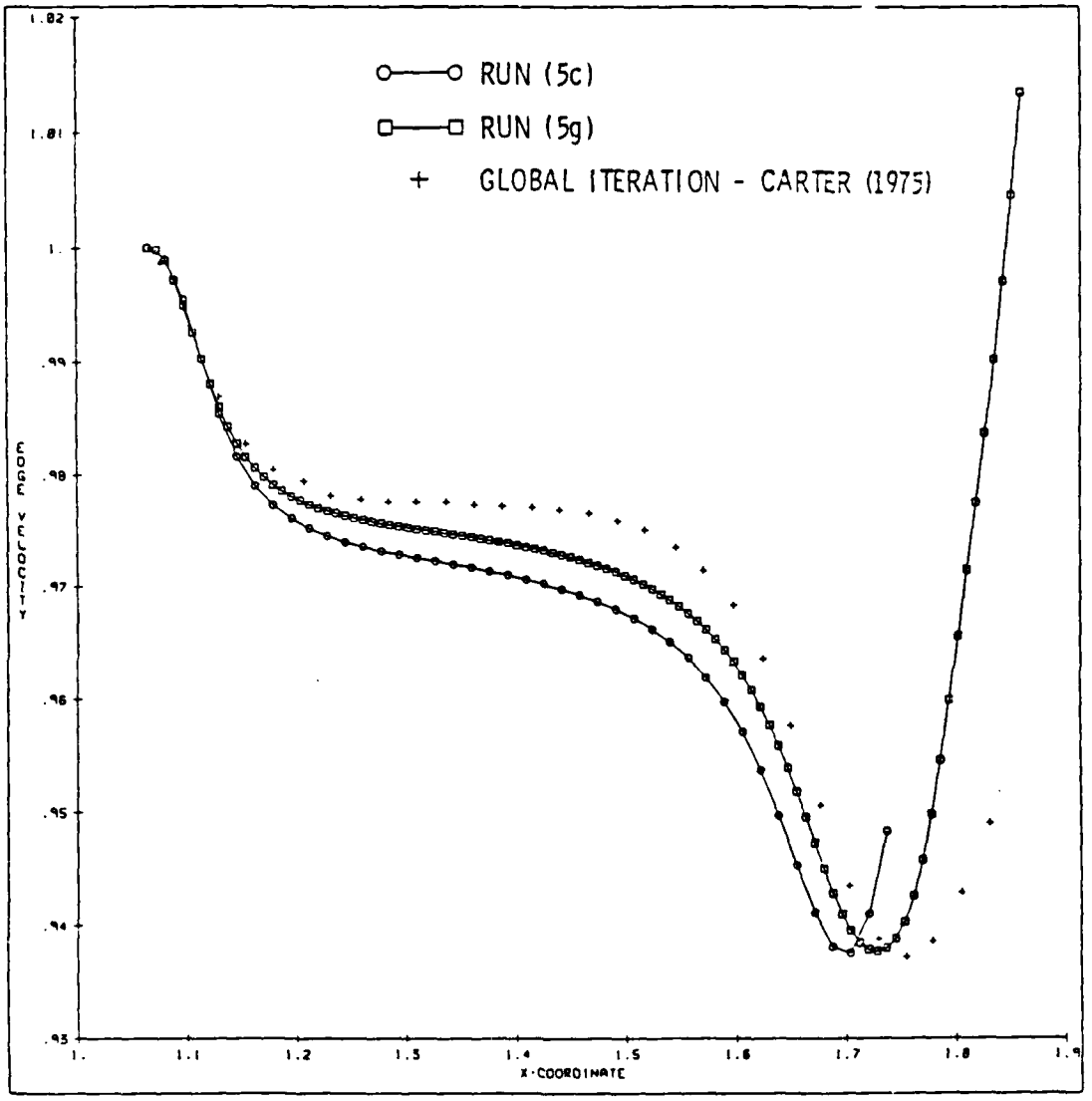

Figure 31. Effect of Streamwise Stepsize Reduction. Comparison of u_e for Case 5 (δ^*_{max} = 8.6).

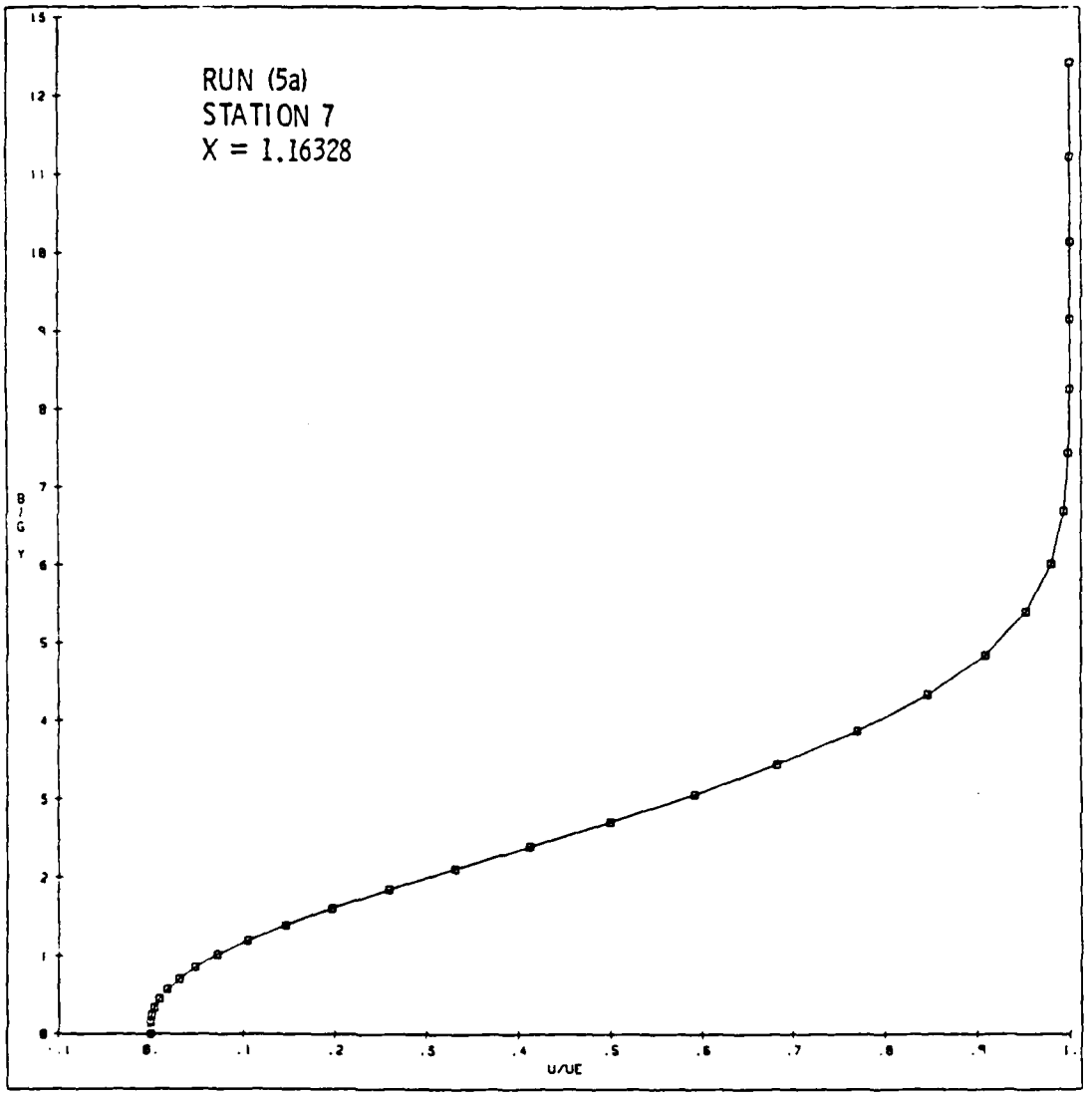

Figure 32. Separation Sequence. Streamwise Velocity Profiles at Three Streamwise Stations for Case 5 (δ^*_{max} = 5.6).

(a) Station 7

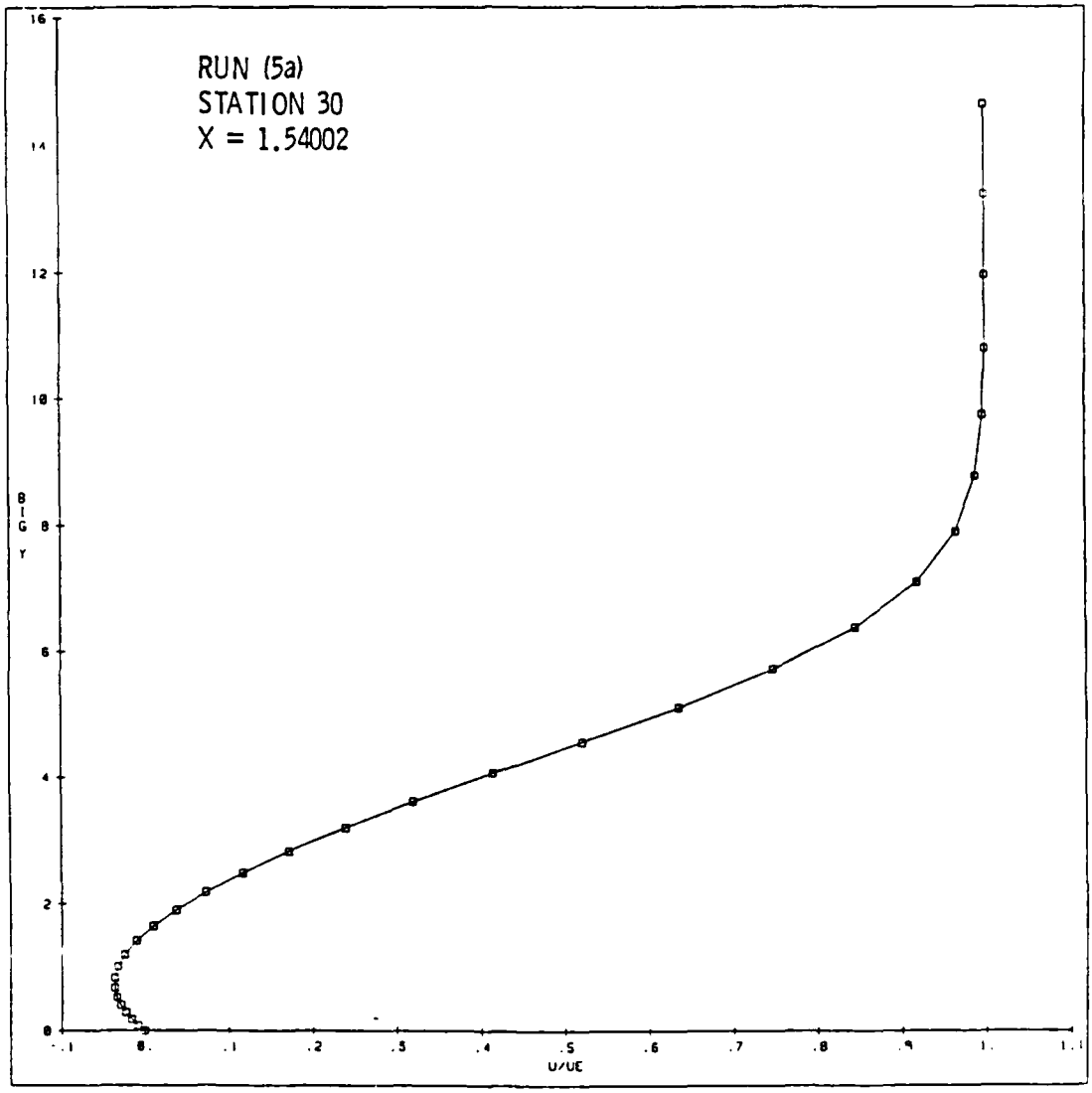

Figure 32. Separation Sequence. Streamwise Velocity Profiles at Three Streamwise Stations for Case 5 (δ^*_{max} = 5.6).

(c) Station 30

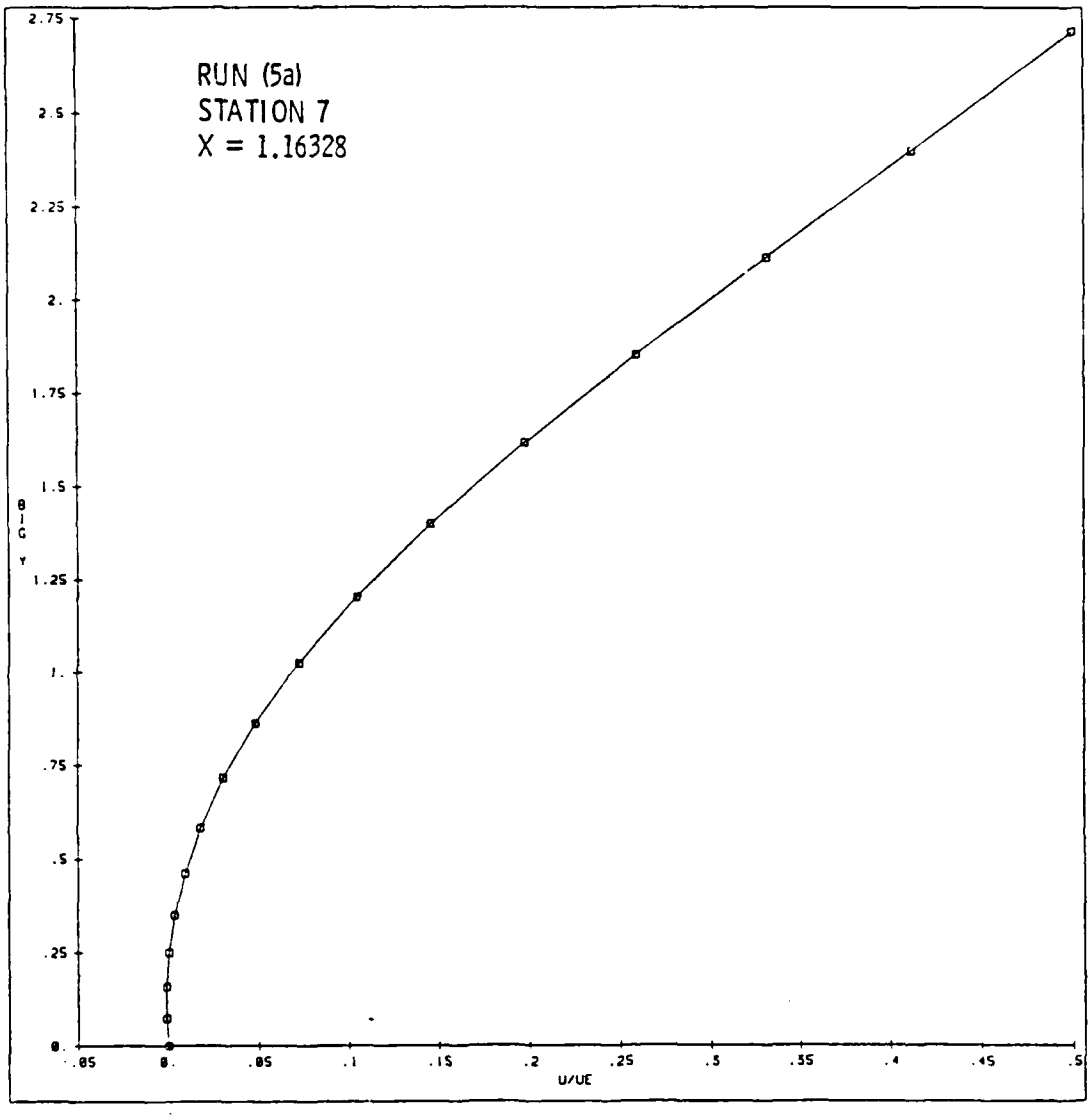

Figure 33. Wall Region Detail of Separation Sequence. Streamwise Velocity Distribution at Three Streamwise Stations for Case 5 (δ^*_{max} = 5.6).

(a) Station 7

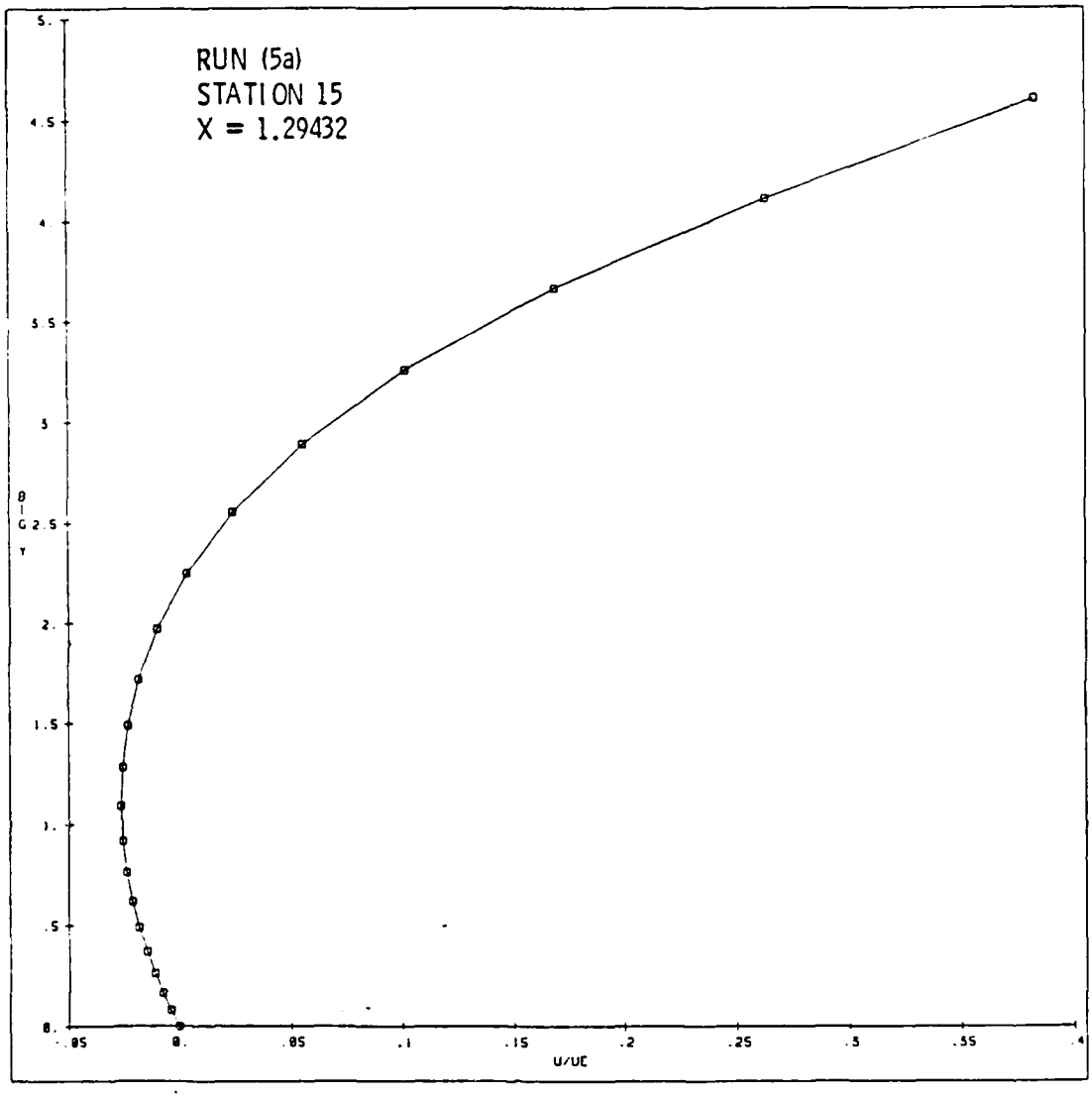

Figure 33. Wall Region Detail of Separation Sequence. Streamwise Velocity Distribution at Three Streamwise Stations for Case 5 (δ^*_{max} = 5.6).

(b) Station 15

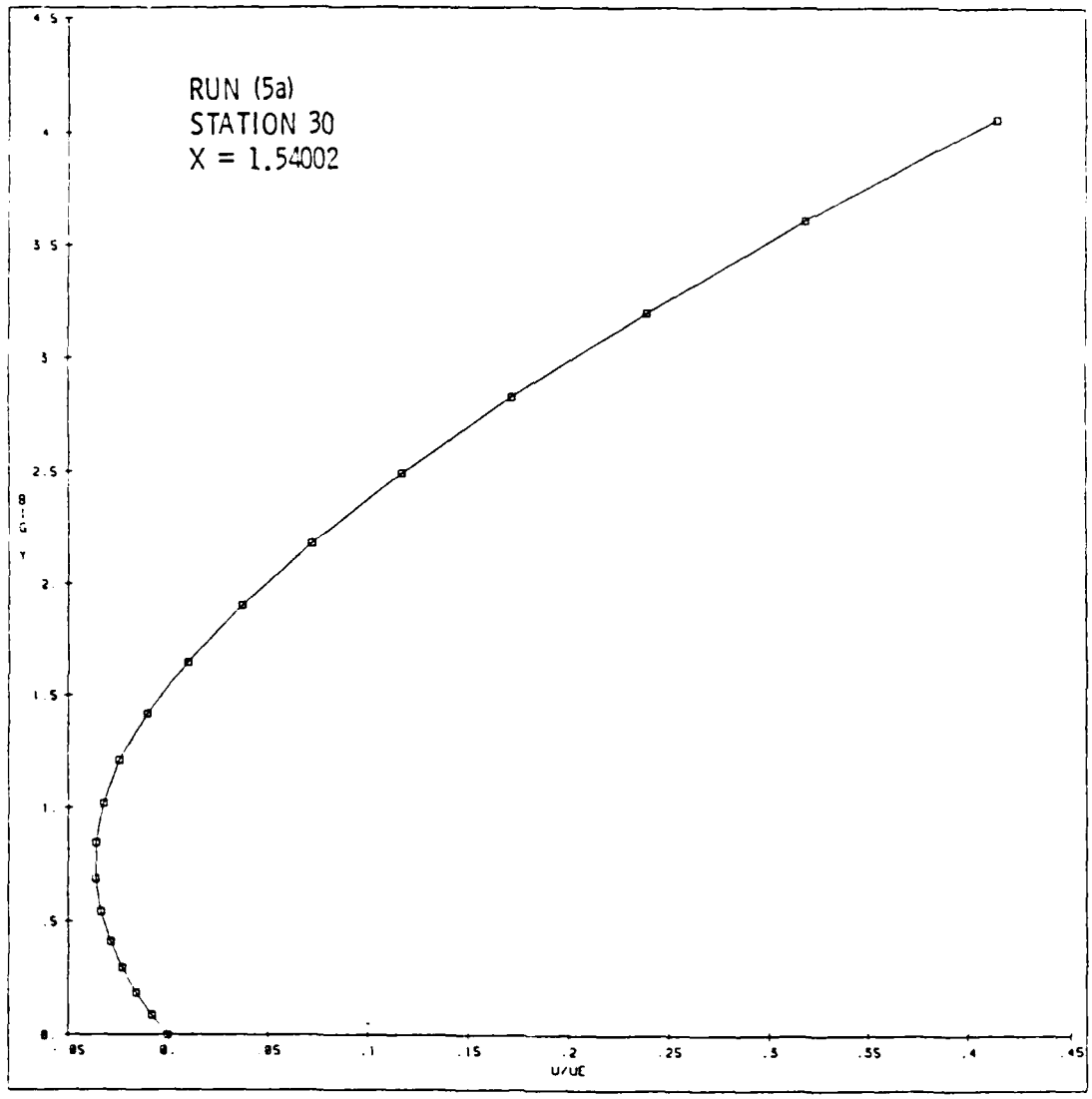

Figure 33. Wall Region Detail of Separation Sequence. Streamwise Velocity Distribution at Three Streamwise Stations for Case 5 (δ^*_{max} = 5.6).

(c) Station 30

point to the maximum negative value of f_w''. Figures 33 a-c provide detailed views of the backflow regions of the same profiles.

3.1.6 Horton Displacement Thickness Distribution

An inverse case using the experimental data of Ntim, as given by Horton [11], and the computational data of Horton from the same reference, was attempted using the displacement thickness method. The original data gathered by Ntim was obtained by placing a circular cylinder over a flat plate to alter the pressure distribution and cause separation. Following Horton, the direct method was used to generate a displacement thickness distribution to a location near separation. The experimental $\delta^* \sqrt{Re}$ distribution of Ntim was then fitted to the computational distribution so that a complete inverse solution could be obtained. Figure 34 shows the $\delta^* \sqrt{Re}$ distribution, resulting from the direct solution and the matched experimental/computational distribution, used as input to the inverse method. Figure 35 is a detail of the direct distribution and the composite distribution around the matching point. The combined distributions are joined using a cubic spline interpolation routine.

Figure 36 displays the input $\delta^* \sqrt{Re}$ distribution with the generated $\delta^* \sqrt{Re}$ distributions from two inverse runs, (6b) and (6c). As was discovered in previous cases, two-point backward differences had to be used once the flow separated to obtain a solution into the separated zone. A noteworthy feature is the deviations between the input displacement thickness and the generated distribution near the matching point. A similar result is apparent in the edge velocity distribution, shown in Figure 37, which peaks above the edge velocity distribution used as input to the direct solution.

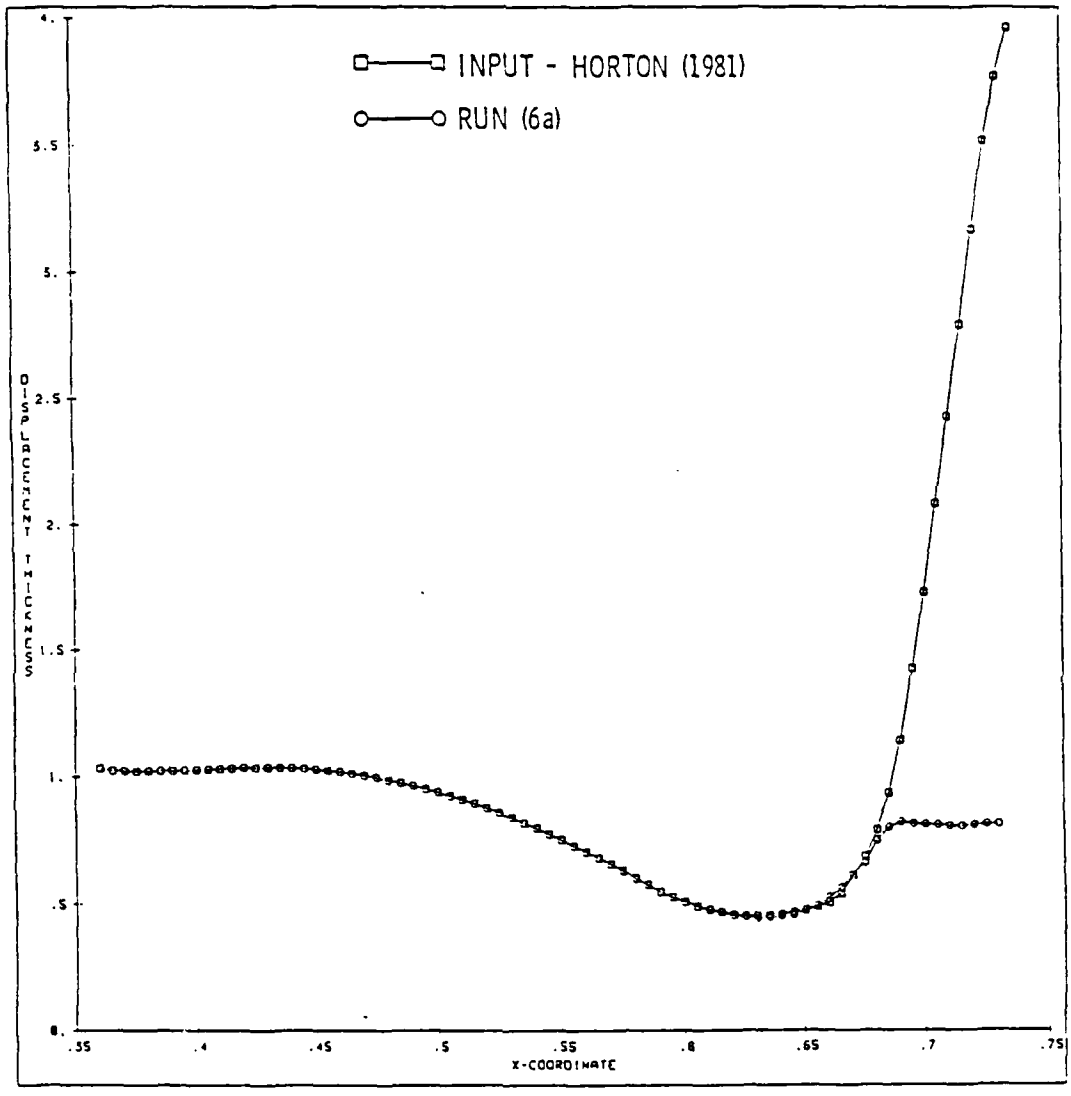

Figure 34. Comparison of $\delta^* \sqrt{Re}$ from Direct Method and Reference 11 for Case 6.

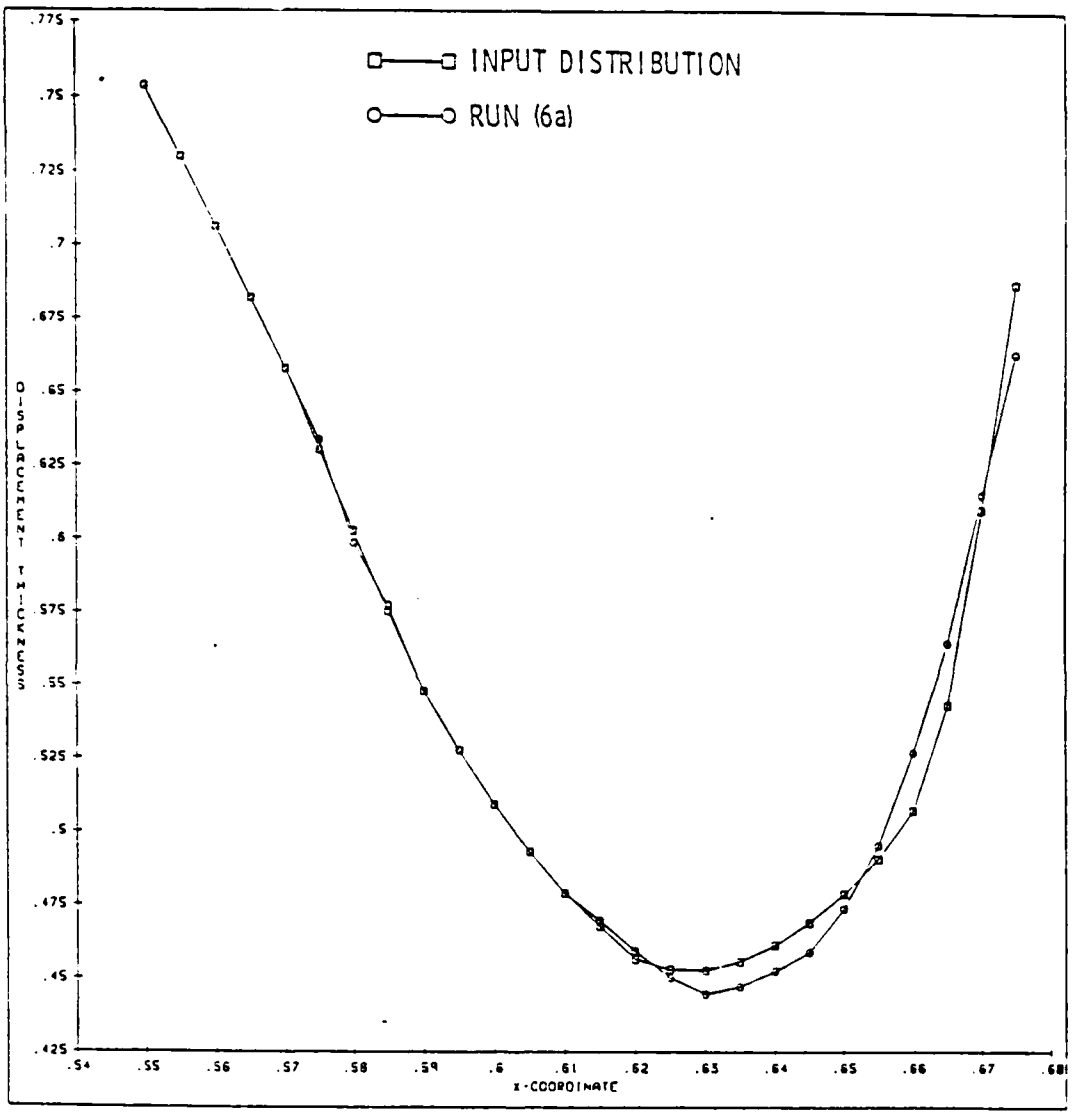

Figure 35. Detail of Comparison of $\delta^* \sqrt{Re}$ Distribution from Direct Method and Reference 11 for Case 6. Matching Region.

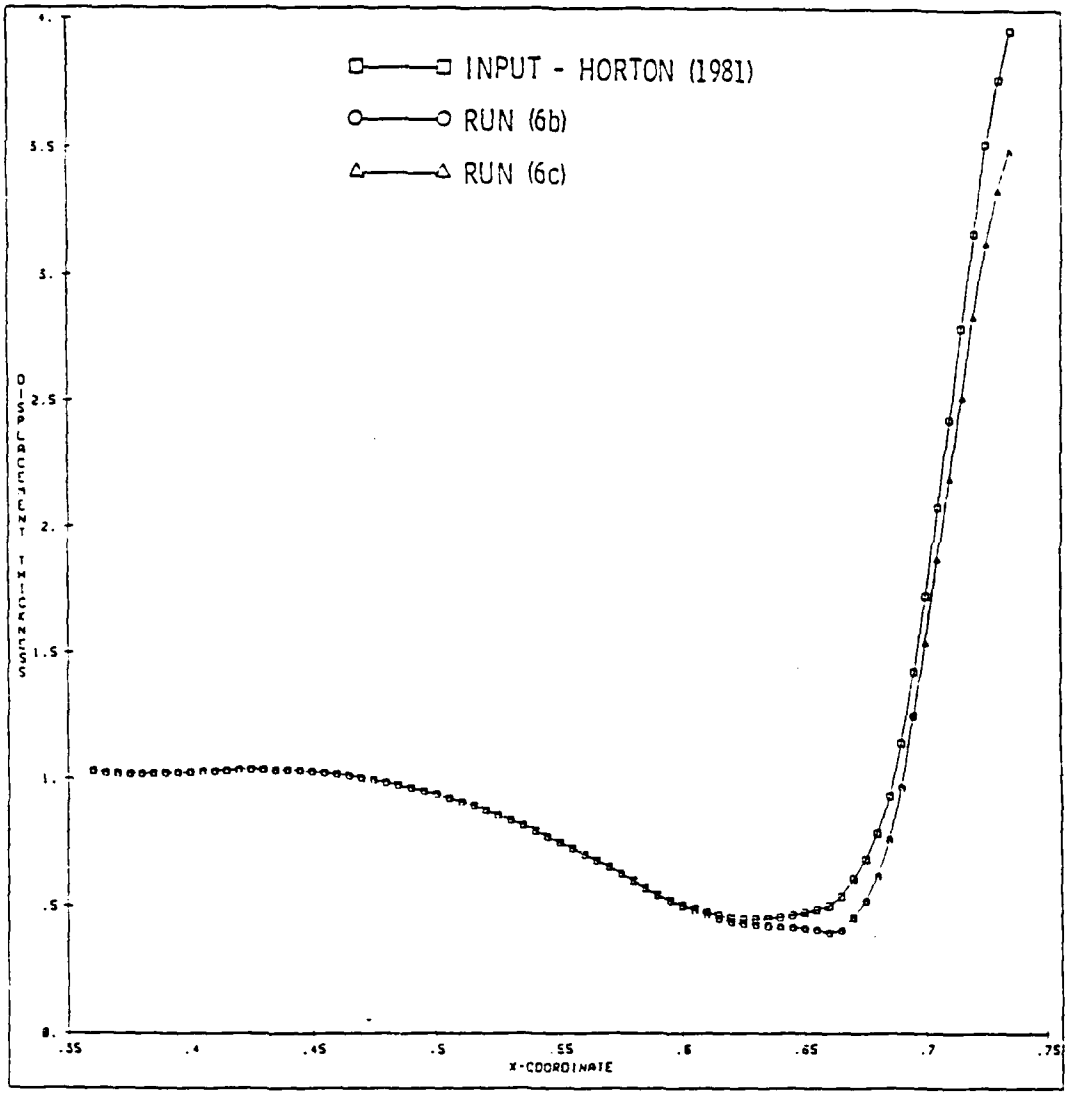

Figure 36. Comparison of $\delta^* \sqrt{Re}$ from Inverse Methods with Reference 11 for Case 6.

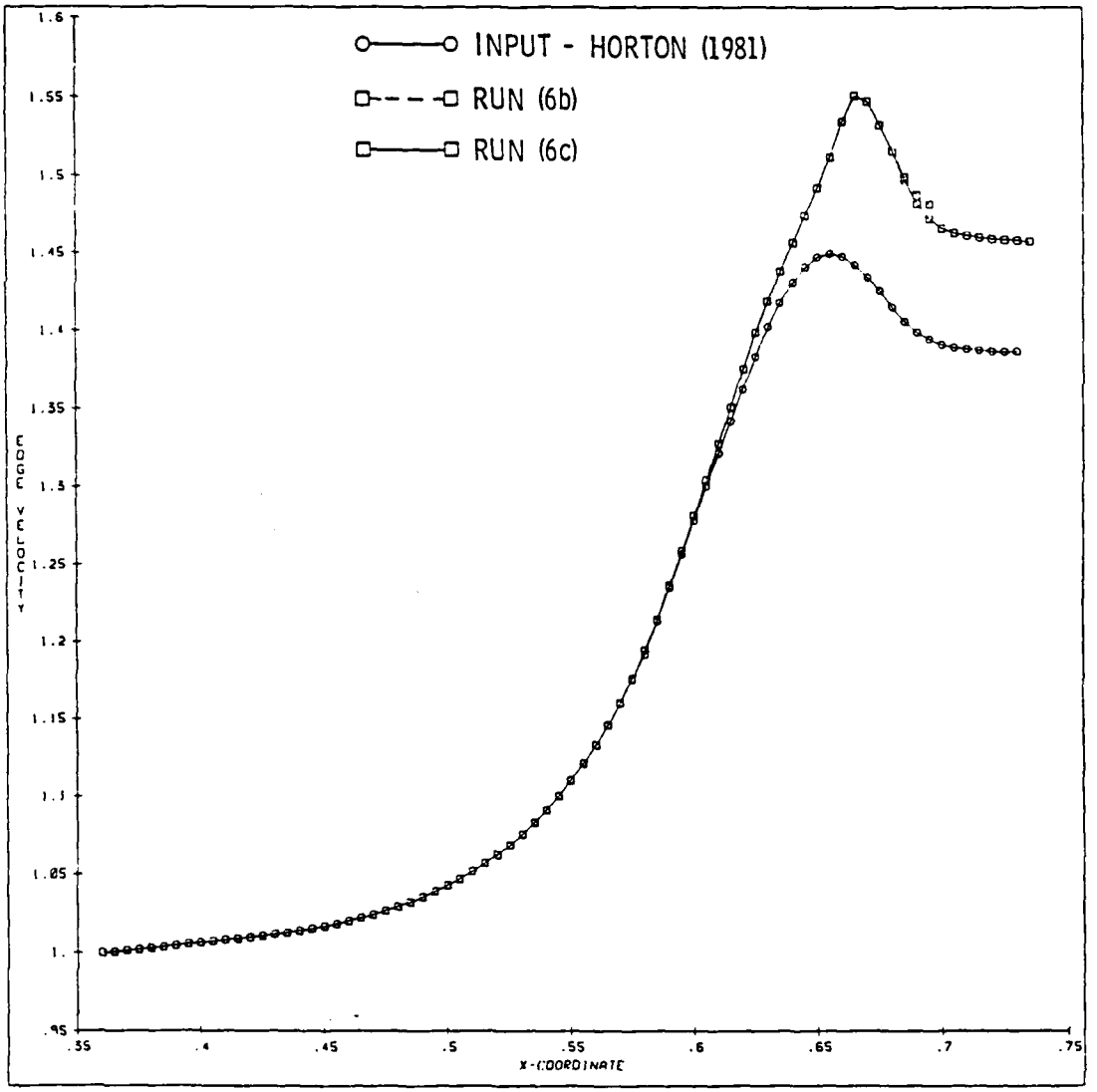

Figure 37. Comparison of u_e from Inverse Methods with Reference 11 for Case 6.

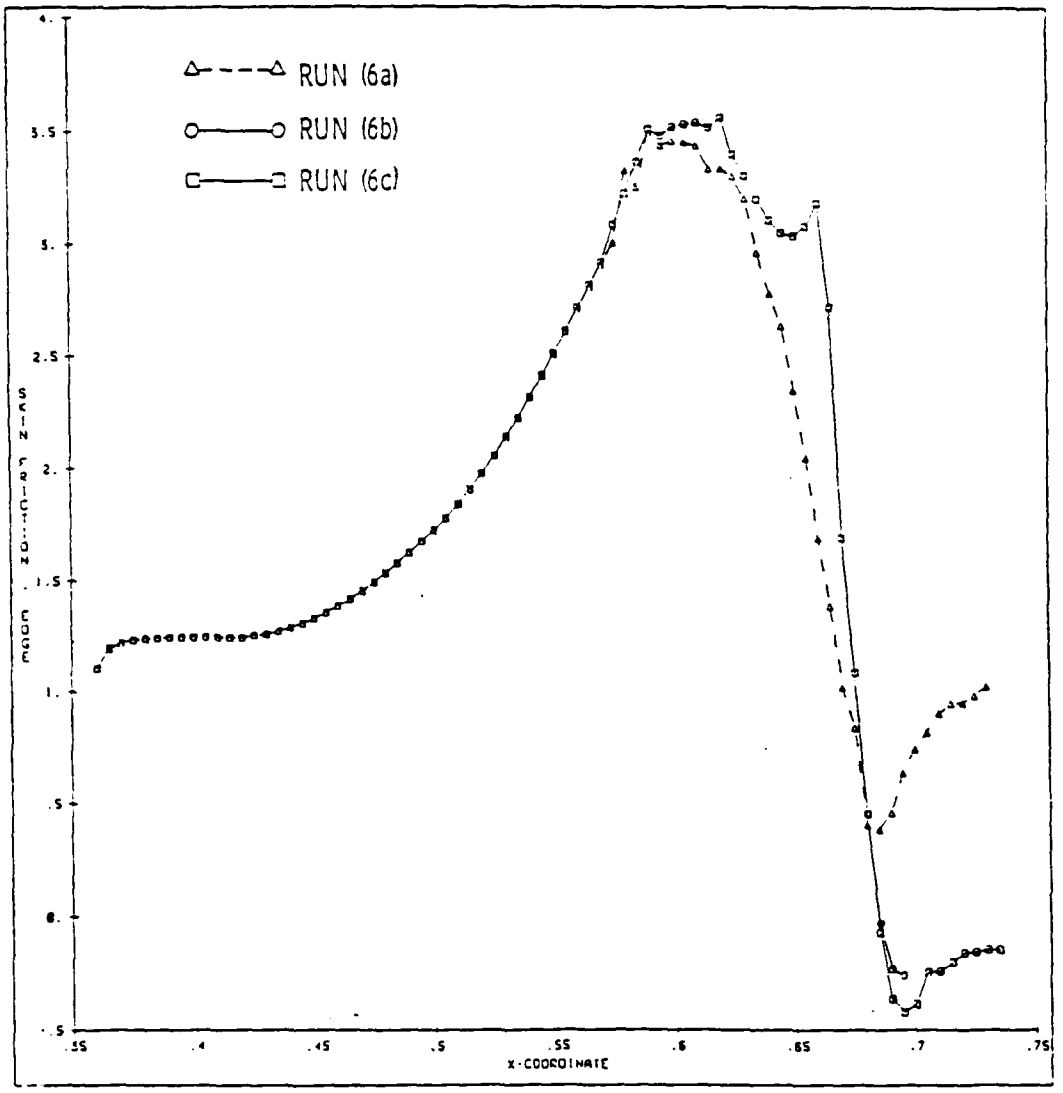

Figure 38. Direct and Inverse Distributions of $C_f \sqrt{Re}_e$ for Case 6.

The cause of this discrepancy becomes more apparent after considering the plot of skin friction coefficients in Figure 38. In this figure, several discontinuities are easily visible near the $\delta^*\sqrt{Re}$ distribution matching points. These peaks in $C_{f_e}\sqrt{Re}$ arise because only the displacement thickness was forced to be continuous at the matching points, and not its derivatives. This procedure was also used in obtaining the edge velocity distribution for the direct solution. Some evidence of the u_e distribution matching is evident in the skin friction coefficients generated by the direct solution. The inverse solution, however, appears to be much more sensitive to such matchings. The mismatched slopes affect the solution because the displacement thickness is related to the streamfunction. The discontinuities become apparent in the skin friction coefficient since C_{f_e} is a function of f_w'', the second derivative of the streamfunction, and differentiation tends to amplify any noise in the calculation procedure.

3.1.7 Klineberg-Steger Wall Shear Distribution

An analytic distribution of wall shear was devised by Klineberg and Steger [9] to test an inverse scheme which they developed. The distribution specifies $\hat{\tau}$, which is related to f_w'' by

$$f_w''(\xi) = \sqrt{\frac{2\xi}{u_e x}}\ \hat{\tau}(x) \quad .$$

The algebraic distribution is given by

$$\hat{\tau}(x) = \frac{0.332}{C_{KS}}(x-x_1)(x-x_2) = \hat{\tau}_1(x), \qquad 0 \le x \le x_1,\ x \ge x_2;$$

$$\hat{\tau}(x) = \hat{\tau}_1(x)[1 + \hat{\alpha}(x-x_1)(x-x_2)], \qquad x_1 \le x \le x_2.$$

Previous calculations show that the wall shear methods work well for some flow situations (Horton's parabolic shear distribution, subsection 3.1.4) but fail completely for other situations where they are expected to work (Carter's analytic displacement thickness cases, subsection 3.1.5). The Klineberg-Steger distribution was used in this investigation to provide a better qualitative understanding of what conditions cause the wall shear cases to fail.

One of the original cases run by Klineberg and Steger with the above distribution of $\hat{\tau}$ sets

$$C_{KS} = 12.0, \quad \hat{\alpha} = 0.0$$

$$x_1 = 2.0, \quad x_2 = 6.0$$

For this investigation, this case appears as run (7a). The constants C_{KS} and x_1, x_2 were then changed for two other runs so that the slope $\frac{d}{dx}(f_w'')$ into the region of separation was decreased. This also decreased the size of the region of separation. For the second and third computations, the constants were set at:

(1) $C_{KS} = 13.75$, $x_1 = 2.5$, $x_2 = 5.5$

(2) $C_{KS} = 15.0$, $x_1 = 3.0$, $x_2 = 5.0$.

This approach was taken since it was suspected that the magnitude of the f_w'' slope into the separation region was a main cause of the wall shear inverse option's inability to successfully treat some cases.

The three cases run are shown in Figures 39 and 40. Figure 39 displays the distributions of f_w''. Run (7c), which has the smallest value of $\frac{d}{dx}(f_w'')$ at separation, passes smoothly through separation and reattaches downstream. This case has the smallest separation bubble, extending from x=3.0 to x=5.0. The middle case, which is separated from x=2.5 to x=5.5, fails to converge in the separated region at x=3.7,

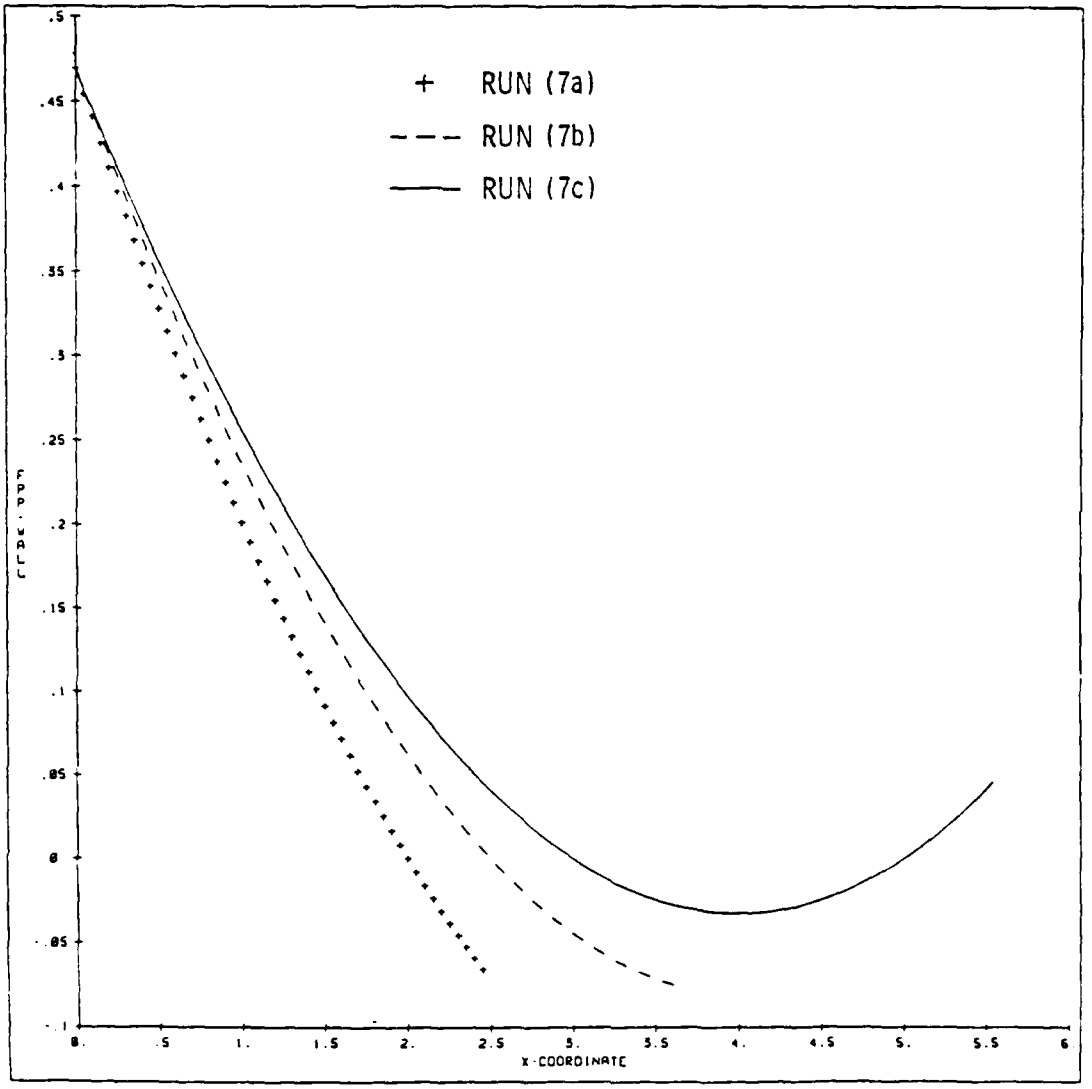

Figure 39. Comparison of f_w'' Distributions for Case 7.

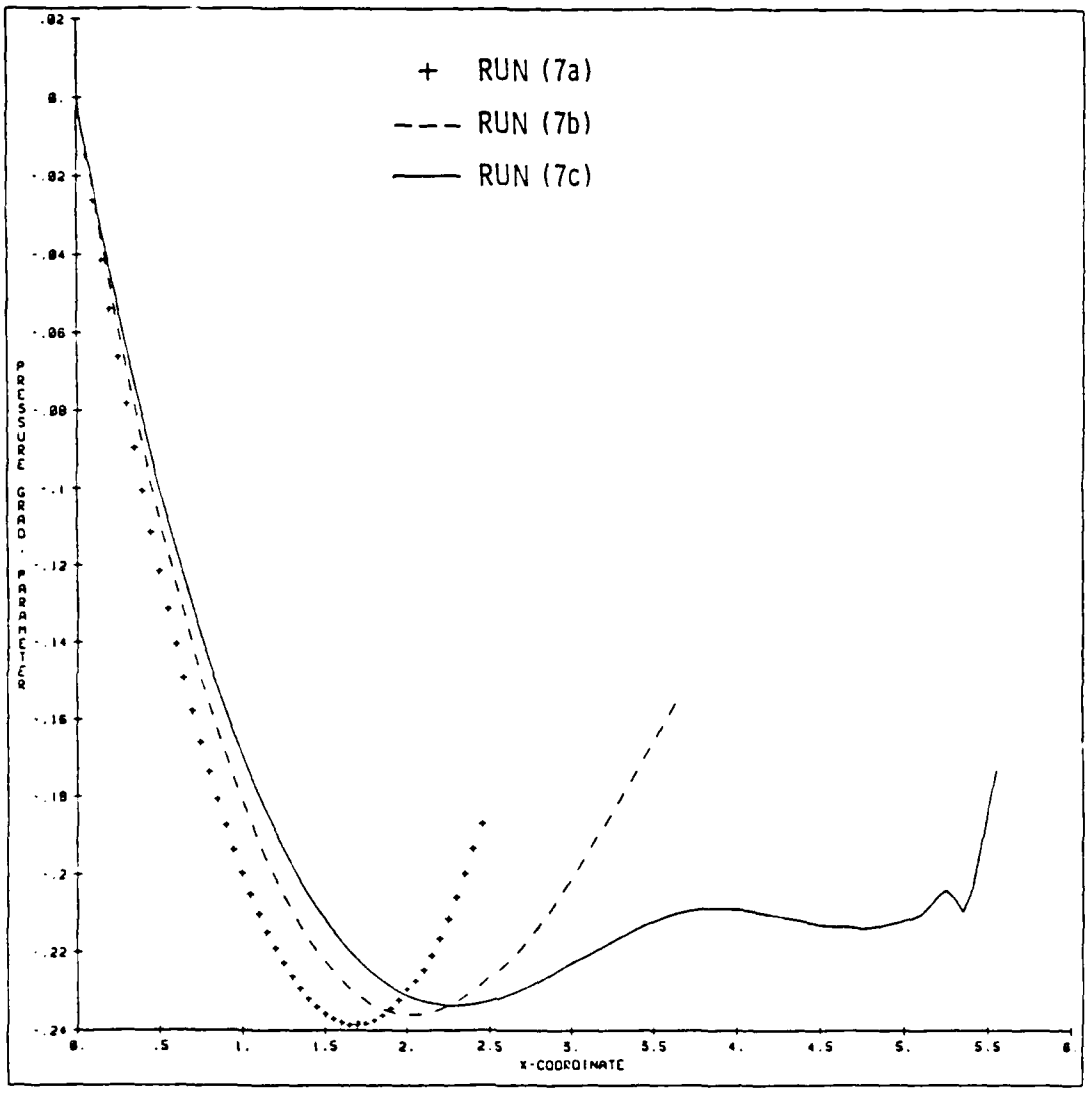

Figure 40. Comparison of β from Inverse Methods for Case 7.

before reaching to the maximum value of f_w''. The most severe case, run (7a), fails to converge properly immediately after reaching separation. The pressure gradient solutions for the three cases are plotted in Figure 40. A discussion of the behavior of the wall shear method is included in the following chapter.

3.2 Turbulent Results

The application of the present method to turbulent boundary layers proved to be disappointing. As a test case, both the direct and inverse methods were us d to compute a turbulent boundary layer on a flat plate. A transition intermittency factor, as described in Appendix B, was used to permit a controlled transition to a fully turbulent flow from a laminar starting solution. A hyperbolic tangent stretching function was used to generate a normal coordinate distribution for the flat plate test.

The resulting direct solution proved to be very unstable, and diverged only several steps downstream after becoming fully turbulent. The number of iterations required for convergence continued to increase as the solution marched downstream even after the full value of the eddy viscosity was reached in the computations. The solution was permitted up to fifty iterations to converge.

The attempted inverse solution proved to be more unstable than the direct solution, and diverged only a short distance into transition. The skin friction distribution generated by the direct method was used as input for the skin friction coefficient solution method. Again, a large number of iterations were permitted.

In an effort to locate the cause of the divergent behavior, two other similar but less complicated eddy viscosity models were coded and

compared with the Baldwin-Lomax model. The standard Cebeci-Smith model [33], in basic form sans corrections, and a simple model applied by Carter and Wornom [14] were used. Both models yielded eddy-viscosity distributions almost identical to those produced by the Baldwin-Lomax model for the flat plate.

An attempt was also made at increasing the transition distance by increasing the constant in the transition intermittency factor. This only slightly prolonged the convergence of the solution downstream.

After a complete check of all analysis and program coding with no errors being found, the attempt at the turbulent solution was abandoned. Future work will be needed to determine the cause of the present method's inability to handle the turbulent case.

Chapter 4

DISCUSSION

4.1 Inverse Methods

In the present investigation, four different inverse methods for boundary-layer flows have been studied. From examining the results, it is clear that for laminar flows, these methods work very well, in general. The methods in their current formulations are not without their problems, however, and for turbulent cases, the problems are severe. The following sections discuss the numerical aspects of the test cases given in the previous chapter in relation to the various methods and formulations used in this investigation.

The inverse methods consist of the transformed wall shear method, the skin friction coefficient methods, the hybrid method, and the displacement thickness method. Each of these methods is discussed individually in the following subsections.

It should be noted that, aside from Horton [10,11], this study is the only one known to the author which formulates the inverse problem in full (streamwise and normal) Levy-Lees coordinates. This study differs from those of Horton in the discretization and solution procedure followed once the equations are cast in pseudo-self-similar form. No other studies exist, to the author's knowledge, which cast the turbulent boundary-layer equations in this form (modified Levy-Lees) for an inverse solution.

4.1.1 Wall Shear Methods

The transformed wall shear method proved to be the least complicated of the inverse formulations, requiring an easy to apply additional boundary condition at the wall. For all cases computed using this boundary condition, quadratic convergence was observed, with only three iterations required typically to satisfy the convergence criteria.

The methods allowing the specification of the skin friction coefficients C_{f_e} and C_{f_∞} are more practical from a physical standpoint. These methods, however, require the development of the complex boundary conditions described in Sections 2.4.2 and 2.9.3. The use of these boundary conditions, which relate the quantities ξ and u_e to the pressure gradient parameter correction, is necessary to accelerate the convergence of the solution. With these boundary conditions installed, quadratic convergence is maintained. Without the correction form of these boundary conditions, convergence is achieved typically only after ten or more iterations.

The wall shear methods do experience a problem with some separated flows. Flows which decelerate rapidly from positive to significant negative values of f_w'' over a small streamwise distance can cause the wall shear methods to fail. Upon examining the distributions of streamfunction, f, and velocity, u, across the boundary layer, an additional reflex in the stream function profile is found near the wall, with an erroneous positive value of f directly adjacent to the wall. This eventually leads to oscillations in the solution. A comparison of incorrect profiles of f and u near the wall and correct profiles for a similar separated region are shown in Figures 41 and 42. This failure

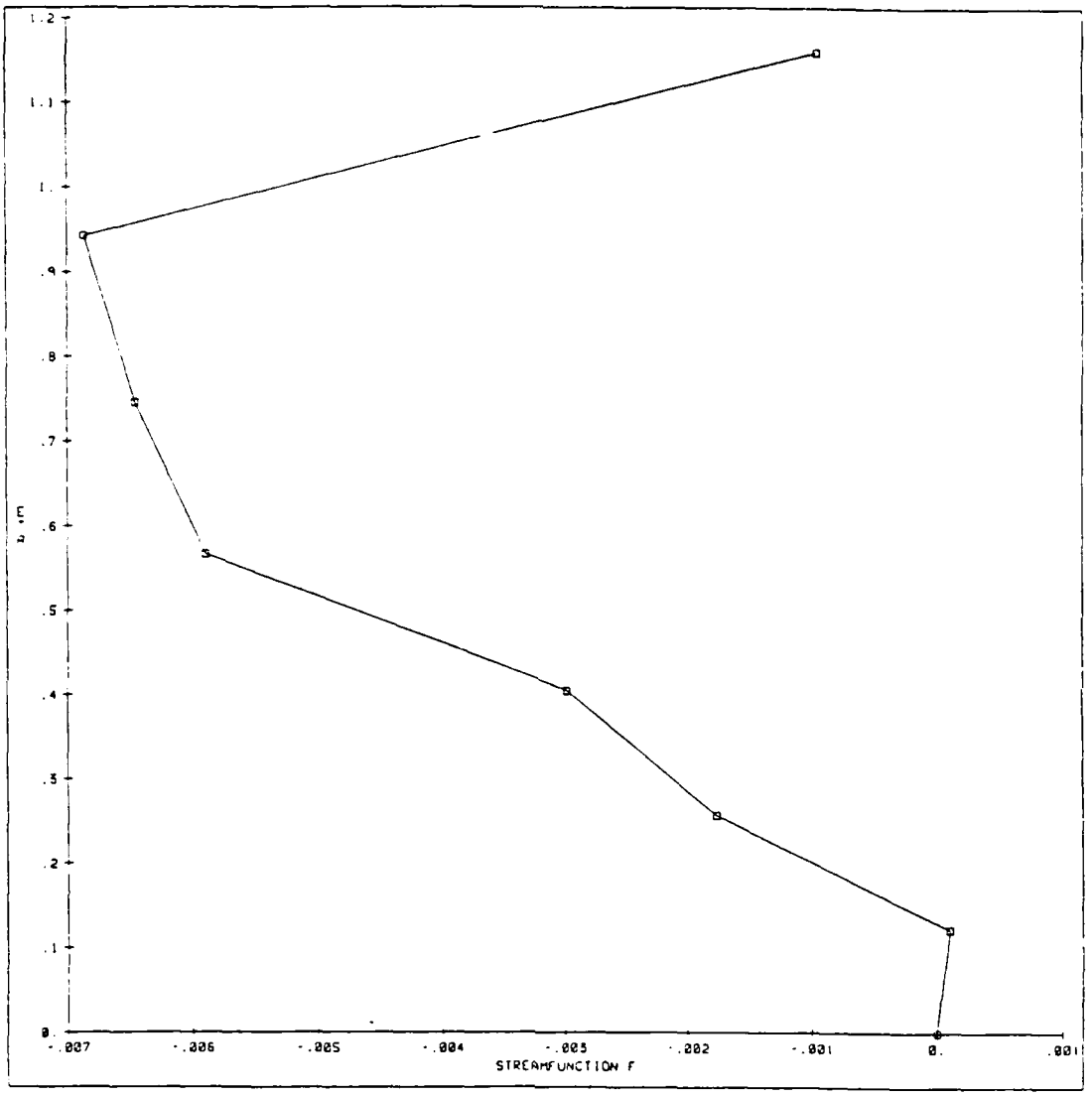

Figure 41. Incorrect Profiles Near Wall from Skin Friction Coefficient Option.

(a) Streamfunction, f

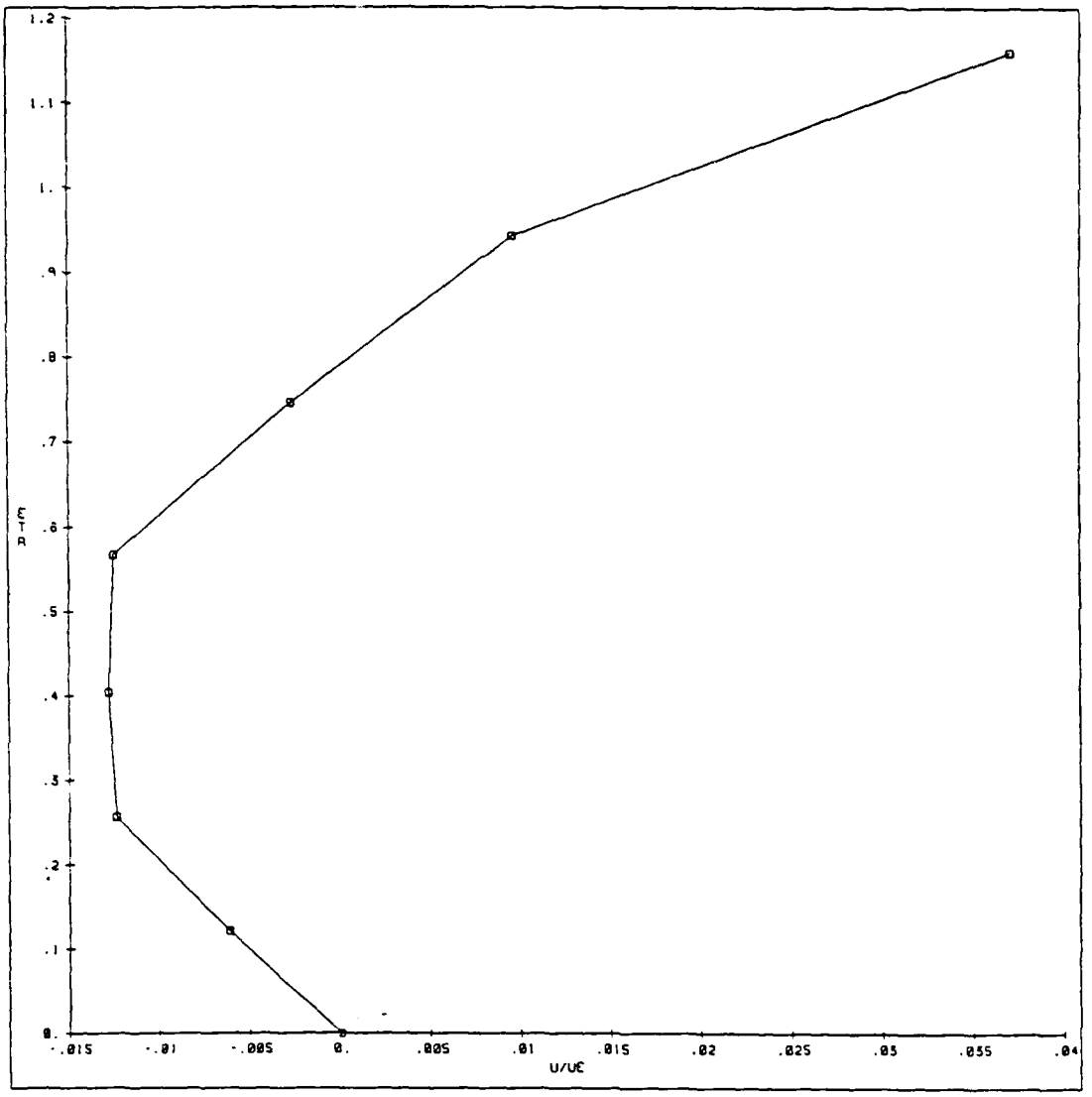

Figure 41. Incorrect Profiles Near Wall from Skin Friction Coefficient Option.

(b) Normalized Velocity, f'

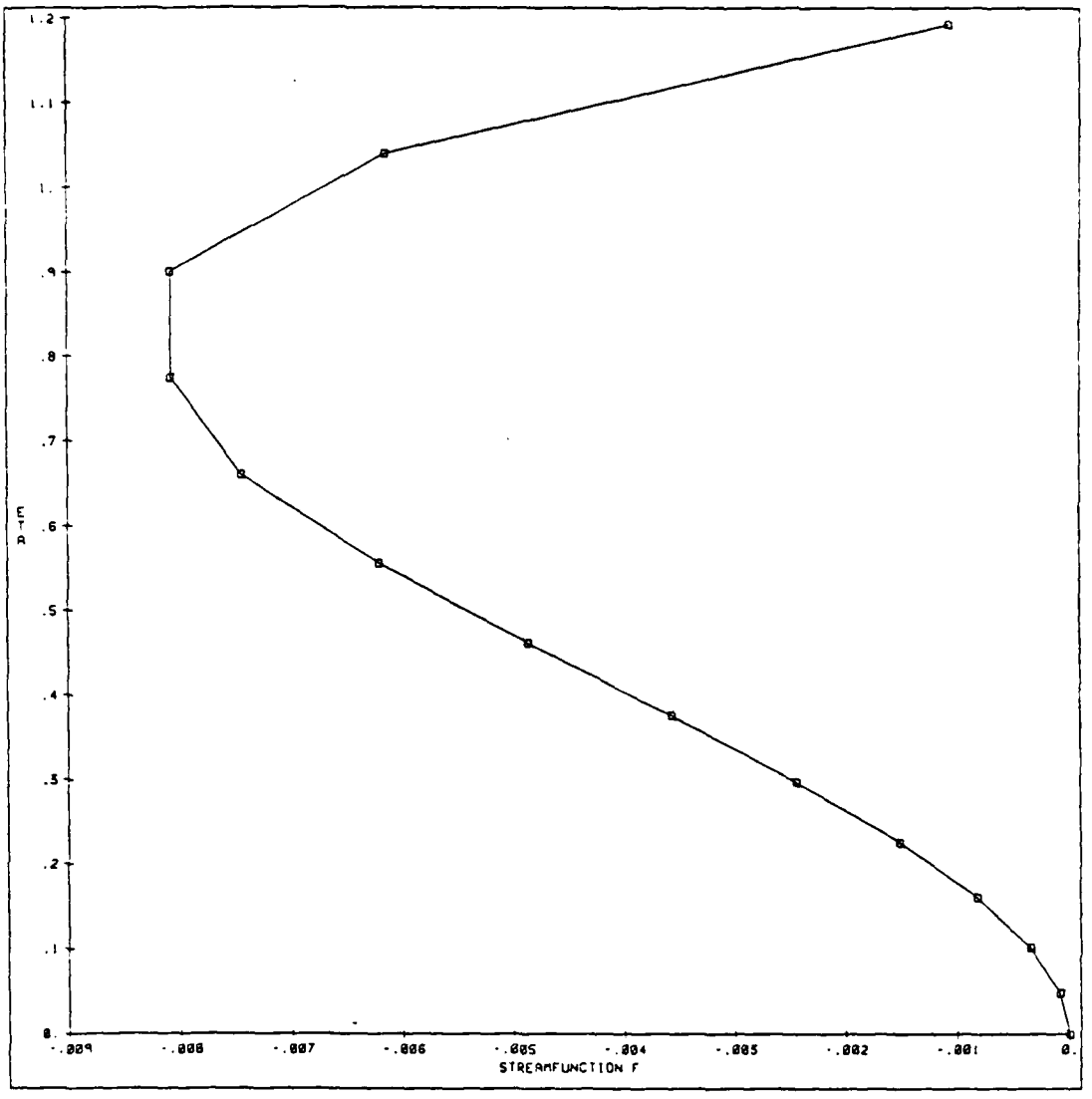

Figure 42. Correct Profiles Near Wall from Displacement Thickness Option.

(a) Streamfunction, f

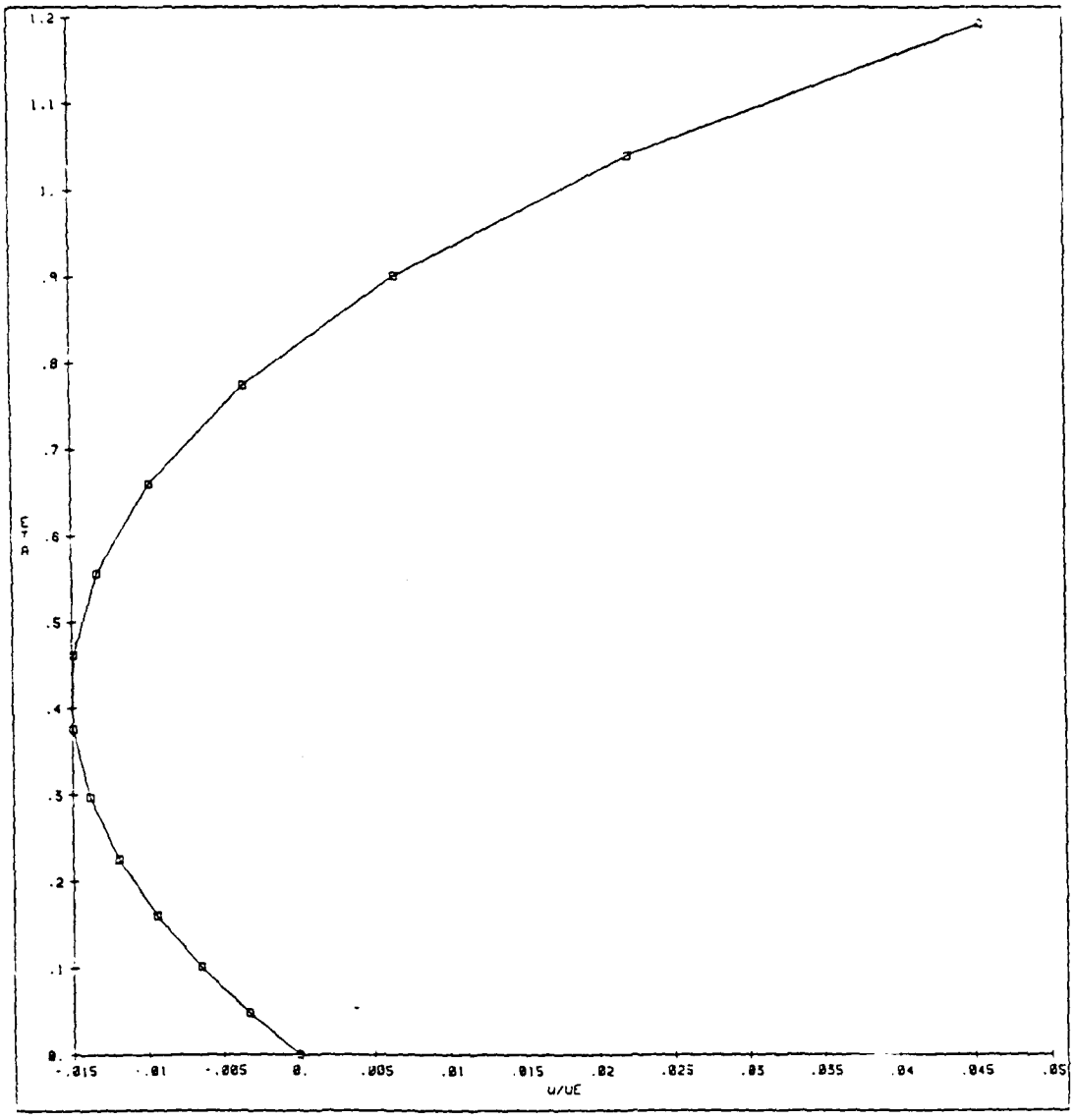

Figure 42. Correct Profiles Near Wall from Displacement Thickness Option.

(b) Normalized Velocity, f'

is apparently inherent in the spline formulation in combination with the boundary conditions applied at the wall for the wall shear methods.

Based upon a comparison of results from the wall shear and displacement thickness methods, it is clear that there is a difference in formulation which must account for the displacement thickness method's ability to successfully calculate regions of separation where the wall shear method fails. This difference is the form of the wall boundary conditions for the two methods. The wall boundary conditions for the wall shear methods only involve the variables f, u, G at j = 1, with no dependence on j = 2 (See subsection 2.8.1). Only the condition on β involves values at both j = 1 and j = 2, but this condition has no effect on the profiles for f, u and G.

The displacement thickness case does include a two-point spline boundary condition at the wall which links the values of f, u, and G at points i = 1 and i = 2. This condition apparently forces the splines to behave in the correct manner near the wall when the flow separates, since the displacement thickness case was used successfully on all occasions. The lack of this two-point condition in the wall shear methods allows the splines to "wiggle" near the wall. This phenomenon seems to occur when the value of $\frac{d}{dx}(f_w'')$ exceeds some undetermined limit near or following separation. This conclusion is based upon the qualitative study of laminar case number 7. This case also demonstrates that the wall shear methods fail when the value of f_w'' exceeds approximately -0.1 or the backflow velocities become larger than one percent of the edge velocity. The inclusion of the two-point boundary condition for the displacement thickness method may be the reason this method can also handle separated zones with values of f_w'' much larger

than the wall shear methods can tolerate. This explains why the wall shear methods perform well for mild cases, such as the Horton parabolic distribution (case number 4) but fail for other problems, such as the separation bubble generated by Carter's analytical distribution of displacement thickness (case number 5).

In the current formulation, however, it is not possible to install a two-point spline boundary condition at the wall for the wall shear methods. Considering the conditions that exist at the wall, only the condition on β may be transferred to the outer edge, since the homogeneous conditions on f and u must remain at the wall, as must the inverse wall shear condition itself. Unfortunately, it was found that transferring the two-point condition on β to the far field produced oscillations there which occurred for attached and separated flow conditions and which significantly decreased marching distance. The conclusion is that, in the present formulation, the required two-point wall boundary condition which would allow the wall shear methods to accurately handle larger regions of separation can not be implemented.

Despite the inability of the wall shear methods to handle larger regions of separation, the methods have proved to be very accurate for milder separated regions and for attached flows. This point is well illustrated by the results for cases 1-4, where the wall shear methods provide excellent results, particularly for Horton's parabolic shear distribution.

4.1.2 Hybrid Method

The hybrid method described in Section 2.4.3 is an inverse method, developed solely for this study, which takes a somewhat different approach to specifying δ^* than other displacement thickness methods,

such as those presented by Carter [12] or Cebeci [15]. Initially the inverse procedure presented here was developed as a wall shear method; and hence the hybrid boundary condition was devised to make use of the wall shear condition for specification of a displacement thickness.

The form presented in this study has not been evolved to the same extent as the wall shear and displacement thickness methods, since it was never completely linearized. Thus the method tends to require more iterations to achieve convergence than the other methods discussed. A standard iteration count at a single streamwise station is typically between five and twelve, depending on the condition of the boundary layer at that location.

A major problem with the hybrid boundary condition is the saddle point occurring in the H-β curve near separation. The value of the derivative $\frac{dH}{d\beta}$ for mild adverse pressure gradients is near -1.0. As the saddle point is approached from upstream, however, the value of $\frac{dH}{d\beta}$ approaches negative infinity, then abruptly switches sign and decreases. The large values of the derivative in the boundary condition lead to a singular matrix and the solution procedure fails.

Several attempts to remedy the saddle point problem were made. Simply neglecting the dependence of H on β made the convergence procedure much more difficult, and the solution would often diverge only a short distance downstream. As an alternative, an ad hoc update procedure for H was implemented, using the following formula:

$$\left(\frac{\delta H}{H}\right)_i^{(n)} = \omega \left(\frac{\delta \beta}{\beta}\right)_i^{(n)}$$

or

$$\left(\frac{dH}{d\beta}\right)_i^{(n)} = \omega \left(\frac{H}{\beta}\right)_i^{(n)}$$

where ω was chosen as a constant less than unity, generally between 0.5 and 0.7. This modified update procedure was used when

$$\left|\frac{dH}{d\beta}\right| > 8.0.$$

This ad hoc update procedure did limit the increasing iteration count as the solution approached separation. The procedure does not, however, recognize the change of sign in the derivative $\frac{dH}{d\beta}$. The location of the saddle point is difficult to determine during computation, since the solution cannot identify the sign switch from an upstream position. The location of the saddle point also seems to vary with different flow situations, sometimes immediately at separation and sometimes ahead of separation. Since the location of the saddle point cannot be accurately determined by the ad hoc procedure, the method also resulted in divergence of the solution or the abrupt jump to another (incorrect) solution curve.

An additional noteworthy feature of the hybrid method is that the error between the specified displacement thickness, $\hat{\delta}^*_{SP}$, and the displacement thickness integrated from the solution, $\hat{\delta}^*_{IN}$, increases linearly as the solution proceeds downstream. This resulted in a slow increase in the solution error and the number of iterations required for convergence. It also lead to slight differences in the solutions for wall shear methods and the hybrid method, although the discrepancies were acceptable.

The combination of these problems indicates that a substantial investigation of the hybrid method is needed. Before the method can be applied constructively, the saddle point problem must be solved and the method more fully understood, although its usefulness is questionable with the success of the displacement thickness method.

4.1.3 Displacement Thickness Method

The displacement thickness method proved to be the most successful of the inverse methods applied in this study. In addition to performing well on the cases treated by the wall shear methods, the displacement thickness method obtained very good results for cases which proved to be too severe for the wall shear methods. In particular, it was used successfully on both analytic displacement thickness distributions devised by Carter [13], for which the wall shear methods were inaccurate.

The ability of the displacement thickness method to handle larger separated regions more accurately than the wall shear methods seems to stem from the use of wall boundary conditions as discussed previously in subsection 4.1.1. The displacement thickness method implements a two-point spline boundary condition at the wall which links the variables f, u, and G at $j = 1$ and $j = 2$. This additional control on the splines prevents the "wiggle" behavior at the wall which is observed in some wall shear method calculations.

Several interesting observations were made during the use of the displacement thickness method. On three occasions, a mild streamwise instability was noted when three-point backward differences were used. This instability was first noticeable through oscillations present in the calculated normal component of velocity, which is dependent upon f_ξ. For these cases, it was necessary to switch to two-point backward differences over the region where separation was present. The use of two-point differences yields accurate solutions through separation without difficulty.

Another unexpected result is the overshoot behavior of the solution following reattachment for the Carter analytic displacement thickness cases. As discussed in the previous chapter, the calculations should return to a flow situation with a near zero pressure gradient, as for a flat plate. For the present method, however, the calculations produce a flow situation which continues to accelerate following reattachment, overshooting the flat plate value of $\delta^*\sqrt{Re}$. The overshoot problem, while present for both displacement thickness distributions, is much more pronounced for the more severe distribution.

The suspected cause for this behavior is streamwise discretization error, which is aggravated by the use of two-point backward differences for the more severe displacement thickness case. As a check, the streamwise stepsize was halved and the cases rerun, as discussed in the previous chapter. The calculations with halved streamwise stepsize show a marked improvement over the initial calculations, although the overshoot behavior is still noticeable. The method has proven to be sensitive to strongly accelerating flows, however, and this sensitivity may be the cause of the remaining discrepancies.

The present formulation was also found to be very sensitive to input data such as displacement thickness or wall shear distributions. This is clear after examining case number 6, treating the Horton displacement thickness distribution obtained experimentally by Ntim [11]. Here, the graphical edge velocity distribution given by Horton was fitted using cubic spline interpolation, and a direct solution was computed to obtain the displacement thickness distribution to a location near the separation point. We note that the edge velocity distribution is matched at two locations, $x = 0.58$ and $x = 0.62$. This is necessary

due to the graphical presentation of the edge velocity in Reference [11].

Once the displacement thickness distribution is obtained from the direct solution, it is fitted, again using cubic spline interpolation, to the distribution given by Horton for the separated region of the boundary-layer flow. The matching procedure is completed over an interval from $x = 0.61$ to $x = 0.66$. A portion of the direct displacement thickness distribution is also smoothed between $x = 0.57$ and $x = 0.585$. Although care is taken to produce continuous distributions of u_e and $\delta\sqrt{Re}$, the derivatives of these quantitied are not forced to be continuous at the matching location.

The inverse solution procedure proved to be very sensitive to the derivative discontinuities, as is shown in Figure 38. The locations of the matching points can be clearly located by the peaks in the skin friction coefficient distribution. From this result, it is clear that for the present formulation, great care must be taken to assure that the input data is as smooth and free of numerical noise as possible to allow for an accurate calculation. The situation here is aggravated by the lack of available tabular data.

4.2 Direct Method

The direct solution option of the present boundary-layer formulation was tested in cases 1, 2, and 3, and used to obtain a displacement thickness distribution in case 6. It performed well for all laminar test cases considered here, with quadratic convergence consistently observed. Upon reaching negative values of f''_w, the solution diverged as expected for standard direct boundary-layer solutions.

The present direct method is interesting since only two boundary conditions must be changed to switch the solution procedure from inverse to direct mode. To obtain a direct solution with the present formulation, the additional condition on β must be enforced and the inverse condition discarded. The direct method retains the 4 X 4 block structure of the inverse methods. The mechul function equation on β becomes a "dummy" equation since β is specified and the equation is satisfied before iteration begins. This suggests that the solution procedure could be easily switched from direct to inverse mode during calculation, although this was not attempted during this study.

With the edge velocity distribution specified, β is obtained using finite difference formulas obtained from the Lagrange interpolation polynomial. In general, three- or four-point backward differences are used. Near the starting solution, forward differences are used if the flow is laminar several stations downstream. If the boundary layer becomes turbulent, β must be updated after each iteration, since it is dependent upon the edge value of μ_t.

Additional comments on the direct method are included in the following sections 4.3, Boundary Conditions, and 4.4, Turbulence Application.

4.3 Boundary Conditions

Throughout the present investigation, the methods developed have proven to be very sensitive to the boundary conditions. A prime example is the results obtained by the wall shear method for certain separated regions, as discussed in section 4.1. This behavior was completely unexpected, since the boundary conditions applied at the wall are quite typical. The use of the splines, however, is not typical.

Unexpected results related to the two-point spline relations were observed in other situations aside from the behavior of the wall shear methods in separated flows. The oscillations produced by transferring the two-point condition on β from the wall to the far field are another instance of such unexpected behavior. Although the boundary condition was expected to be satisfactory at the far field, the resulting oscillations caused the solution to diverge at a streamwise location short of the distance obtained when the condition on β is implemented at the wall.

Similar behavior was observed for the direct method. Replacing Eq. (66a) with Eq. (66c), both of which should perform satisfactorily in the far field, caused the u-velocity profile near η_∞ to overshoot the specified value of unity at η_∞. This overshoot tended to increase as the solution proceeded downstream, and caused a decrease in solution accuracy.

Other instances of such behavior were observed in the current investigation, but only the most severe cases are discussed here. In all instances, however, the solution procedure was found to be extremely sensitive to the particular implementation of the two-point spline relations. Often it was found that one condition adversely affected the solution while another provided accurate results, although both were expected to be adequate. The cause of this sensitivity is unclear from the results of the current investigation.

4.4 Turbulent Application

As noted in the previous chapter, the attempt at obtaining a solution for a turbulent boundary layer was far less successful than the laminar solutions. As a test case, the present direct and inverse

methods were used to compute a turbulent boundary layer on a flat plate. As the solution proceeds downstream, however, the accuracy in the far field rapidly deteriorates. The value of the shear (f'') near the edge grows steadily with downstream distance, while the values of u (f') near η_∞ overshoot the edge value of unity. Oscillations in the far field follow, leading to divergence of the solution only a short distance downstream.

The far field boundary conditions were initially suspected as the cause of this phenomena, since the methods had previously been shown to be sensitive to the particular two-point spline conditions implemented. While changing the particular implementation of the two-point spline conditions produced minor adjustments in the solution, such as slightly smaller values of shear near the edge, the modifications did not prevent the oscillations or the early divergence of the solution.

At present, two possibilities exist which may be the cause of the turbulent solution's behavior. The most likely cause is the presence of a streamwise instability in the present formulation which has a minimal effect on laminar calculations, but which is much more important for turbulent calculations. This is a prime suspect since streamwise fluctuations were found in the turbulent solution attempts. Oscillations were also noted in the normal velocity profile, similar to those found for the laminar displacement thickness cases. For the turbulent case, switching to two-point backward differences prolongs solution convergence by several streamwise stations, but does not prevent the solution from diverging.

The other possibility is that the present formulation is not compatible with the use of the modified Levy-Lees transformation.

Although this possibility is more remote, it cannot be rejected at this stage. It is also possible that the behavior of the turbulent solution is the result of a combination of these causes. The actual cause cannot be definitely identified without further investigation.

Because a turbulent solution was never successfully completed, the adaptive grid coordinate in its present form was never fully tested. The laminar section of the coordinate was tested on several laminar cases, yielding results typical of a hyperbolic normal distribution. Numerical results for these laminar cases are not included here since they are not noteworthy.

4.5 Advantages and Disadvantages of Similarity Transformations

Several advantages of the modified Levy-Lees transformation have been discussed in Chapter Two, such as the ability to capture the laminar and turbulent boundary-layer growth and to provide a self-starting solution. This transformation, or the more familiar original Levy-Lees form, has been a standard part of many direct boundary-layer solutions. For inverse flows, the use of the transformation is not standard. In most cases, the streamwise coordinate x is left alone, although the normal coordinate may be put into similarity form. This is mainly because the transformed streamwise coordinate ξ is a function of the edge velocity, which is obtained during an inverse solution, rather than known beforehand for a direct solution.

Leaving the streamwise coordinate untransformed, however, precludes the use of the modified Levy-Lees transformations and its desirable effect of capturing the turbulent boundary-layer growth. This study has shown that with proper linearization, use of the transformed streamwise

coordinate need not result in additional iterations, particularly for laminar flows.

For direct laminar solutions, the use of the modified Levy-Lees transformation is straightforward, since u_e is specified and μ_{t_e} reduces to the molecular viscosity. For direct turbulent solutions, the use of the transformation becomes more complicated since μ_{t_e} must be estimated and updated at each streamwise station because of its dependence on the eddy viscosity, ε.

Inverse solutions are complicated further since u_e is obtained during the solution procedure. Further, for inverse turbulent solutions, ξ must be updated with u_e and μ_{t_e} as both change during the solution iteration. Although this additional update procedure may tend to slow the convergence rate, this inconvenience is outweighed by the advantages provided by applying the transformation. Additional iterations required for convergence can also be reduced by proper linearization, as discussed in section 2.9. Unfortunately, due to the lack of success with the turbulent solution in this study, the usefulness of the modified Levy-Lees transformation could not be verified beyond its simplification of equation form and algorithm development.

4.6 Pivoting

The present direct and inverse methods employ partial pivoting in the L-U decomposition to prevent the buildup of roundoff error. In an effort to determine whether an ideal ordering of the equations exists, the pivoting indices in the block matrix solver were observed during solution of a nonsimilar boundary-layer flow. By checking these indices, it is possible to determine the pivoting elements of the L-U

decomposition procedure. If the decomposition routine pivots consistently about the same elements, an ideal order of the equations in block matrix form is implied.

The check of the pivoting indices, however, shows no such consistencies. Not only does the pivoting order change continually across the boundary layer, but it also changes as the solution proceeds downstream. This indicates that no predetermined order of the equations exists. Thus, regardless of the equation ordering, pivoting is an essential process for obtaining an accurate solution.

Chapter 5

CONCLUSIONS AND RECOMMENDATIONS

A unified approach to calculating direct and inverse solutions for two-dimensional boundary layers has been presented. By a simple interchange of boundary conditions, the method is capable of providing a direct solution, with a pressure distribution specified, or one of several inverse solution options, depending upon the specification of wall shear, skin friction coefficient, or displacement thickness distributions. A modified form of the mechul function method is used to obtain the inverse solutions. Spline/finite difference discretization yields a fully implicit scheme which converges quadratically for laminar flows, when proper linearization is applied.

For laminar flows, the method works quite well, although it was discovered that the wall shear/skin friction coefficient options do not converge properly for separation regions with backflow velocities greater than one percent of the edge velocity. This behavior is due to the nature of the splines combined with the lack of a sufficiently strong two-point boundary condition at the wall. Without proper control through the wall conditions, the splines allow oscillations in the solution profiles in regions of separation. The displacement thickness option, which does employ such a wall boundary condition, is capable of treating regions of separation with larger backflow velocities (approximately ten percent of the edge velocity).

The solution procedure is also sensitive to the use of the three-point backward differences, sometimes requiring the use of two-point backward differences for accurate results. For laminar flows, this sensitivity appeared during the calculation of separated regions, and

was manifested by oscillations in the normal component of velocity. It is believed that this sensitivity is connected to the instability noted during the attempted turbulent calculations. In addition to the normal velocity oscillations, streamwise fluctuations were also noted in the turbulent cases. This instability resulted in the failure of the turbulent calculations. It is unclear why this instability strongly affects the turbulent case while having little effect on the laminar results.

These conclusions cast some doubt on the utility of spline discretization for all but a small portion of boundary-layer flows, and particularly for cases concerning regions of separation or turbulence. The sensitivity of the present method to the two-point spline boundary conditions contributes strongly to this conclusion. It should be noted, however, that the spline formulation performed excellently in many instances, yielding very accurate results with a minimum of mesh points. The use of a strong, two-point boundary condition at the wall is essential for solutions involving reversed flow. Satisfactory results have been obtained only when such a condition is used. Unfortunately, this form of boundary condition is sometimes difficult to implement, as demonstrated by the wall shear/skin friction options.

The work of Rubin and Khosla [44] indicates that turbulent, non-separating boundary layers can be successfully treated by spline discretization. Therefore, prior to completely discarding the spline/finite difference formulation, a full stability analysis must be performed to determine the source of the streamwise instability which prevents the calculation of accurate turbulent results and impedes the calculation of some separated solutions for this method formulation.

Further research into the application of an adequate boundary condition for the wall shear option is also required to establish the minimum requirements of such a condition and how it could best be implemented.

REFERENCES

1. Smith, A.M.O., and Clutter, D. W., "Solution of the Incompressible Laminar Boundary-Layer Equations," AIAA J., Vol. 1, 1963, pp. 2062-2071.

2. Golstein, S, "On Laminar Boundary-Layer Separation," Quart. J. Mech. and Appl. Math., Vol. 1, 1948, pp. 43-69.

3. Brown, S. N. and Stewartson, K., "Laminar Separation," Ann. Rev. Fluid Mech., Vol. 1, 1969, pp. 45-72.

4. Catherall, D., and Mangler, K. W., "Integration of the Two-Dimensional Laminar Boundary-Layer Equations Past the Point of Vanishing Skin Friction," J. Fluid Mech., Vol. 26, Pt. 1, 1966, pp. 163-182.

5. Reyhner, T. A., and Flugge-Lotz, I., "The Interaction of a Shock Wave with a Laminar Boundary Layer," Int. J. Non-Linear Mech., Vol. 3, 1968, pp. 173-199.

6. Williams, P. G., "A Reverse Flow Computation in the Theory of Self-Induced Separation," Proc. Fourth Int. Conf. Numerical Methods in Fluid Dynamics, Lecture Notes in Physics, Springer-Verlag, 1975, pp. 445-451.

7. Cebeci, T., Keller, H. B., and Williams, P. G., "Separating Boundary-Layer Flow Calculations," J. Comp. Physics, Vol. 31, 1979, pp. 363-378.

8. Keller, H. B., and Cebeci, T., "An Inverse Problem in Boundary-Layer Flows: Numerical Determination of Pressure Gradient for a Given Wall Shear," J. Comp. Physics, Vol. 10, 1972, pp. 151-161.

9. Klineberg, J. M. and Steger, J. L., "The Numerical Calculation of Laminar Boundary-Layer Separation," NASA TN D-7732, July 1974.

10. Horton, H. P., "Separating Laminar Boundary Layers with Prescribed Wall Shear," AIAA J., Vol. 12, No. 12, Dec. 1974, pp. 1772-1774.

11. Horton, H. P., "Comparisons Between Inverse Boundary-Layer Calculations and Detailed Measurements in Laminar Separated Flows," Aeronautical Quart., Aug. 1981, pp. 169-187.

12. Carter, J. E., "Solutions for Laminar Boundary Layers with Separation and Reattachment," AIAA Paper No. 74-583, 1974.

13. Carter, J. E., "Inverse Solutions for Laminar Boundary-Layer Flows with Separation and Reattachment," NASA TR R-447, Nov. 1975.

14. Carter, J. E., and Wornom, S. F., "Solutions for Incompressible Separated Boundary Layers Including Viscous-Inviscid Interaction," NASA SP-347, 1975.

15. Cebeci, T., "An Inverse Boundary-Layer Method for Compressible Laminar and Turbulent Boundary Layers," J. Aircraft, Vol. 13, No. 9, Sept. 1976, pp. 709-717.

16. Carter, J. E., "Inverse Boundary-Layer Theory and Comparison with Experiment," NASA TP-1208, 1978.

17. Whitfield, D. L., Swafford, T. W., and Jacocks, J. L., "Calculation of Turbulent Boundary Layers with Separation and Viscous-Inviscid Interaction," AIAA J., Vol. 19, No. 10, Oct. 1981, pp. 1315-1322.

18. Liebeck, R. H., "On the Design of Subsonic Airfoils for High Lift," AIAA Paper 76-406, 1976.

19. Veldman, A. E. P., "New Quasi-Simultaneous Method to Calculate Interacting Boundary Layers," AIAA J., Vol. 19, No. 1, Jan. 1981. pp. 79-85.

20. Vatsa, V. N., and Verdon, J. M., "Viscous/Inviscid Interaction Analysis of Separated Trailing-Edge Flows," Vol. 23, No. 4, April 1985, pp. 481-489.

21. Rubin, S. G., and Khosla, P. K., "Polynomial Interpolation Methods for Viscous Flow Calculations," J. Comp. Physics, Vol. 24, 1977, pp. 217-244.

22. Cebeci, T. and Keller, H. B., "Laminar Boundary Layers with Assigned Wall Shear," Proceedings Third Int. Conf. Numerical Methods in Fluid Dynamics, Lecture Notes in Physics, Vol. 19, Springer-Verlag, 1973, pp. 79-85.

23. Kaufman, K. C., and Hoffman, G. H., "Inverse Laminar Boundary-Layer Problems with Assigned Shear. The Mechul Function Revisited," Int. J. Num. Methods in Fluids, Vol. 5, 1985, pp. 1035-1045.

24. Baldwin, B. S., and Lomax, H., "Thin Layer Approximation and Algebraic Model for Separated Turbulent Flows," AIAA Paper 78-257, 1978.

25. Carter, J. E., Edwards, D. E., and Werle, M. J., "Coordinate Transformation for Laminar and Turbulent Boundary Layers," AIAA J., Vol. 20, No. 2, Feb. 1982, pp. 282-284.

26. Schlicting, H., Boundary-Layer Theory, McGraw-Hill Book Company, New York, 1979.

27. Whitfield, D. L., "Analytical Description of the Complete Turbulent Boundary-Layer Profile," AIAA J., Oct. 1979, pp. 1145-1147.

28. Clauser, F. H., "The Turbulent Boundary Layer," Advances in Applied Mechanics, Vol. 4, 1956, pp. 1-51.

29. Edwards, D. E., Carter, J. E., and Werle, M. J., "Analysis of the Boundary-Layer Equations Including a New Composite Coordinate Transformation--The ABLE Code," UTRC 81-30, May 1982.

30. Swafford, T. W., "Analytical Approxiamtion of Two-Dimensional Separated Turbulent Boundary-Layer Profiles," Arnold Engineering Development Center Report AEDC-TR-79-99, 1979.

31. Whitfield, D. L., "Integral Solution of Compressible Turbulent Boundary Layers Using Improved Velocity Profiles," Arnold Engineering Development Center Report AEDC-TR-78-42, 1978.

32. Anderson, D. A., Tannehill, J. C., and Pletcher, R. H., Computational Fluid Mechanics and Heat Transfer, Hemisphere Publishing Company, McGraw-Hill Book Company, New York, 1984.

33. Cebeci, T., and Smith, A. M. O., Analysis of Turbulent Boundary Layers, Academic Press, New York, 1974.

34. Blottner, F. G., "Introduction to Computational Methods in Boundary Layers," Sandia Report No. 79-0893, Sandia Laboratories, Albuquerque, NM, Sept. 1979.

35. Keller, H. B., "Numerical Solution of Two Point Boundary Value Problems," *Regional Conference Series in Applied Mathematics*, Society for Industrial and Applied Mathematics, 1976.

36. Rosenhead, L., Laminar Boundary Layers, Oxford University Press, Oxford, 1963.

37. Bradshaw, P., Cebeci, T. and Whitelaw, J. H., Engineering Calculation Methods for Turbulent Flow, Academic Press, New York, 1981.

38. Vinokur, M., "On One-Dimensional Stretching Functions for Finite Difference Calculations," NASA Contractor Report 3313, 1980.

39. Thompson, J. F., Warsi, Z. U. A., and Mastin, C. W., Numerical Grid Generation Foundations and Applications, Elsevier Science Publishing Co., Inc., New York, 1985.

40. White, F. M., Viscous Fluid Flow, McGraw-Hill Book Company, New York, 1974.

41. Howarth, L., "On the Solution of the Laminar Boundary-Layer Equations," Proc. Roy. Soc. London, Ser. A, Vol. 164, pp. 547-579.

42. Terrill, R. M., "Laminar Boundary-Layer Flow Near Separation With and Without Suction," Phil. Trans., Vol. 253, 1960, pp. 50-100.

43. Cebeci, T. and Bradshaw, P., Momentum Transfer in Boundary Layers, Hemisphere Publishing Company, McGraw-Hill Book Company, New York, 1977.

44. Rubin, S. G., and Khosla, P. K., "Turbulent Boundary Layers With and Without Mass Injection," Computers and Fluids, Vol. 5, 1977, pp. 241-259.

Appendix A: BACKWARD DIFFERENCES WITH VARIABLE STEPSIZE

Streamwise differencing with variable stepsize is essential for the present inverse method since the transformed streamwise coordinate, ξ is determined with the solution. Thus, although a constant stepsize in x may be specified with the input data, the values of $\Delta\xi$ between each streamwise station will vary. To obtain accurate difference formulas with variable stepsize, the Lagrange interpolation formula is used to derive three- and two-point backward differences.

The quadratic Lagrange interpolation formula is

$$f(x) = f(x_1)\frac{(x-x_2)(x-x_3)}{(x_1-x_2)(x_1-x_3)} + f(x_2)\frac{(x-x_1)(x-x_3)}{(x_2-x_1)(x_2-x_3)} + f(x_3)\frac{(x-x_1)(x-x_2)}{(x_3-x_1)(x_3-x_2)} . \tag{A.1}$$

Letting $f(x) = y - y_1$, Eq. (A.1) becomes

$$y = y_1 + \frac{A_1}{B_1}(y_2-y_1) + \frac{A_2}{B_2}(y_3-y_1) \tag{A.2}$$

where

$$A_1 = (x-x_1)(x-x_3)$$

$$A_2 = (x-x_1)(x-x_2)$$

$$B_1 = (x_2-x_1)(x_2-x_3)$$

$$B_2 = (x_3-x_1)(x_3-x_2)$$

The difference formula for $\frac{dv}{dx}$ is then

$$\frac{dv}{dx} = \frac{A_1'}{B_1}(y_2-y_1) + \frac{A_2'}{B_2}(y_3-y_1) \tag{A.3}$$

where

$$A_1' = (x-x_1) + (x-x_3)$$

$$A_2' = (x-x_1) + (x-x_2)$$

In terms of the streamwise index i, the three point backward difference formula at x is

$$\left(\frac{dv}{dx}\right)_i = \frac{A_1'}{B_1}(y_{i-1} - y_i) + \frac{A_2'}{B_2}(y_{i-2} - y_i) \qquad (A.4)$$

where

$$A_1' = x_i - x_{i-2}$$

$$A_2' = x_i - x_{i-1}$$

$$B_1 = (x_{i-1} - x_i)(x_{i-1} - x_{i-2})$$

$$B_2 = (x_{i-2} - x_i)(x_{i-2} - x_{i-1})$$

Equation (A.4) can be written in the alternative form

$$\left(\frac{dv}{dx}\right)_i = -\left(\frac{A_1'}{B_1} + \frac{A_2'}{B_2}\right) y_i + \frac{A_1'}{B_1} y_{i-1} + \frac{A_2'}{B_2} y_{i-2} \qquad (A.5)$$

or

$$\left(\frac{dv}{dx}\right)_i = ay_i + by_{i-1} + cy_{i-2} \qquad (A.6)$$

Equation A.6 is the form used to discretize the streamwise derivatives.

For a two-point backward difference formula, Eq. (A.4) reduces to

$$\left(\frac{dv}{dx}\right)_i = \frac{A_1'}{B_1}(y_{i-1} - y_i) \qquad (A.7)$$

where

$$A_1' = 1$$

$$B_1 = x_{i-1} - x_i$$

or

$$\left(\frac{dv}{dx}\right)_i = ay_i + by_{i-1} \qquad (A.8)$$

with

$$a = \frac{1}{x_i - x_{i-1}}$$

$$b = - a$$

Appendix B: TRANSFORMED EDDY VISCOSITY FORMULAS

The untransformed eddy-viscosity model of Baldwin and Lomax [24] is described in Section 2.6. For this problem, the eddy-viscosity equations must be non-dimensionalized and transformed to (ξ, η) coordinates. The following is a complete list of all transformed quantities related to the turbulence model.

Inner region:

$$\varepsilon_i = \sqrt{Re}\ k^2\ \sqrt{2\xi}\ \eta^2\ \ell_c^2\ |f_{\eta\eta}|\ \gamma_{tr} \tag{B.1}$$

where

$$\ell_c = 1 - \exp\left(-\frac{y^+}{A^+}\right) \tag{B.2}$$

$$y^+ = Re^{1/4}\ \eta\ [\sqrt{2\xi}\ |f_{\eta\eta}|_w]^{1/2} \tag{B.3}$$

Outer region:

$$\varepsilon_o = Re\ K\ C_{CP}\ F_{WAKE}\ F_{KLEB}(\eta)\ \gamma_{tr} \tag{B.4}$$

where

$$F_{WAKE} = \left\{ \begin{array}{l} Re^{-1/2}\ \frac{\sqrt{2\xi}}{u_e}\ \eta_{MAX}\ F_{MAX} \qquad (B.5) \\ \\ Re^{-1/2}\ C_{WK}\ \frac{\sqrt{2\xi}}{u_e}\ \eta_{MAX}\ u_{DIF}^2/F_{MAX} \qquad (B.6) \end{array} \right\} \text{ the smaller}$$

$$F(\eta) = u_e \eta |f_{\eta\eta}|\ [1 - \exp\left(-\frac{y^+}{A}\right)] \tag{B.7}$$

$$F_{MAX} = \text{maximum } [F(\eta)] \Big|_0^{\eta_\infty}$$

$$\eta_{MAX} = \eta \text{ where } F(\eta) = F_{MAX}$$

$$u_{DIF}^2 = u_e^2 \left[f_\eta^2 + 2\xi Re^{-1} \mu_{t_e}^2 \left(f_\xi + \frac{f}{2\xi} + \eta_\xi f_\eta\right)^2\right] \qquad (B.8)$$

$$\eta_\xi = \frac{\eta}{2\xi}(\beta-1) \qquad (B.9)$$

$$F_{KLEB}(\eta) = \left[1 + 5.5\left(\frac{C_{KLEB}\eta}{\eta_{MAX}}\right)^6\right]^{-1} \qquad (B.10)$$

The transition intermittency factor is

$$\gamma_{tr} = 1 - \exp\left[\bar{G}\, u_e^3 \int_{x_{tr}}^{x} dx \int_{x_{tr}}^{x} \frac{dx}{u_e}\right] \qquad (B.11)$$

where

$$\bar{G} = -\frac{1}{1200} Re^2 R_{x_{tr}}^{-1.34} \qquad (B.12)$$

$$R_{x_{tr}} = Re \cdot x_{tr} \cdot u_e \qquad (B.13)$$

The constants are:

$A^+ = 26$ $\qquad$ $C_{KLEB} = 0.3$

$k = 0.4$ $\qquad$ $C_{WK} = 0.25$

$K = 0.0168$ $\qquad$ $C_{CP} = 1.6$

Note: For the present study, C_{KLEB} was set to zero so that $F_{KLEB}(\eta)=1$.

Appendix C: SPLINE AND BLOCK TRIDIAGONAL COEFFICIENTS

In block matrix form, the system of spline equations for the nodal points $2 \leq j \leq N$ at a streamwise station i are as follows:

$$B_j \, Z_{j-1} + A_j \, Z_j + C_j \, Z_{j+1} = R_j$$

where

$$B_j = \begin{bmatrix} \frac{\sigma_2}{N'_{j-1}} \hat{A}_{j-1} & \frac{\sigma_2}{N'_{j-1}} \hat{B}_{j-1} & \frac{\sigma_2}{N'_{j-1}} \hat{D}_{j-1} & \frac{\sigma_2}{N'_{j-1}} G_{j-1} \\ \frac{\sigma_3}{h_j} & -\frac{\sigma_2}{N'_{j-1}} & 0 & 0 \\ 0 & \frac{\sigma_3}{h_j} & \frac{\sigma_2}{N'_{j-1}} b^*_{j-1}(e_{j-1}-1) & 0 \\ 0 & 0 & 0 & 1 \end{bmatrix}$$

$$A_j = \begin{bmatrix} \frac{\sigma_1}{N'_j} A_j & \frac{\sigma_1}{N'_j} \hat{B}_j & \frac{\sigma_1}{N'_j} \hat{E}_j & \frac{\sigma_1}{N'_j} G_j \\ \frac{\sigma_4}{h_j} & -\frac{\sigma_1}{N'_j} & 0 & 0 \\ 0 & \frac{\sigma_4}{h_j} & \frac{\sigma_1}{N'_j} b^*_j(e_j-1) & 0 \\ 0 & 0 & 0 & \sigma_j \end{bmatrix}$$

$$C_j = \begin{bmatrix} \frac{1}{N'_{j+1}} \hat{A}_{j+1} & \frac{1}{N'_{j+1}} \hat{B}_{j+1} & \frac{1}{N'_{j+1}} \hat{F}_{j+1} & \frac{1}{N'_{j+1}} G_{j+1} \\ \frac{\sigma_5}{h_j} & - \frac{1}{N'_{j+1}} & 0 & 0 \\ 0 & \frac{\sigma_5}{h_j} & \frac{b^*_{j+1}}{N'_{j+1}} (e_{j+1}-1) & 0 \\ 0 & 0 & 0 & \sigma_6 \end{bmatrix}$$

and

$$Z_j = \begin{bmatrix} \delta f \\ \delta u \\ \delta G \\ \delta \beta \end{bmatrix}_j \qquad R_j = \begin{bmatrix} T \\ L \\ P \\ Q \end{bmatrix}_j$$

with the following coefficients definitions:

$$\sigma_1 = (1 + \sigma)^2$$

$$\sigma_2 = \sigma^2$$

$$\sigma_3 = - \frac{2\sigma(2 + \sigma)}{1 + \sigma}$$

$$\sigma_4 = \frac{2(\sigma-1)(1+\sigma)^2}{\sigma}$$

$$\sigma_5 = \frac{2(1 + 2\sigma)}{\sigma(1 + \sigma)}$$

$$\sigma_6 = \frac{1}{\sigma}$$

$$\sigma_7 = - \frac{1 + \sigma}{\sigma}$$

$$\sigma = \frac{h_{j+1}}{h_j}, \quad h_j = N_j - N_{j-1} \quad \text{or} \quad h_j = \eta_j - \eta_{j-1} .$$

and

$$\hat{A}_j = C_{2_j}\, b_j^* G_j$$

$$\hat{B}_j = 2u_j\,(\beta_j + \Theta_j\, C_{1_j}) + R_j(\Theta_j - 1)\, b_j^*\, G_j$$

$$\hat{C}_j = b_j^*(i-e_j)[C_{2_j}\, f_j + R_j(\Theta_j - 1)u_j + C_{3_j}]$$

$$\hat{D}_j = \hat{C}_j - \frac{N_j'}{h_j}\frac{\sigma_3}{\sigma_2}$$

$$\hat{E}_j = \hat{C}_j - \frac{N_j'}{h_j}\frac{\sigma_4}{\sigma_1}$$

$$\hat{F}_j = \hat{C}_{j+1} - \frac{N_j'}{h_j}\sigma_5$$

$$\hat{G}_j = u_j^2 - 1$$

$$R_j = 2\xi\left(\frac{N_\xi}{N_\eta}\right)_j$$

The backward differencing coefficients are defined as

$$C_{1_{ij}} = a\xi_i$$

$$C_{2_{ij}} = -(2a\xi_i + 1)$$

$$C_{3_{ij}} = -\,2\xi_i\,(bf_{i-1} + cf_{i-2})_j$$

$$C_{4_{ij}} = \xi_i\,(bu_{i-1}^2 + cu_{i-2}^2)_j$$

with a, b, and c as given in Appendix A. The eddy viscosity

coefficients are

$$b_j^* = b_j^{-1}$$

$$b_j = \frac{\mu_t}{\mu_{t_e}}$$

$$\mu_t = 1 + \varepsilon$$

$$\mu_{t_e} = 1 + \varepsilon_o$$

$$e_j = \begin{cases} e_j = \dfrac{\varepsilon_i}{2\varepsilon_i + 1} & \text{for inner region} \\ 0 & \text{for outer region} \end{cases}$$

END

4-87

DTIC